

**Charles University**  
**1<sup>st</sup> Faculty of Medicine**



**UNIVERZITA KARLOVA**  
**I. lékařská fakulta**

Postgraduate Ph.D. program in Biomedicine  
Field of study: Imaging Methods in Medicine

**MUDr. Masego Candy BUDKA MOKOTEDI**

Imaging methods in monitoring organ function of critically ill patients with an emphasis on  
lung ultrasound

Ph.D. Thesis

Supervisor: doc. MUDr. Martin BALÍK, Ph.D., EDIC

Prague, 2024

**Declaration:**

I declare that I have prepared this final thesis independently and that I have listed and cited all the sources and literature used. At the same time, I declare that this work has not been used to obtain another or the same qualification/title.

**I agree** to the permanent storage of the electronic version of my thesis in the database of the interuniversity project system Theses.cz to serve as a continuous control of the similarity of qualification theses.

In Prague, 31.01.2024

MUDr. Masego Candy BUDKA MOKOTEDI

**Prohlášení:**

Prohlašuji, že jsem závěrečnou práci zpracovala samostatně a že jsem řádně uvedla a citovala všechny použité prameny a literaturu. Současně prohlašuji, že práce nebyla využita k získání jiného nebo stejného titulu.

Souhlasím s trvalým uložením elektronické verze mé práce v databázi systému meziuniverzitního projektu Theses.cz za účelem soustavné kontroly podobnosti kvalifikačních prací.

V Praze, 31.01.2024

MUDr. Masego Candy BUDKA MOKOTEDI

**Identification record:**

BUDKA MOKOTEDI, Masego Candy. *Imaging methods in monitoring organ function of critically ill patients with an emphasis on lung ultrasound*. Prague, 2024. 58 pages. Ph.D. dissertation thesis. Charles University, 1. Faculty of Medicine, Department of Anesthesiology and Intensive Care, 1. Faculty of Medicine, Charles University, and the General Faculty Hospital in Prague. Supervisor BALÍK, Martin.

**Identifikační záznam:**

BUDKA MOKOTEDI, Masego Candy. *Imaging methods in monitoring organ function of critically ill patients with an emphasis on lung ultrasound*. Praha, 2024. 58 stran. Disertační práce. Univerzita Karlova, 1. Lékařská fakulta, Klinika anesteziologie, resuscitace a intenzivní medicíny, 1. lékařská fakulta, Univerzita Karlova a Všeobecná fakultní nemocnice Praha. Vedoucí práce BALÍK, Martin.

## **Acknowledgement**

First and foremost, I would like to express my deepest appreciation to my supervisor, Doc. MUDr. Martin Balík, Ph.D., EDIC, for his unwavering support and for imparting his knowledge unto me to be able to make this project a success. I had the pleasure of working with his team and my thanks go to them for their invaluable support.

Second, this endeavour would not have been possible without my husband, Karel, and my family for believing in me and encouraging me to see this project through.

Lastly, I would like to thank the committee chair for her patience and guidance.

## **Abstract**

There are different methods monitoring thoracic organ function in the critically ill by using various imaging methods (chest x-ray, computed tomography, magnetic resonance, and the newly popular lung ultrasound as a stand-alone method or combined with echocardiography). The disadvantages of these methods make lung ultrasound in this group of patients an exquisite bed side imaging tool to assess and diagnose a myriad of lung pathologies, gauge therapeutic interventions and ultimately assess the diaphragm, extradiaphragmatic apparatus and cardiopulmonary changes during weaning of mechanical ventilation and as thus predict its potential failure or success. Furthermore, lung ultrasound has also proved to be extremely useful during the COVID-19 pandemic in assessing COVID-19 pneumonia and its complications with a resultant reduction in potential cross-contamination of staff and patients due to transport to and from the radiology department for imaging. Moreover, vital information can be attained on the hemodynamics of a patient when lung ultrasound is combined with vascular assessment and echocardiography.

This doctoral thesis delved into evaluating chest drain positioning on chest x-ray using several simple parameters (chest drain inclination, tortuosity of the chest drain and its foreshortening) and we further sought to locate a chest drain on lung ultrasound post drainage. These investigations into chest drain positioning help in the diagnosis of chest drain malposition which can potentially lead to residual/occult pneumothoraces which further can have dire implications in mechanically ventilated patients. We also challenged the established method of quantifying pleural fluid volume on lung ultrasound wherein this method could give erroneous pleural fluid estimates in patients with consolidated lungs and lastly, we sought the impact of serial imaging with the growing popularity of lung ultrasound on the intensive care unit outcome of patients with COVID-19, acute respiratory distress syndrome treated with extracorporeal membrane oxygenation.

**Keywords:** Lung ultrasound, chest x-ray, computed tomography, pneumothorax, pulmonary consolidation, pleural effusion, pulmonary edema, COVID- 19 pneumonia, acute respiratory distress syndrome, pulmonary embolism, fluid loading, extravascular lung water, proning, weaning failure, diaphragm dysfunction

## Abstrakt

Existují různé metody monitorování funkce hrudních orgánů u kriticky nemocných pacientů pomocí různých zobrazovacích metod (rentgen hrudníku, počítačová tomografie, magnetická rezonance a nově populární ultrazvuk plic jako samostatná metoda nebo v kombinaci s echokardiografií). Nevýhody těchto metod dělají z ultrazvuku plic u této skupiny pacientů vynikající zobrazovací metodu vyšetření na lůžku k posouzení a diagnostice mnohých plicních patologií, k provedení terapeutických intervencí a dále k posouzení dysfunkce bránice, extradiafragmatického aparátu a kardiopulmonálních změn během odvykání od umělé mechanické ventilace a eventuální predikce jeho úspěchu či potenciálního selhání. Kromě toho se ultrazvuk plic také ukázal jako mimořádně užitečná metoda během pandemie COVID při hodnocení COVID pneumonie a jejích komplikací s výsledným snížením potenciální křížové kontaminace personálu a pacientů v důsledku transportu na radiologického oddělení za účelem vyšetření. Kromě toho lze získat důležité informace o hemodynamice pacienta, v případě, když je ultrazvuk plic kombinován s vaskulárním vyšetřením a echokardiografií.

Tato disertační práce se ponořila do hodnocení umístění hrudního drénu na rentgenu srdce a plic pomocí několika jednoduchých parametrů (sklon hrudního drénu, tortuozita hrudního drénu a jeho zkrácení) a dále jsme hledali umístění hrudního drénu po drenáži. Tato vyšetření umístění hrudního drénu pomáhají při diagnostice malpozice hrudního drénu, která může potenciálně vést k reziduálním/okultním pneumotoraciím, které dále mohou mít vážné důsledky u mechanicky ventilovaných pacientů. Zpochybnili jsme také metodu kvantifikace objemu pleurální tekutiny na ultrazvuku plic, kde by tato metoda mohla poskytnout chybné odhady objemu pleurální tekutiny u pacientů s konsolidovanými plícemi, a nakonec jsme hledali dopad sériového zobrazování s rostoucí popularitou ultrazvuku plic na výsledky léčby pacientů na jednotce intenzivní péče se syndromem akutní dechové tísně při COVID-19 léčených pomocí mimotělního oběhu.

Klíčová slova: Ultrazvuk plic, rentgen srdce a plic, počítačová tomografie, pneumotorax, plicní konsolidace, pleurální výpotek, plicní edém, COVID-19 pneumonie, syndrom akutní dechové tísně, plicní embolie, tekutinová zátěž, extravaskulární plicní voda, pronační poloha, selhání odvykání/weaning, dysfunkce bránice.

## **List of abbreviations**

AAL - *anterior axillary line*

ACE - *angiotensin-converting enzyme*

AFOP - *acute fibrinous and organizing pneumonitis*

AI – *artificial intelligence*

ALARA – *as low as reasonably achievable*

APACHE - *acute physiology and chronic health evaluation*

ARDS - *acute respiratory distress syndrome*

AUC - *area under the curve*

BIPAP - *bilevel positive airway pressure*

BLUE - *bedside lung ultrasound in emergency*

BMI - *body mass index*

CD - *chest drain*

CDI - *chest drain index*

CEPPIS - *chest echography and procalcitonin pulmonary infection score*

CEUS - *contrast enhanced lung ultrasound*

CI - *confidence interval*

CIN - *contrast induced nephropathy*

CO - *cardiac output*

COPD - *chronic obstructive pulmonary disease*

COVID-19 - *coronavirus disease of 2019*

CPIS - *clinical pulmonary score*

CT - *computed tomography*

CTAG - *pulmonary computed tomography angiography*

CW - *continuous wave doppler*

CXR - *chest x-ray*

DB - *deep breathing*

DL – *deep learning*

DM - *diabetes mellitus*

ECMO - *extracorporeal membrane oxygenation*

EUR - *Euro*

EVLW - *extravascular lung water*

FALLS - *fluid administration limited by lung sonography*  
GGO - *ground glass opacities*  
H1N1 - *Influenza A virus subtype H1N1*  
HT - *hypertension*  
ICU - *intensive care unit*  
IHD - *intermittent hemodialysis*  
IPPV - *intermittent positive pressure ventilation*  
IQR - *inter-quartile range*  
LV - *left ventricle*  
LVDA - *left ventricular end diastolic area*  
LVEDP - *left ventricular end diastolic pressure*  
LVEF - *left ventricular ejection fraction*  
LUS - *lung ultrasound*  
MA - *Massachusetts*  
MCL - *midclavicular line*  
MLA - *machine learning algorithm*  
MRI - *magnetic resonance imaging*  
NNT - *number needed to treat*  
OR - *odds ratio*  
PA - *postero-anterior projection on chest x-ray*  
PAOP - *pulmonary artery occlusion pressure*  
PLAPS - *posterior and/or lateral alveolar and/or pleural syndrome*  
PNO - *pneumothorax*  
PE - *pleural effusion*  
PEEP - *positive end-expiratory pressure*  
PEmb - *pulmonary embolism*  
PERC - *pulmonary embolism rule-out criteria*  
PSV - *pressure support ventilation*  
PVR - *pulmonary vascular resistance*  
QB - *quiet breathing*  
REPE - *re-expansion pulmonary edema*  
ROC - *receiver operating characteristic*  
RR - *relative risk*



RTG - *radiographic*

RV - *right ventricle*

RVDA - *right ventricular end diastolic area*

SBT - *spontaneous breathing trial*

SOFA - *sequential organ failure assessment*

UK - *United Kingdom*

US - *ultrasound*

USA - *United States of America*

VAP - *ventilator associated pneumonia*

VS - *spontaneous sniffing*

VV-ECMO - *veno-venous extracorporeal membrane oxygenation*

# Contents

<b>1 Introduction</b> .....	<b>1</b>
<i>1.1 Chest imaging</i> .....	1
<i>1.2 Chest radiography</i> .....	3
<i>1.3 Computed tomography</i> .....	4
<i>1.4 Magnetic resonance</i> .....	5
<i>1.5 Basics of lung ultrasound</i> .....	5
1.5.1 How lung ultrasound works .....	5
1.5.2 Tools of the trade .....	6
1.5.3 Method of examination.....	7
1.5.4 Artefacts of LUS .....	8
1.5.5 Findings and signs at LUS.....	9
1.5.6 Reporting the findings .....	13
<i>1.6 Lung ultrasound in various clinical scenarios</i> .....	14
1.6.1 Pneumothorax.....	14
1.6.2 Pulmonary oedema .....	15
1.6.3 Pleural effusion .....	16
1.6.4 Consolidation of the lung.....	18
1.6.5 COVID-19 pneumonia and pulmonary embolism .....	21
1.6.6 Fluid loading/ extravascular lung water .....	27
1.6.7 Weaning failure .....	27
1.6.8 Proning.....	29
1.6.9 Ventilation apparatus assessment .....	30
<b>2 Aims and hypotheses</b> .....	<b>35</b>
<b>3 Investigations</b> .....	<b>37</b>
<i>3.1 Part 1: Studies evaluating CD positioning on CXR and LUS</i> .....	37
3.1.1 Study 1 - X-ray indices of chest drain malposition after insertion for drainage of pneumothorax in mechanically ventilated critically ill patients .....	37
3.1.2 Study 2 - Interpleural location of chest drain on ultrasound excludes pneumothorax and associates with a low degree of chest drain foreshortening on the antero-posterior chest x-ray .....	42
<i>3.2 Part 2 - Challenging the established method of quantifying pleural fluid volume on LUS in patients with consolidated lungs</i> .....	46
3.2.1 Study 3 - Pulmonary consolidation alters the ultrasound estimate of pleural fluid volume when considering chest drainage in patients on ECMO.....	46

3.3 Part 3 - <i>The impact of serial imaging with the growing popularity of LUS on the ICU outcome of patients with COVID-19 ARDS treated with ECMO</i> .....	50
3.3.1 Study 4 Prognostic Impact of Serial Imaging in Severe Acute Respiratory Distress Syndrome on the Extracorporeal Membrane Oxygenation .....	50
<b>4 Discussion</b> .....	<b>57</b>
<b>5 Conclusion</b> .....	<b>65</b>
<b>6 References</b> .....	<b>66</b>
<b>A Appendix</b> .....	<b>78</b>
<i>A.1 Publications included in this thesis</i> .....	78
<i>A.2 Publications on the topic not included in this thesis</i> .....	78

# 1 Introduction

## 1.1 Chest imaging

Chest imaging is pivotal in the diagnosis and management of patients with respiratory pathologies, especially in the intensive care unit (ICU). There are different imaging methods available for imaging the chest being: chest x-rays (CXR), lung ultrasound (LUS), computed tomography (CT) and magnetic resonance imaging (MRI).

The limitations brought on by the aforementioned methods with the exception of LUS, make LUS the go to method of assessing critically ill patients, and when paired with echocardiography, LUS is a force to be reckoned with, with diagnostic capabilities similar to CT.

LUS helps to evaluate the dynamics of pulmonary consolidation, pneumothoraces (PNOs), and pleural effusions (PEs) and is also excellent in guiding thoracentesis. This reduces serial mobilised bedside chest X-rays, and as thus, a reduction in unnecessary radiation exposure of patients (for reference, one non-contrast chest CT (effective dose of 8mSv) equals about 400 chest postero-anterior (PA) chest x-ray examinations and 1 chest x-ray has an effective dose of about 0.02mSv), and the side effects of contrast administration notably contrast induced nephropathy (CIN) and a potential allergic reaction to contrast media.

LUS has also been an incredible tool in the recent and ongoing COVID-19 pandemic whereby it is used for triage and in assessing COVID-19 pneumonia and its complications while reducing potential cross contamination of patients and staff caused by transport to and from the radiology department (Mokotedi et al., 2023).

The bedside CXR is particularly lackluster in diagnosing discrete pulmonary consolidations, small to moderate pleural effusions (PEs), pneumothoraces (PNOs) or eventually an alveolar interstitial syndrome (Engdahl et al., 1993; Bouhemad et al., 2007) due to technical complications that arise when a bedside CXR is performed. The spatial resolution of the CXR is compromised by the fact that the patient can't do a breath hold, as thus, there is movement of the thorax, furthermore, due to film cassette positioning (between the bed and the patient) the x-ray beam is shortened because of shorter acquisition distance. This leads

to suboptimal images that can be particularly challenging to interpret accurately. (Bouhemad et al., 2007)

In critically ill patients who are closely monitored by various invasive devices, CT scanning is not only cumbersome, transporting these patients to the CT suite and positioning of such patients in the gantry is a task in itself, with the potential for significant respiratory and haemodynamic derangements (Peris et al., 2010). In the morbidly obese patients, CT scanning is not possible to obtain as the table itself has a weight limit and the gantry itself is only so big. Another important factor is the potential for contrast induced nephropathy, which further complicates care of the already critically patient, as is a potential allergic reaction to contrast, if unknown. Furthermore, unless ICU related complications arise, or in cases where CT scanning is imperative, substituting CT imaging by CXR, LUS in combination with echocardiography confers a financial benefit (Balik et al., 2023).

This is where, in particular, LUS shines- it can be performed at the bedside when needed and waiting for a radiology report is eliminated as clinical information is acquired in a matter of a few seconds if not minutes. LUS as a portable mobile imaging tool does not have a steep learning curve in contrast to echocardiography and other imaging modalities; however, the combination of LUS coupled with echocardiography is extremely valuable not only in the evaluation of lung pathology, but also in the evaluation of hemodynamics of a patient.

For many years, LUS has been considered impossible and not feasible due to the very nature of the lungs being air-containing organs; radiologists know how much air, for example, in the bowels, can be a hindrance in evaluating the underlying organs. The fact that air in the lungs creates specific artefacts is the very backbone on which LUS operates to tell a story.

For our dissertation work we evaluated chest drain (CD) positioning on CXR using several simple parameters (CD inclination, tortuosity of the CD and its foreshortening) and we further sought to locate a CD on lung ultrasound post drainage. These investigations into CD positioning help in the diagnosis of CD malposition which can potentially lead to residual/occult pneumothoraces which further can have dire implications in mechanically ventilated patients. We also challenged the established method of quantifying pleural fluid volume (PEv) on lung ultrasound wherein this method could give erroneous pleural fluid

estimates in patients with consolidated lungs and lastly, we sought the impact of serial imaging with the growing popularity of lung ultrasound on the intensive care unit outcome of patients with COVID-19 acute respiratory distress syndrome (ARDS) treated with extracorporeal membrane oxygenation (ECMO).

The following sections will look briefly at the aforementioned methods and extensively at LUS.

## **1.2 Chest radiography**

Over 30 years ago, early digital imaging systems known as ‘computed radiography’ utilized a photostimulable phosphor image receptor plate. Some departments still use CR systems due to their compatibility with conventional radiography equipment, but they have largely been replaced by direct radiography (DR) systems. DR systems employ methods for converting x-ray photons into electrical charges to generate an electrical signal that can be read directly. Direct conversion is achieved through photoconductors within flat panel detectors, such as amorphous selenium, or using a selenium drum (Adam et al., 2021).

Indirect conversion uses a scintillator associated with either a charge-coupled device or FPD and commonly relies on thallium-doped caesium iodide-based or gadolinium-based compounds in the case of more recent developments. Indirectly converted images offer many advantages over conventional film-screen radiography, including wider latitude which decreases error and repeat examination rates, reusable detectors, integration with picture archiving and communication system (PACS) capabilities, and superior image quality, especially in the case of DR configurations (Adam et al., 2021).

### **1.2.1 Portable radiography**

When patients cannot be easily or safely mobilised, portable anteroposterior radiographs are obtained to monitor patient cardiopulmonary status, assess the position of monitoring and life support tubes, lines and catheters, as well as detect complications related to their use (Klein et al., 2019).

There are technical challenges with portable bedside radiography due to inherent physiological changes. Portable units require longer exposures to penetrate cardiomeastinal structures due to their maximal kilovoltage potential. Critically ill patients also pose difficulties in positioning for these radiographs, leading to possible inaccuracies in directing the x-ray beam perpendicular to the patient resulting in distorted images. Additionally, there is magnification of intrathoracic structures due to the short focus-to-film distance and the AP technique used, which brings about physiological implications such as an increase in cardiac diameter on an AP radiograph by 15% to 20%. This makes interpretation challenging, where normal values differ from other types of radiographs (Klein et al., 2019; Schaefer-Prokop, 2011).

Physiologically, patients who are supine can elevate the diaphragm leading to compression of the lower lobes and decreased lung volumes, making the assessment difficult, especially when determining pulmonary venous hypertension or detection. Physiological widening of the vascular pedicle is caused by increased systemic return to the heart in supine patients and therefore pathological changes can be difficult to delineate. The gravitational layering effect of a fluidothorax further compounds this challenge by hiding free-flowing fluid within the upper mediastinum. Since a PNO rises to the non-dependent regions of the thorax, identifying it on these radiographs may be difficult (Klein et al., 2019; Schaefer-Prokop, 2011).

### **1.3 Computed tomography**

The basic principles underlying CT imaging remain largely unchanged since its introduction by Sir Godfrey Hounsfield; it involves an x-ray source emitting a fan beam, a rotating gantry housing this source, along with a ring containing a detector array located opposite to the x-ray source, which captures signals emitted from passing through patients' bodies. This data is then reconstructed into an anatomical image using a computer processing system utilising three-dimensional (3D) pixels known as voxels displayed on differing densities emphasising scanned volumes. Depending on the requirements, thicker/thinner slices can be further reconstructed by computers after scanning is finished (Adam et al., 2021).

Several methods are available for obtaining chest CT scans. The most common approach is the spiral mode, where the patient continuously moves through the CT scan table while

images are acquired, resulting in a single large-volume scan. Most CT scanners utilise a multi-detector array with 256 to 320 detectors that provide thin sections of the entire lung in one breath hold acquisition. Scans can be done with or without contrast administration depending on the clinical question at hand (Klein et al., 2019).

The main benefits of CT scanning include its exceptional contrast resolution and cross-sectional display format, which enables clear visualisation of thoracic structures due to lack of superimposition. This high contrast resolution allows differentiation between metal, air, calcium/bone, soft tissue, fluid, and fat content within the body (Klein et al., 2019).

## **1.4 Magnetic resonance**

The application of MRI in thoracic imaging is gradually increasing, evolving from a tool for problem-solving and research on chest wall and mediastinal issues to regular clinical practice. MRI offers excellent soft tissue contrast and avoids ionising radiation, but historically, its use in lung imaging has been hampered by factors such as a low signal-to-noise ratio due to the lack of protons in lung tissue, breathing-related motion artefacts worsened by long scan times, and very short T2\* decay times caused by the diverse magnetic properties of the pulmonary interfaces. Ultrashort and zero echo-time pulse sequences are not yet commonly used in clinical practice. They use readout gradients immediately after or during the radiofrequency pulse, combined with radial k-space mapping. This allows tissues with very short T2\* decay, like the lung parenchyma, to produce detectable signals. However, these techniques are still not as effective as CT for evaluating pulmonary parenchymal lesions structurally (Adam et al., 2021).

## **1.5 Basics of lung ultrasound**

### **1.5.1 How lung ultrasound works**

The transmission of ultrasound rays is disrupted by bones and air; therefore, a normally aerated lung does not transmit ultrasound rays; instead, only the pleural line is visible on ultrasound. As such, LUS is restricted to examination of lesions in the pleura and subpleura through intercostal spaces. The pleura produces artefacts during ultrasonography because



the air in the lung has a different acoustic impedance than the superficial structures (Lê et al., 2022).

The primary goal of LUS is to identify a pleural shift by identifying the pleural line and lung sliding, which entails visualising the parietal pleura's horizontal back and forth movement underneath the two visualized consecutive ribs in B-mode (dynamic mode). A thin, echogenic line that extends only deep to the intercostal muscle between the ribs is known as the pleural line and is visually seen on ultrasound- this visualisation of the two ribs with a pleural line in between is known as the bat sign (the ribs form the “wings” of the bat). A typical pleural line is between 0.2 and 0.3 mm in width. The M-mode enables a more accurate assessment of lung sliding at the same spot, and on ultrasound it is seen as the seashore sign (Lê et al., 2022).

### **1.5.2 Tools of the trade**

The three standard ultrasound probes can all be used to perform LUS (**Figure 1**), the choice of which is dependent on the biometrics of the patient and/or the potential pathology being examined.

The convex probe, albeit having the lowest frequency (3-5 Hz), has the largest footprint, enabling the visualisation of deeper structures due to deeper penetrance and can visualise both superficial and deep pathologies. The linear probe has a smaller footprint but has a higher frequency (8-12 Hz) and enables for the visualisation and assessment of superficial structures due to its better superficial penetrance, it is thus better for examining superficial pleural pathologies like a PNO. The last probe available, the phased array, has the smallest footprint and is typically used for echocardiography, and has a similar frequency to the convex probe and can be used to examine deeply located pathologies, e.g., PEs and/consolidations (Lê et al., 2022; Bouhemad et al., 2015).



**Figure 1** - Ultrasound probes: On the left is a linear probe, the middle is a curvilinear probe, and the phased array is on the right.

### **1.5.3 Method of examination**

A standardised protocol should be utilised to carefully evaluate each hemithorax. By using the anterior and posterior axillary lines as anatomical landmarks, three regions (anterior, lateral and posterior) can be identified for each hemithorax. Each area is divided into two areas: an upper area and a lower area. In a given region of interest, the lung surface of all adjacent intercostal spaces should be carefully examined. Rotating the patient slightly to the contralateral side allows for a more detailed examination of the posterior area (right up to the spine). Assessing the upper posterior region can be difficult because the scapula (bone) can create a blind spot (Bouhemad et al., 2015).

Lichtenstein (Lichtenstein, 2014, 2015; Lichtenstein & Mezière, 2008b) initially proposed a simpler method of examining each hemithorax, calling each area examined a bedside lung ultrasound in emergency (BLUE) point. The examiner places each hand on the patient's hemithorax, one placed below the other, therefore identifying the location of the lung. The upper hand's margin lies along the clavicle, and the lower margin of the lower hand identifies the diaphragm. The upper BLUE point is a region in the middle of the upper palm, and the lower BLUE point is located by the lower palm. Furthermore, the Posterior and/or Lateral Alveolar and/or Pleural Syndrome (PLAPS) point is an area where the horizontal line at the

level of the lower BLUE-point and a vertical line at the posterior axillary line cross. Therefore, by this technique, 3 points per hemithorax are identified (**Figure 2**).

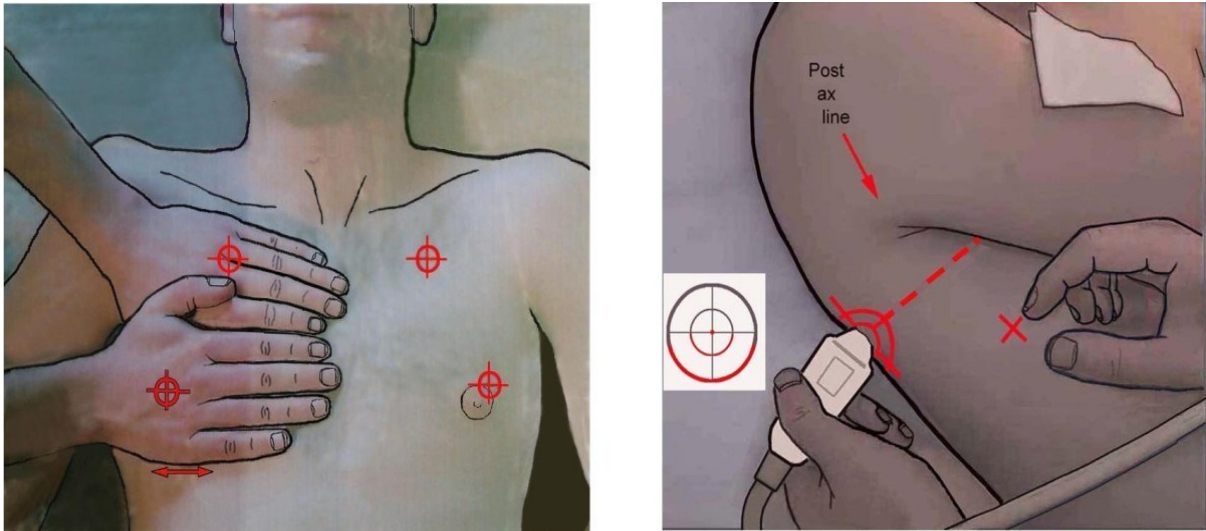


**Figure 2** - BLUE points. Image from (Lichtenstein, 2014).

#### 1.5.4 Artefacts of LUS

The A lines and B lines seen on LUS are reverberation artefacts representing reflections of the pleura at regular intervals. The A lines represent the horizontal hyperechoic lines between 2 ribs and are seen in a normally aerated lung- they are a reflection of the hyperechoic pleural line. The B lines represent vertical hyperechoic lines, known as lung comet tail artefacts; these lines always arise from the pleura and move in concert with the lung during breathing and are caused by the thickening of the pulmonary interstitium caused by various pathologies. In normal lungs, solitary B lines (fewer than two per intercostal space) may be present. The density and appearance of B lines directly correlate to disease severity and can be used to calculate the degree of lung alveolo-interstitial syndrome and lung consolidation (**Figure 3, Figure 4**) (Bouhemad et al., 2015).

Lung score	Description	Classic interpretation on LUS	Modified interpretation on LUS
Score 0	Normal aeration	A lines, 2 B-lines maximum	A lines, 2 B-lines maximum
Score 1	Moderate loss of aeration	≥ 3 well-spaced B lines	Involvement of the pleura < 50%
Score 2	Severe loss of aeration	Coalescent B lines	Involvement of the pleura > 50%
Score 3	Complete loss of aeration	Tissue- like pattern	Tissue- like pattern

**Figure 3** - The lung score, adapted from (Mongodi et al., 2017). Pleural involvement is described as subpleural consolidations or B- lines (singular or coalescent). Tissue like pattern = consolidation.

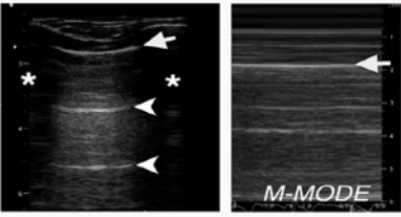
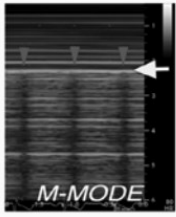
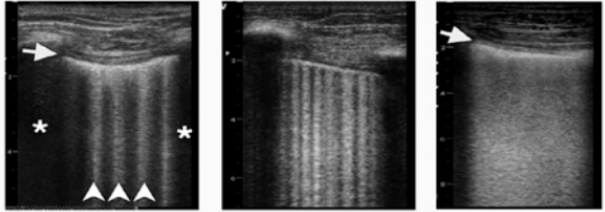
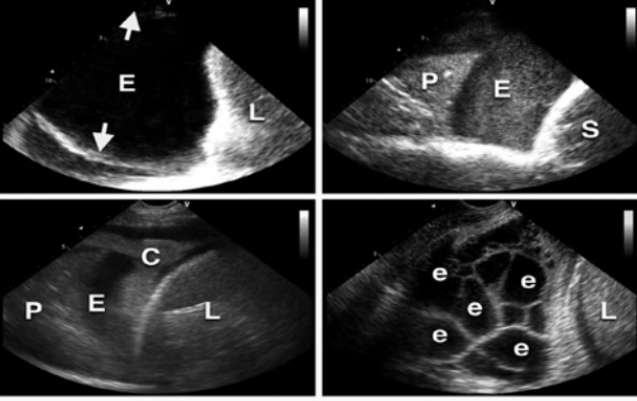
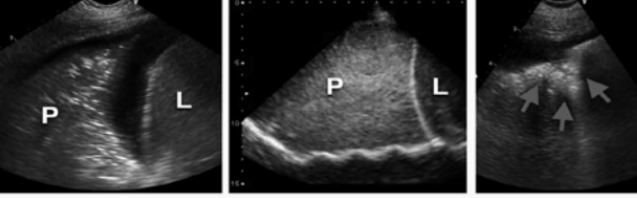
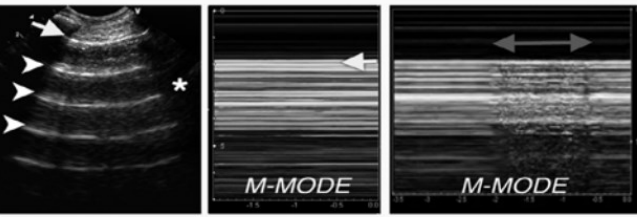
### 1.5.5 Findings and signs at LUS

**Lung sliding** is the movement of the pleural line synchronised with tidal ventilation, which indicates that both visceral and parietal pleura are in contact, and that regional ventilation is intact. **The seashore sign** consists of straight lines above the pleural line and a sandy pattern below it when visualised in M-mode, confirming lung sliding. On the other hand, the **stratosphere sign** shows straight horizontal lines both above and beneath the pleural line in M-mode, indicating the absence of pleural line movement seen in conditions such as a PNO (Figure 4) emphysematous bullae, severe hyperinflation, and pleural adhesions. **The lung pulse** (Figure 4) is recognised in the absence of lung sliding and refers to movement of the hyperechoic pleura synchronous with cardiac rhythm; it can indicate impaired regional ventilation. Meanwhile, the **lung point** represents where the collapsed lung meets a PNO (Rocca et al., 2023).

What we see in cases involving consolidations and effusions: **The shred sign** represents a subpleural echo-poor area bordered by irregular borders indicative of a superficial small consolidation. **A tissue-like pattern** reveals a homogeneous texture similar to abdominal

parenchyma (i.e. liver-like tissue) which corresponds to complete loss of aeration within a lobe. *An air bronchogram* consists of a hyperechoic intraparenchymal structure seen within tissue-like patterns representing trapped air within consolidations (**Figure 4**). *PE* (**Figure 4**) appears as a hypoechoic or anechoic area between pleural layers which settles in the dependent area of the chest. The character of its echogenicity differentiates between transudative (homogeneously anechoic) from exudative types (anechoic or homogeneously echogenic with internal particles, or even septation) (Rocca et al., 2023).

These findings obtained from the LUS examination can be further interpreted in a stepwise manner as in (**Figure 5**). Furthermore, in patients with acute respiratory failure, the BLUE protocol can be used; it also incorporates vascular assessment (duplex ultrasound) of the lower extremities to rule out the source of potential pulmonary embolisation (PE) (**Figure 6**). The final results can then be reported in a fashion similar to (**Figure 8**).

<p><b>A</b></p> 	<p><b>B</b></p> 	<p><b>NORMAL ("A-Pattern") (1A)</b></p> <p>2-D/M-Mode anterior scans. <b>Pleural line</b> (arrow) + <b>A lines</b> (arrowheads) + <b>Lung sliding</b> ("sandy" appearance of M-Mode pattern beneath pleural line = "seashore sign")</p> <p><b>Lung Pulse (1B)</b></p> <p>In absence of ventilation pleural sliding is substituted by heart-beat synced pleural motion (rhythmic changes in M-Mode artifacts beyond pleural line, arrowheads)</p>
<p><b>C</b></p> 		<p><b>Sonographic INTERSTITIAL SYNDROME ("B-Pattern")</b></p> <p>2-D anterior scans. Multiple (&gt;3 / intercostal space) <b>B-lines</b> (left panel, arrowheads) originate from pleural line (arrow), and substitute A-lines. B-lines can be well-spaced (left), crowded (mid) or coalescent (right panel) ("white lung" pattern). Note pleural line thickening in left &amp; right panels (arrows)</p>
<p><b>D</b></p> 		<p><b>PLEURAL EFFUSION</b></p> <p>2-D longitudinal scans at the posterior axillary line; diaphragm appears as bright curvilinear boundary on the left of liver (L) or spleen (S). <b>Transudative effusion</b> (E) appears as anechoic space between the pleuras (left upper panel, arrows). <b>Complex exudative effusion</b> (E) with particulated internal echoes (right upper panel, empyema) and consolidated lung (P) inside. <b>Complex hemorrhagic effusion</b> (E) with free-floating clot (C) and consolidated lung (P) inside (left lower panel). <b>Complex septated effusion</b> with multiple loculated collections (e) separated by septa (right lower panel)</p>
<p><b>E</b></p> 		<p><b>CONSOLIDATION</b></p> <p>2-D longitudinal scans at the posterior axillary line (left and mid panels). Tissue-like echotexture of the lung (P), similar to the liver (L). Presence in it of white dots/lines, reinforced at inspiration ("dynamic bronchograms", suggests a patent airway (left); their <b>absence</b> equates to atelectasis (mid). Small subpleural consolidation (right panel, arrows)</p>
<p><b>F</b></p> 		<p><b>PNEUMOTHORAX ("A-Pattern")</b></p> <p>2-D parasternal scan (left panel) shows pleural line (arrow) and A-lines (arrowheads). M-Mode investigation (mid panel) indicates <b>sliding abolition</b>, representing the artifacts as parallel straight lines ("stratosphere sign") beneath the pleural line (arrow). At a more lateral point, M-Mode depicts inspiratory reappearance of sliding as transient (double-headed arrow) seashore sign ("<b>lung point</b>")</p>

**Figure 4** - Example of findings at LUS. Image from (Via et al., 2012). 1A = the normal A pattern, 1B = lung pulse, C = sonographic interstitial syndrome (B pattern), D = pleural effusion, E = consolidation, F = pneumothorax.

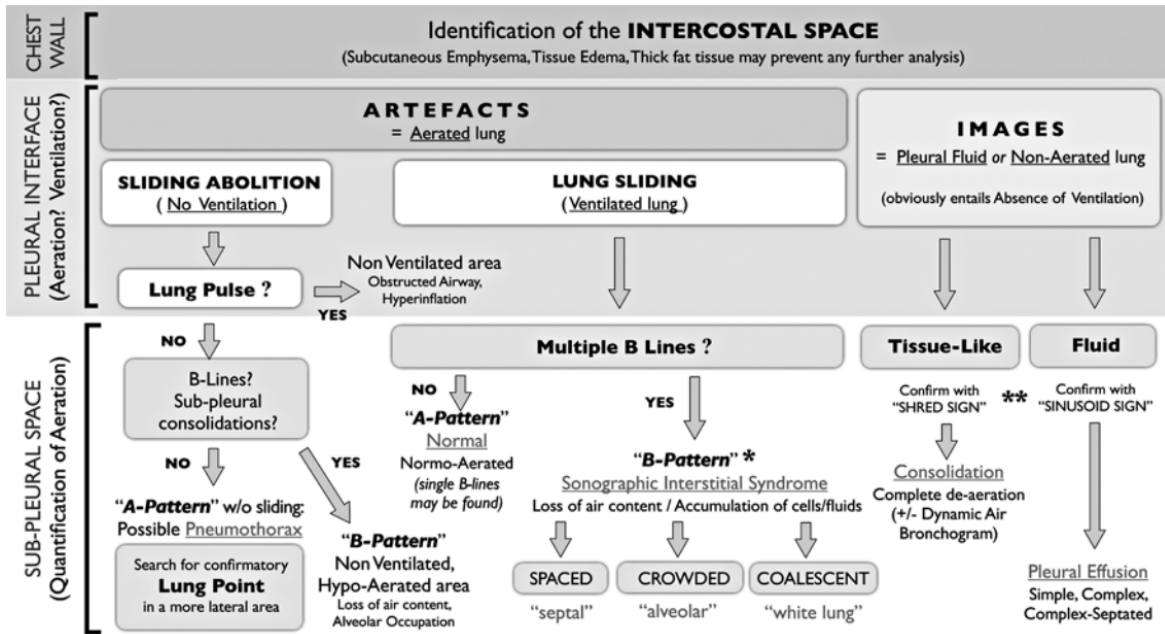


**Figure 5** - Flow chart showing interpretation of LUS findings in a single scan field at three levels (the chest wall, pleural interface, and subpleural space). Image from (Via et al., 2012).

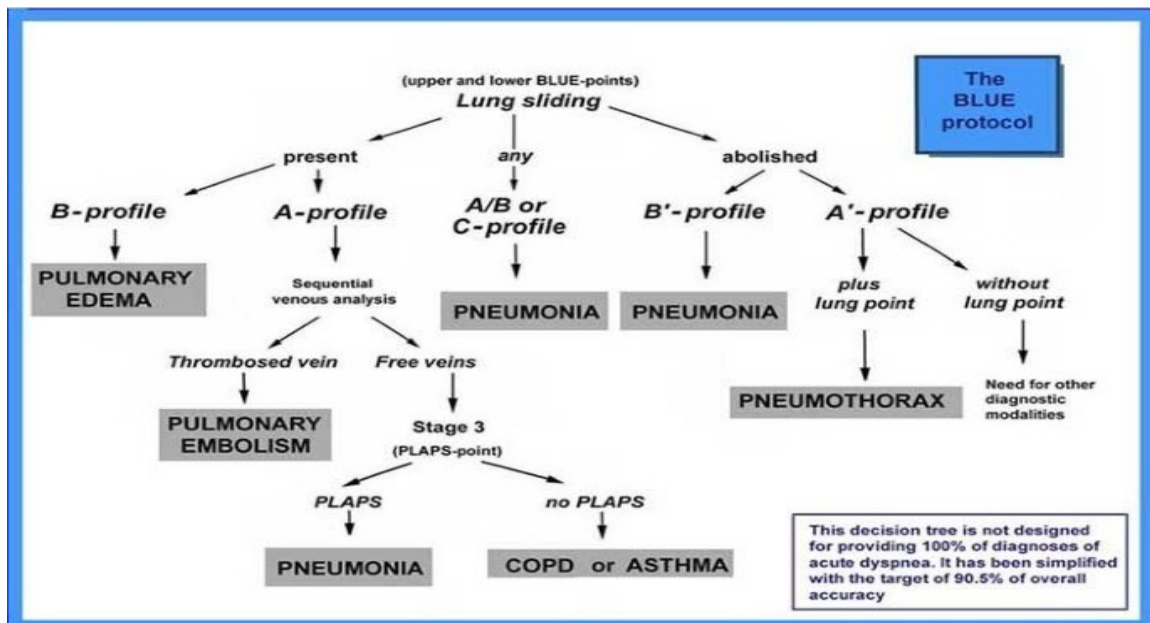


**Figure 6** - BLUE protocol flow diagram. A profile = normal pattern, A' = A profile with lung comets and abolished lung sliding, B profile = anterior lung sliding with lung comets, B' = B profile with abolished lung sliding, C profile = anterior lung consolidation. Image from (Lichtenstein, 2014).

In patients with shock (i.e., obstructive, distributive, cardiogenic, or hypovolemic), the fluid administration limited by lung sonography (FALLS) protocol is recommended and incorporates LUS with the concomitant use of echocardiography (Figure 7).

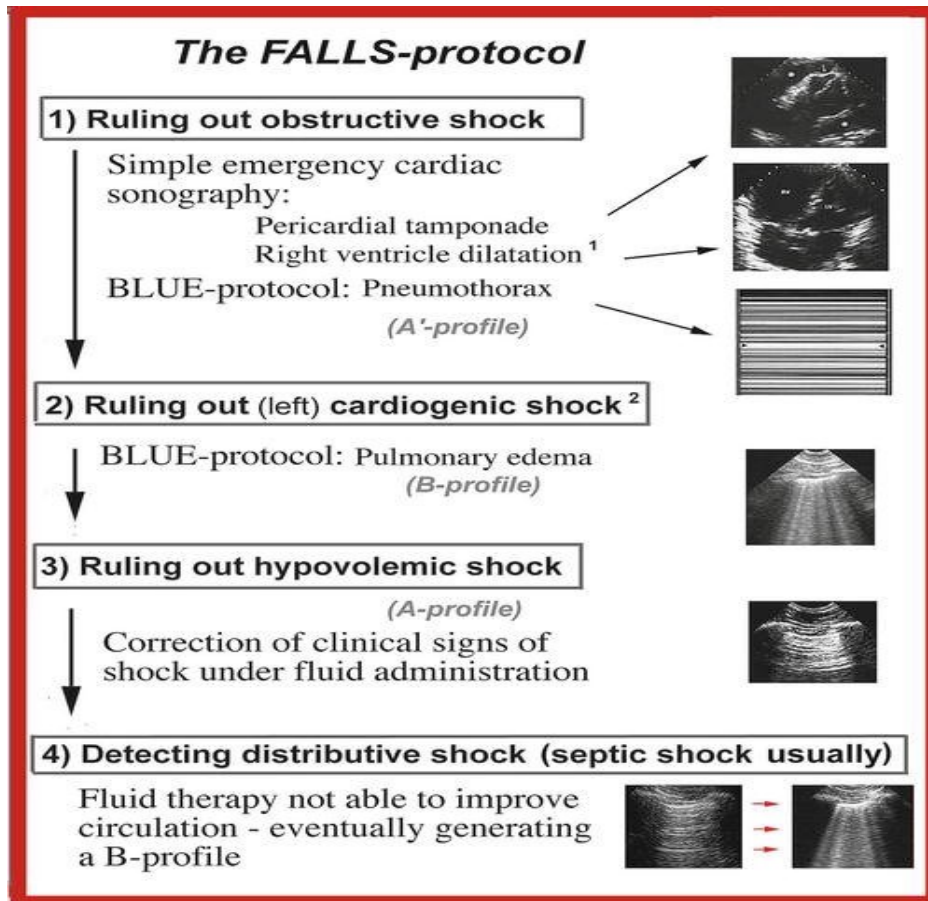


**Figure 7** - The FALLS protocol. A profile = normal pattern, A' = A profile with lung comets and abolished lung sliding, B profile = anterior lung sliding with lung comets. Image from (Lichtenstein, 2014).

### 1.5.6 Reporting the findings

This report template (Figure 8) allows for rapid reporting of diagnostic, screening, monitoring, and procedure-guidance LUS examinations. Visual representation of different regions explored (6 per hemithorax) and a number-coded rating of findings provide instantaneous interpretation of the general lung ultrasound examination. Calculation of a



LUS score allows semi-quantitative analysis of the state of aeration of the entire lung. An additional free-text description and presumptive diagnosis complete the report. For improved interpretation of the examination, detailed patient history, clinical conditions, and ventilation are reported (Via et al., 2012).

<span style="font-size: 24px; font-weight: bold; margin: 0 10px;">LUNG ULTRASOUND</span>	
Report Form	
PATIENT NAME: ..... GENDER: <input type="checkbox"/> M <input type="checkbox"/> F DATE OF BIRTH: ..... OPERATOR: ..... EXAM DATE: ..... HOUR ..... STORAGE CODE ..... HISTORY: ..... ..... SPONT VENTILATION: RR = ..... Resp Distress: <input type="checkbox"/> Yes <input type="checkbox"/> No DECUBITUS: <input type="checkbox"/> Sup <input type="checkbox"/> Lat <input type="checkbox"/> Pron <input type="checkbox"/> Semirec MECH VENTILATION: a) Modality: <input type="checkbox"/> PCV <input type="checkbox"/> DuoPAP <input type="checkbox"/> ASV <input type="checkbox"/> PSV <input type="checkbox"/> SIMV <input type="checkbox"/> NIV <input type="checkbox"/> CPAP b) Settings/Pattern: PEEP/Ps = ..... /..... Ppeak ..... Pplat ..... RR ..... I:E ..... VT ..... EGAVEAB: pH ..... pCO2 ..... HCO3- ..... BE ..... PO2 ..... P/F ..... SpO2% ..... Hb .....	
INDICATION: <input type="checkbox"/> DIAGNOSTIC <input type="checkbox"/> SCREENING <input type="checkbox"/> MONITORING <input type="checkbox"/> PROCEDURAL GUIDANCE TYPE OF EXAM: <input type="checkbox"/> simplified <input type="checkbox"/> comprehensive <input type="checkbox"/> focused (ANT / POST)	
<div style="display: flex; justify-content: space-around;"> <div style="text-align: center;"> <p><b>R</b></p> <p>ANT</p> </div> <div style="text-align: center;"> <p><b>L</b></p> <p>ANT</p> </div> </div>	<div style="display: flex; justify-content: space-around;"> <div style="text-align: center;"> <p><b>R</b></p> <p>LAT</p> </div> <div style="text-align: center;"> <p><b>L</b></p> <p>LAT</p> </div> </div>
LUS Score = _____	
<b>Legenda:</b> 0 = A-Pattern (or nearly normal); 1 = B-Pattern (B-lines >3/field, well spaced); 2 = B-Pattern (crowded, coalescent +/- subpleural consolidations) 3 = Consolidation* E= Effusion*; Pn = Pneumothorax**; NS= Sliding Abolition; LP=Lung Pulse *(3 and E: characterize below in description) **(indicate Lung Point(s) )	
DESCRIPTION ..... ..... .....	
DIAGNOSIS ..... <input type="checkbox"/> Suspected <input type="checkbox"/> Not made <input type="checkbox"/> Second Opinion needed	
----- Signature	

**Figure 8** - A sample report form to report the findings at LUS. Image from (Via et al., 2012).

## 1.6 Lung ultrasound in various clinical scenarios

### 1.6.1 Pneumothorax

In supine patients with a pneumothorax (PNO), air rises to the anterior aspect of the hemithorax and also accumulates in the basal areas, therefore detection by chest x-ray can be evasive, unless if the PNO is very large and the lung itself is compliant to the compressive

mechanism of the PNO. On supine CXR if the PNO is not seen, one has to rely on other indirect signs that may allude to the presence of PNO, for example, the deep sulcus sign, an area with absent bronchovascular markings, a well demarcated border of the heart shadow/vascular structures/mediastinum/diaphragm, double diaphragm sign, and a rounded area that is darker than the surrounding lung (Schaefer-Prokop, 2011). With this in mind, LUS can be an excellent substitute to serial CXR imaging to diagnose and evaluate the dynamics even after drainage of PNOs.

The diagnosis of a PNO depends on the presence of a lung point, the absence of B- lines, lung sliding, lung pulse and the visualisation of the stratosphere sign on M-mode (Volpicelli, 2011; Lichtenstein, 2017). Most often than not, supine patients in ICU tend to have an underestimation of occult PNOs and/or residual PNOs after drainage- LUS has an accuracy on par with the gold standard CT in the detection and evaluation of occult/residual pneumothoraces and their extension (Silveri et al., 2008). This is important because when the patient's lungs are subjected to high ventilatory pressures and volumes, there is a potential for barotrauma, volutrauma, and biotrauma (Ball et al., 2003). Therefore, even a small occult or residual PNO has the potential to enlarge on intermittent positive pressure ventilation (IPPV), and it is imperative that it is observed/diagnosed to help guide therapy. The influence of PNOs on pulmonary mechanics may be a subject of further research as a large PNO creates a V/P mismatch and shunt formation. In the ventilated patient, increases in peak and plateau pressures may indicate the likelihood of a PNO.

With the drainage of a PNO, the presence of a chest drain (CD) under the anterior chest wall on LUS excludes a PNO (Maly et al., 2022) however, not rarely, CD migration can be encountered. The migration of a CD observed on CXR can be an indicator of suboptimal drainage of a PNO, and thus the detection of CD foreshortening in CXR can be used to predict a possible residual PNO that is occult in CXR and warrants further evaluation by LUS for its presence/absence (Mokotedi & Balik, 2018; Maly et al., 2022).

### **1.6.2 Pulmonary oedema**

On LUS, multiple B lines that are 7 mm apart have been shown to be caused by interlobular septal thickening, a characteristic of interstitial oedema. In contrast, B lines that are spaced

3 mm or less apart are caused by ground-glass areas which are characteristic of alveolar edema (Bouhemad et al., 2007).

Maw et al. (Maw et al., 2019) found that LUS is more sensitive in the diagnosis of pulmonary oedema than CXR in a pooled estimate, while the two methods revealed the same specificity (LUS sensitivity 0.88 (95% CI, 0.75-0.95) and 0.90 (95% CI, 0.88-0.92) for specificity. In contrast, the sensitivity of CXR was 0.73 (95% CI, 0.70-0.76) and the specificity was 0.90 (95% CI, 0.75-0.97) – this is an absolute difference of 15%.

### **1.6.3 Pleural effusion**

An area where LUS shines exceptionally is in the assessment of pleural effusions (PE). When large, PEs cause a restrictive syndrome by compression of the lung parenchyma, as thus thoracentesis has a positive effect on arterial oxygenation and therefore shortens the duration of mechanical ventilation (Goligher et al., 2011; Remérand et al., 2010). Therefore, in critical care, there is a potential for quantitative assessment of lung re-aeration using LUS after therapy to gauge lung recruitment by positive end expiratory pressure (PEEP) or a recruitment manoeuvre (Bouhemad et al., 2007).

With computed tomography, a PE can be assessed by measuring its Hounsfield units with the potential (to some degree), to differentiate whether the PE is a haemothorax, a transudate, or an exudate. Unfortunately, with this modality, the presence of septations can be elusive to assess, if not impossible. In patients with signs of a PE on CXR and CT, it is important to assess the affected hemithorax by ultrasound to rule out any septations as this has an impact on the success of a thoracentesis as their presence will often necessitate a thoracotomy with eventual resection and decortication of these pleural septations (Esmadi et al., 2013).

CT can also be used to quantify the PE, but that is a tedious process that needs one to trace the outer edges of the PE itself per few slices so as to calculate the volume (Remérand et al., 2010). This is overcome by the ability to quantify the PE by LUS at the bedside. There are a few equations put forth to help quantify PE (Remérand et al., 2010; Balik et al., 2006; Ibitoye et al., 2018; Roch et al., 2005.). The most commonly used method of quantification (and the

least complicated) used is by Balík (Balík et al., 2006) based on interpleural separation (the maximum distance between the visceral and parietal pleura (separation)), and they ended up with a simple equation: **Volume (ml) = 20 x separation (mm)**. In mechanically ventilated critically ill patients, the greatest interpleural distance is seen in expirium, and in spontaneously ventilating patients the greatest separation is seen in inspirium; that is why it is imperative to work with the type of patient you have so as to accurately assess the separation.

However, as a downside, this quantification does not take into consideration a circumferential PE due to large pulmonary consolidations or atelectases, or eventually fluid that has tracked into the pulmonary fissures; the scapula being a bone also interferes with the assessment of cranially located PEs by casting a shadow which ends up obscuring the 1<sup>st</sup> intercostal space (Remérand et al., 2010).

In large PEs (>1000ml), pulmonary effusion volume (PEv) can be underestimated due to lower lobe consolidation owing to passive/compressive atelectasis, and this consolidation, by virtue of its weight (collapsed lung is heavier than aerated lung), then displaces the effusion (think of putting an orange in a bowl of water). In patients with heavily consolidated lungs (e.g. grade 3 according to LUS) detected by the visualisation of liver-like tissue on LUS with or without a bronchogram (a dynamic bronchogram indicates airway patency, whilst the absence of a bronchogram indicates an atelectasis) and the absence of B- lines; therefore a better estimation of PEv put forth in such patients is thus **V (ml) = 540 + 17 x lateral separation (mm)** (Balík et al., 2022).

Seeing as that there is no agreeable standard on what constitutes as a mild, moderate, or large PE, there may be consequences to draining large PEs (usually >1000ml), in patients with concomitant heart failure, i.e., where the left ventricle (LV) is overloaded with increased left ventricular end-diastolic pressure (LVEDP) ascertained by echocardiography. There is a potential for re-expansion pulmonary oedema (RE-PE) (purportedly a rare occurrence in literature) due to heart- lung interactions when introducing pleural drainage, meaning, a heart that is used to functioning at higher pressures than normal is inadvertently adapted to the increased pleural pressure caused by the coexisting PE. In the ICU, patients who are on mechanical ventilation may experience higher pressures generated in inspirium, therefore,

the impact of pleural fluid drainage on the LV pressure could be mitigated due to higher mean airway and plateau pressures.

When, for example, drainage of a PE leads to a decrease in pleural pressure, there is a parallel increase in left ventricular transmural pressure (to cope with the decreasing pleural pressure), which inadvertently causes an increased afterload of the LV which can furthermore cause LV failure and a subsequent pulmonary oedema. This is why, in particular, the evaluation of cardiac function is important before pleural drainage to aid in estimating the likelihood of whether (or not) draining a large PE may potentially result in a RE-PE (Mokotedi & Balik, 2017) (**Figure 9**). In the same breath, this same narrative can be expected in the drainage of large pneumothoraces, as the mechanisms and changes in intrathoracic pressure are similar. RE-PE on LUS will invariably be seen as the presence of a B- profile.

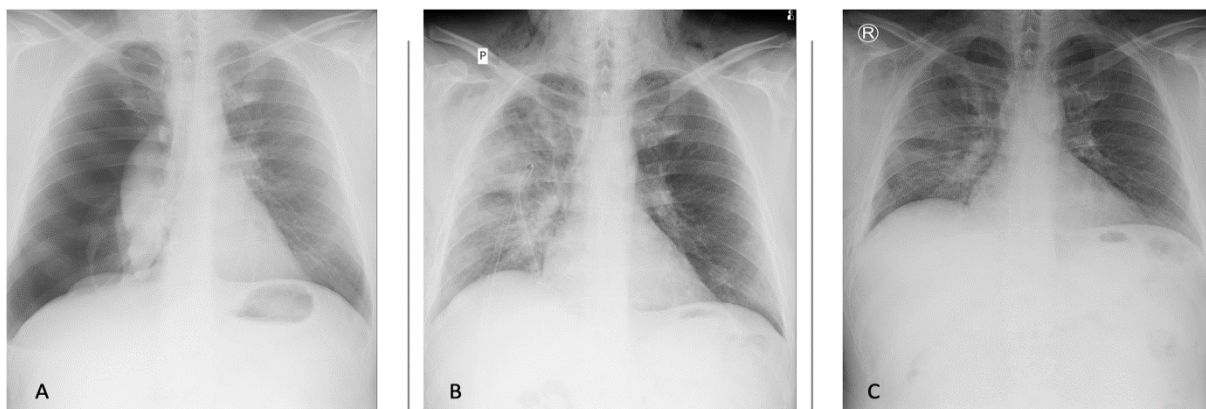


**Figure 9** - Development of a RE-PE (B) after drainage of a large right sided PNO (A) and its resolution (C) seen on CXR.

Image reproduced with permission from the archives of the Department of Diagnostic Radiology, Faculty Hospital Bulovka, Prague, Czech Republic.

#### 1.6.4 Consolidation of the lung

Bedside LUS as a dynamic examination also helps in differentiating whether a lung consolidation seen on CXR or CT is probably a pneumonia or a resorptive atelectasis. To do this on LUS, it is imperative to identify an air bronchogram and evaluate whether it is dynamic or not- this feature is believed to be due to the presence of air in the airways and,

therefore, indicating their patency- hence why it is seen in pneumonia and not as much in resorptive atelectasis, with a 97% positive predictive value and 94% specificity (Lichtenstein et al., 2009), and this is important because then a bronchoscopy is acutely not needed to look for an obstruction.

The use of the clinical pulmonary score (CPIS) has been used to diagnose ventilator-associated pneumonia (VAP) in a ventilated patient. However, due to its low specificity and sensitivity, the use of LUS has been incorporated into the diagnostic workup to differentiate from the colonization of the lower airways and the infiltration of lung parenchyma, where classic LUS signs of an infectious consolidation (pneumonia) are seen with the picture of a dynamic bronchogram, and together with the quantitative analysis of microbiology from a tracheal aspirate or bronchoscopy. The CPIS has been delegated for its modified counterpart, the chest echography and procalcitonin pulmonary infection score (CEPPIS), which further incorporates the evaluation of procalcitonin (Bouhemad et al., 2018).

Not only does LUS aid in diagnosing VAP, but it helps in tracking progress or resolution of the pneumonia after initiation of treatment (**Figure 10**). For example, complicated effusions with septations can be easily identified on ultrasound, whereas abscess formation is seen on LUS (as is the case elsewhere in the body) as a demarcated hypoechoic area which can be further drained under US guidance. Cavity formation in a consolidation/pneumonia is seen as a hypoechogenic area with hyperechogenic particles that are non-dependent and are created by the lung tissue/gas interface (Bouhemad et al., 2007). LUS goes on further to facilitate drainage of these aforementioned complications (**Figure 11**).

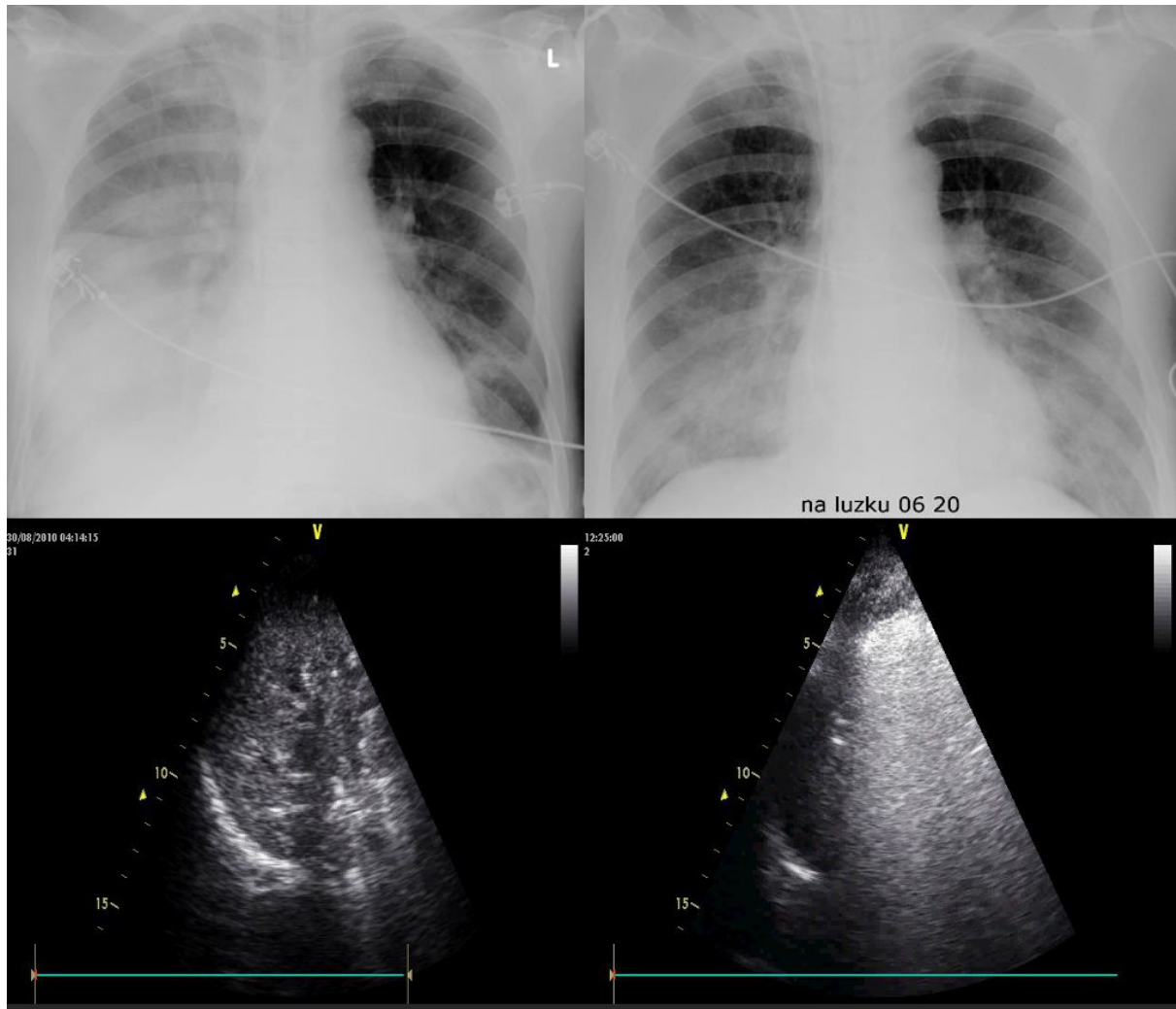


**Figure 10** - Evolution of a unilateral consolidation of the right lung; the upper panels show depiction at CXR and the lower panels on LUS. These changes from right to left on both panels were seen within 36 hours after initiation of treatment.

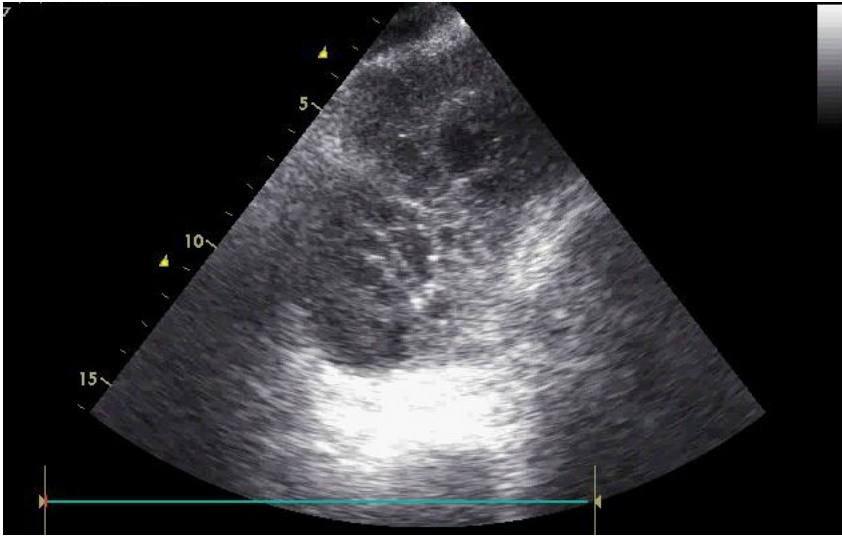


**Figure 11** - Ultrasound depiction of a pulmonary empyema. The septations are largely appreciated on ultrasound than on other imaging modalities.

### 1.6.5 COVID-19 pneumonia and pulmonary embolism

In this current climate of the worldwide pandemic due to COVID-19, there has been a greater need for accessible and safer means of imaging, and in this sense LUS can be extremely useful (as it was during the H1N1 pandemic) to evaluate patients at the bedside for the evolution (either the progression or regression) and the efficacy of any treatment initiated for COVID-19 pneumonia and can confer an easier and dynamic method of assessment, as an ultrasound machine is widely available in specialised ICU units and is easier to clean and disinfect. This reduces the potential of complicated transport to the CT suite for imaging (unless other confounding factors are at play, which can only be assessed by CT) and reduces unnecessary exposure of personnel (Mokotedi et al., 2023).

COVID-19 pneumonia has an evolution, it starts off as microvascular damage, which then progresses to acute fibrinous and organising pneumonitis (AFOP) and less typically to a diffuse alveolar damage (DAD), and both may fulfil the diagnostic criteria of acute respiratory distress syndrome (ARDS) (**Figure 12**). On CT it typically has these features: predominantly peripheral ground glass opacities (GGOs) with or without consolidations or crazy paving, with a bibasilar predominance (Huang et al., 2020; Ko et al., 2020; Mokotedi et al., 2023; Soldati et al., 2020) (**Figure 15**). These features can be seen on LUS as an



interstitial profile with singular or confluent B- lines extending to the surface of the pleura, a thickened and irregular pleural line (resulting in diminished lung sliding), and with further progression, small patchy subpleural consolidations are seen; then, the evolution and progression of these subpleural consolidations can be seen in a picture mirroring the pattern of ARDS that would require ventilatory support (Corradi et al., 2014; Mokotedi et al., 2023; Smith et al., 2020; Soldati et al., 2020; Zhang et al., 2021) (**Figure 13 and 14**). As thus, a complete examination of all the lung zones (anterior, lateral, and posterior) needs to be performed.

In a clinical setting/ intensive care, usage of LUS can also help guide the clinician on which way to go in terms of therapy. If a patient is admitted and ventilating on his own, the presence of the A-pattern/profile largely excludes significant COVID-19 pneumonia. With a LUS image showing a progression from the normal A - profile picture to the B-lines and eventually further progression to the confluent B- lines picture as disease progresses, this can guide admission to intensive care, or indicate impending intubation (Ko et al., 2020) (**Figure 13**).

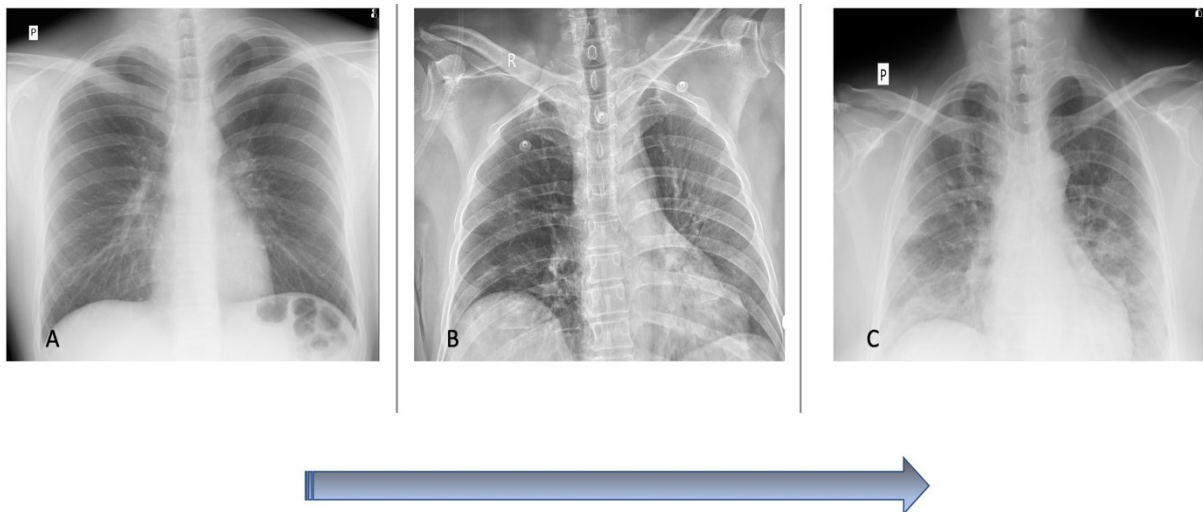


**Figure 12** – Different stages of COVID-19 infection on CXR, from no detectable pulmonary changes as in A to significant pulmonary changes as seen in C. Image from (Mokotedi et al., 2023).

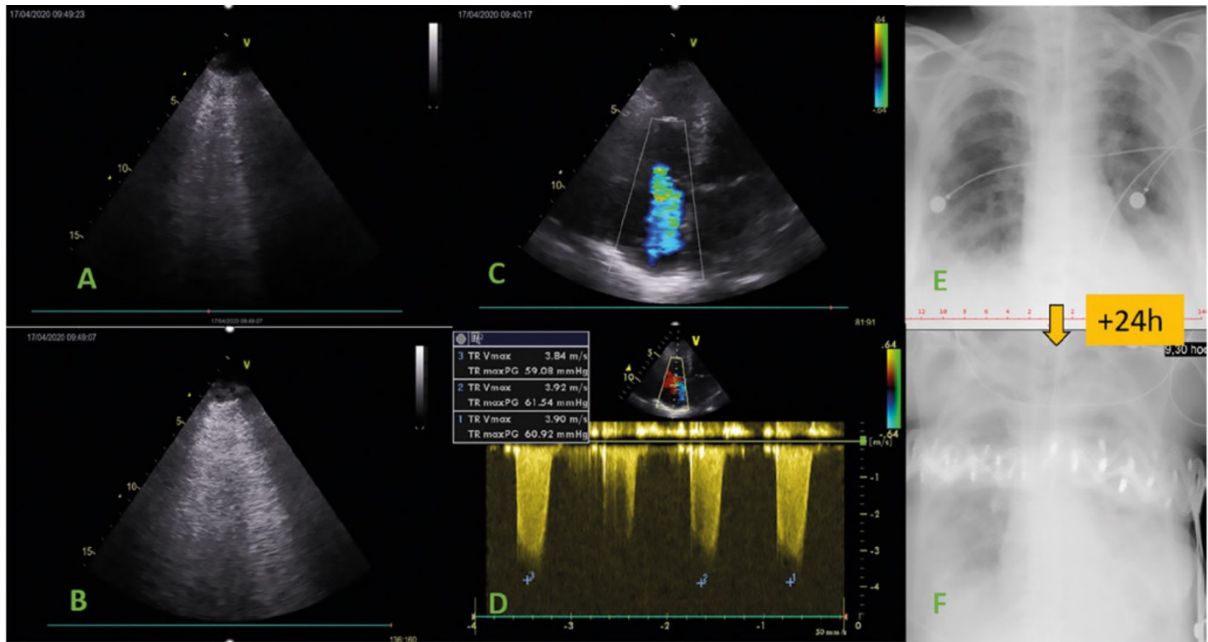


**Figure 13** - Early stage of severe COVID-19 on LUS and echocardiography, the patient is after intubation due to hypoxaemic respiratory insufficiency. CXR on admission and 24 hours later depicts delayed progression on radiographic methods: A apical LUS with multiple B3-4 lines, B basal LUS with coalescent B lines, C apical four-chamber view with dilated right ventricle and severe tricuspid regurgitation, D trans-tricuspid CW Doppler gradient of 60 mmHg in a patient with absent cardiac history, E CXR at the time of LUS and echocardiography showing CXR changes disproportionate to disease severity, F CXR after 24 hours showing severe ARDS; note the bioimpedance belt across the chest. Pulmonary embolism was excluded by CT scanning prior to admission. Image from (Mokotedi et al., 2023).

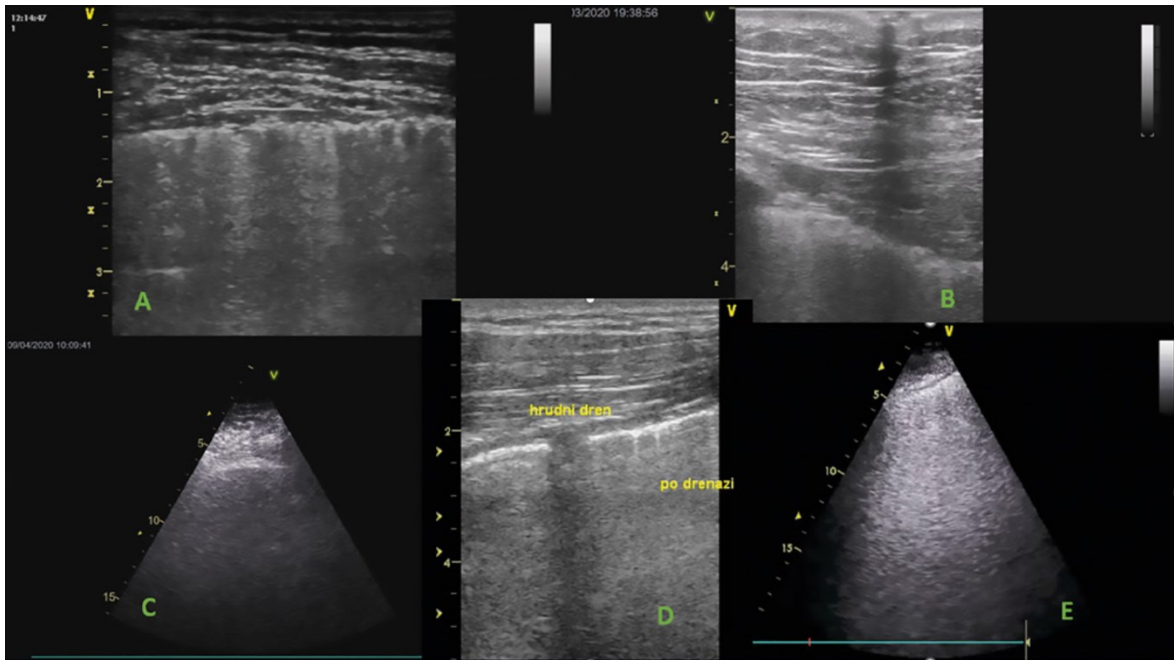


**Figure 14** - LUS findings of severe COVID-19: A thickened hyperechogenic pleura with multiple B3-4 lines, B thickened pleura with coalescent B-lines on the left side of the image, correlating with ground-glass opacities; C thickened pleura due to inflammation; D pleural space after drainage of PNO due to barotrauma; note the chest drain in between the pleural layers confirming full lung expansion; E coalescent B-lines, 2nd degree alveolo-interstitial syndrome and ARDS. Image from (M. C. Mokotedi et al., 2023).

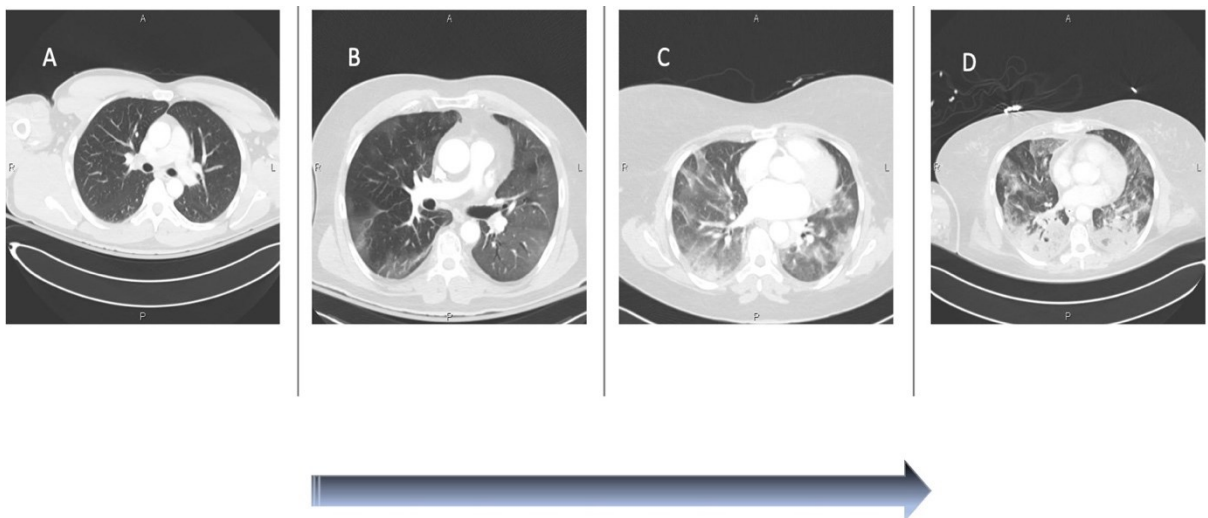


**Figure 15** – Different stages of COVID-19 infection on CT from no pulmonary changes (A) to significant pulmonary changes (D). Image from (Mokotedi et al., 2023).

Due to the fact that the coronaviruses bind to the angiotensin converting enzyme 2 (ACE2) which is predominantly found in the endothelium and epithelium of alveoli and as thus the viruses are able to enter the cells. When endothelial cells are activated, this gives rise to the escalating complication of intravascular thrombosis seen in COVID-19 patients (Price et al., 2020).

Particularly in the first 48 hours, LUS can be used as a great triage tool since COVID-19 pneumonia when subtle can be missed on CXR, especially in the first 48 hours (Figure 12), and with the prothrombic nature of the COVID-19 infection, some patients who had negative CXRs and initially tested negative or had no positive COVID-19 contacts, were sent with shortness of breath and elevated d-dimers for the exclusion/confirmation of a pulmonary embolism at pulmonary angiography CT (CTPA), which according to literature has a cumulative incidence of up to 30% (Bompard et al., 2020; Suh et al., 2021; Roncon et al., 2020) and is mostly seen in ICU patients. In this process of pulmonary embolism (PEmb) diagnosis/exclusion at CTPA, there is often an incidental finding of subtle COVID-19 pneumonia (GGO) and in this instance, the lung changes described beforehand can be readily seen earlier on LUS.

The pulmonary embolism rule out criteria (PERC) rule (**Figure 16**) can be utilised to stratify patients suspected to have a low risk for PEmb. For patients who are high risk for PEmb, combining LUS with echocardiography and Duplex ultrasound of the legs (multiorgan US) (**Figure 17**) in the ICU unit can aid in the early detection of PEmb. (Nazerian et al., 2014). Furthermore, Nazerian (Nazerian et al., 2017) found that multi-organ US in combination with D-dimers and Wells score can safely reduce CT pulmonary angiography exams and as thus reduce the radiation burden, not only in ICU patients, but in all patients with a suspected pulmonary embolism.

Furthermore, CTPA has enabled increased visualisation of subsegmental pulmonary emboli, which pose a diagnostic problem for clinicians - are they recent? Is it microembolization? Is something bigger coming? Are they clinically significant to treat?

PERC rule	Wells criteria	rGENEVA score	YEARS criteria
Age <50	Clinical signs and symptoms of PE (3points)	Age >65 (1 point)	Clinical signs and symptoms of PE?
Pulse <100bpm	HR > 100 (1.5 points)	Previous DVT/PE (3 points)	Hemoptysis?
SpO <sub>2</sub> >94%	PE is #1 diagnosis OR very likely (3 points)	Fracture of a lower limb or surgery in the past month (2 points)	PE is #1 diagnosis OR very likely?
Absence of unilateral leg swelling/ pain	Previous, objectively diagnosed PE or DVT (1.5 points)	Presence of malignancy (2 points)	
Absence of hemoptysis	Hemoptysis (1 point)	Unilateral lower limb pain (3 points)	
Absence of recent trauma/surgery	Immobilization at least 3 days OR surgery in the previous 4 weeks (1.5 points)	Hemoptysis (2 points)	
No exogenous estrogen use	Malignancy w/ treatment within 6 months or palliative (1 point)	Heart rate: 75 - 94 bpm = 3 points 95 bpm or more = 5 points	
Absence of previous DVT or PE		Pain on palpation of the deep veins of the lower limb and unilateral limb swelling (4 points)	

**PERC rule**  
 Patient low risk and meets all criteria? - no further work-up  
 Patient low risk and meets any of the criteria? - Order D- Dimer, if it is positive consider CTPA or V/Q scan

**Wells criteria**  
 0-1: low risk  
 2-6: moderate risk  
 >6: high risk

**rGeneva score**  
 low probability 0-3 points  
 intermediate probability 4-10 points  
 high probability >10 points

**YEARS criteria**  
 0 YEARS items and D-dimer <1000ng/mL - PE is considered excluded.  
 1+ YEARS items and a D-dimer <500mg/mL - PE is considered excluded.

**Figure 16 - Different pulmonary embolism criteria.**



**Figure 17 - Extensive thrombosis of the subrenal aorta extending caudally to the arteries of both lower limbs (arrows) in a COVID-19 positive patient which can be detected by vascular ultrasound. Note the partially visualised PE.**

(Image reproduced with permission from the archives of the Department of Diagnostic Radiology, Faculty Hospital Bulovka, Prague, Czech Republic).

### **1.6.6 Fluid loading/ extravascular lung water**

During fluid loading, there is at least a 10-15 % increase in the cardiac index in previously diagnosed volume-responsive patients, a subsequent decrease of the pulmonary shunt and an increase of arterial oxygenation. In systemic inflammation, interstitial lung disease, or in patients with elevated cardiac filling pressures, a concomitant worsening of lung aeration due to a rise in pulmonary microvascular hydrostatic pressure gives the picture of interstitial-alveolar edema, revealing LUS as a potential excellent monitoring medium to safeguard against overhydration (Caltabeloti et al., 2014).

Agricola et al. (Agricola et al., 2005) further demonstrated that the number of B-lines on LUS correlates with extravascular lung water (EVLW) measured by transpulmonary thermodilution.

In patients undergoing dialysis, there is a notable clearance of the of pulmonary B-lines (**Figure 3, 5, 6**) following fluid removal, as these patients tend to have fluid overload, showing that there is a causal relationship between water balance and B-lines on LUS and, therefore, additionally incorporating inferior vena cava measurements enhances the prediction of overhydration (Trezzi et al., 2013).

At the other end of the spectrum, Volpicelli et al. (Volpicelli et al., 2014) found that the pulmonary B-pattern on LUS combined with diminished LVEF on echocardiography is highly indicative of an elevated pulmonary artery occlusion pressure (PAOP).

### **1.6.7 Weaning failure**

Weaning failure, by definition, is spontaneous breathing trial (SBT) failure or the requirement of mechanical ventilation (invasive or non-invasive) after extubation of a patient within 48 hours (Boles et al., 2007) seen as postextubation respiratory distress.

Furthermore, when a significant PE is present, it raises the pressure of the thorax with the resulting loss of recoil of the inspiratory muscles, and therefore the ability of the diaphragm to generate the pressure needed for ventilation is reduced (Razazi et al., 2014).

By incorporating the LUS score (**Figure 3** and **Figure 18**), weaning failure can be anticipated by the visualisation of aeration changes of the lung on LUS before extubation and/or during an SBT. Furthermore, using a LUS score combined with the evaluation of the dynamics of the left ventricle (LV) (i.e., diastolic dysfunction) can predict successful or potential failure of extubation (S. Silva et al., 2017; Soummer et al., 2012). When patients are placed on mechanical ventilation with positive pressures, there is a reduction in venous return, preload, and afterload of the LV. Therefore, when a patient is liberated from mechanical ventilation leading to an SBT, the ensuing decrease of intrathoracic pressure as a result of this transition raises the central blood volume, the systemic venous return pressure gradient, the preload of the right ventricle (RV) and as thus, the preload of the LV (interventricular dependence). The rise of LV transmural pressure leads to an increase in the afterload of the LV. All these factors contribute to an increase in the work of breathing and ultimately, pulmonary oedema (Routsi et al., 2019).

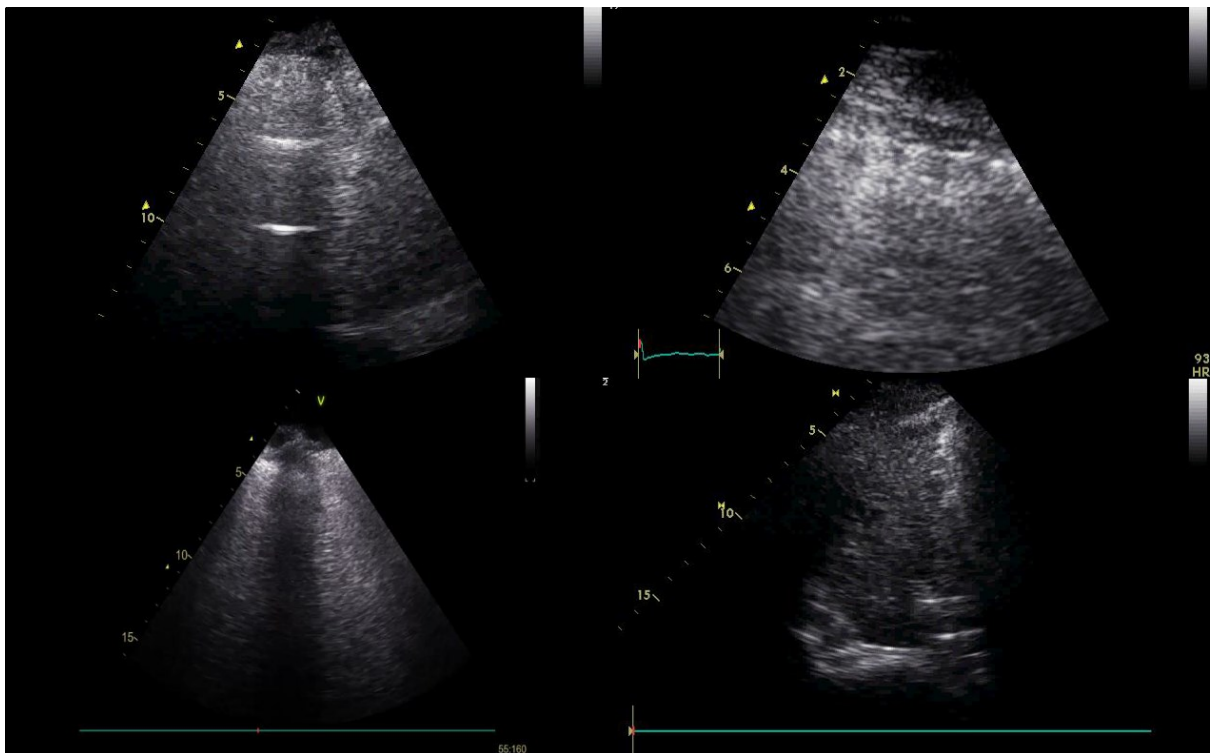


**Figure 18** - Ultrasonographic representation of the lung score. Upper left: Score 0, Upper right: Score 1, Bottom left: Score 2, Bottom right: Score 3.

### 1.6.8 Proning

Proning improves lung oxygenation, compliance, and ventilation/perfusion matching by promoting a more even distribution of tidal volume and inducing recruitment of the dorsal areas of the lungs (Guérin et al., 2020; Ibarra-Estrada et al., 2020).

As mentioned by Lichtenstein (Lichtenstein & Mezière, 2008b), the posterior interstitial syndrome is not particularly searched for due to the physiologic gravitational changes seen in the posterior parts of the lungs (hypostatic-hypoventilation changes). However, in patients admitted to the hospital, LUS evaluation can help with US-guided proning in patients who have lung pathology, especially in the posterior zones, while the anterior and lateral zones may be better aerated on LUS, to help ventilate these affected areas (Ko et al., 2020) (**Figure 19**) and thus potentially improving clinical data related to this therapy.





**Figure 19** - Improvement in aeration of the lungs seen after pronation. When evaluating these (bottom) images based on the lung ultrasound score, there is a shift from coalescent B lines to distinctive B lines followed by changes in gas exchange.

### 1.6.9 Ventilation apparatus assessment

The physiology of ventilation of the lungs is an intricate process that brings in multiple muscular players being the diaphragm (being the key player), muscles of the abdomen, intercostal muscles, and accessory muscles, the likes of which being the sternocleidomastoid and scalene muscles. Diaphragmatic dysfunction is a loss of muscle strength that can be either partial (manifesting as weakness) or total (manifesting as paresis), resulting in decreased inspiratory capacity and respiratory muscle fatigue. Ultrasound of the diaphragm

assesses not only the function, but the anatomy of the diaphragm as well, focusing on its thickening and excursion (Santana et al., 2020).

Diaphragmatic paralysis is seen as the absence of mobility of the diaphragm during quiet and deep breathing, concomitantly with diaphragmatic paradoxical motion during deep breathing or voluntary sniffing. Diaphragmatic weakness can be seen as reduced excursion during deep breathing, with or without paradoxical motion during voluntary sniffing. To assess diaphragm atrophy and contraction, diaphragm thickness and thickening fraction must be determined, respectively. Chronic paresis of the diaphragm is observed as a thin, atrophic diaphragm, with no thickening during inspiration. However, in acute or subacute diaphragmatic paresis, the diaphragm thickness may be normal, but the thickening fraction will be reduced to less than 25% (Santana et al., 2020), (**Figure 20, Figure 21 and Figure 22**). This assessment can largely replace the fluoroscopic evaluation of the diaphragm.

$$\text{Thickening fraction} = \frac{\text{diaphragm thickness (insp)} - \text{diaphragm thickness (exp)}}{\text{diaphragm thickness (exp)}} \times 100$$

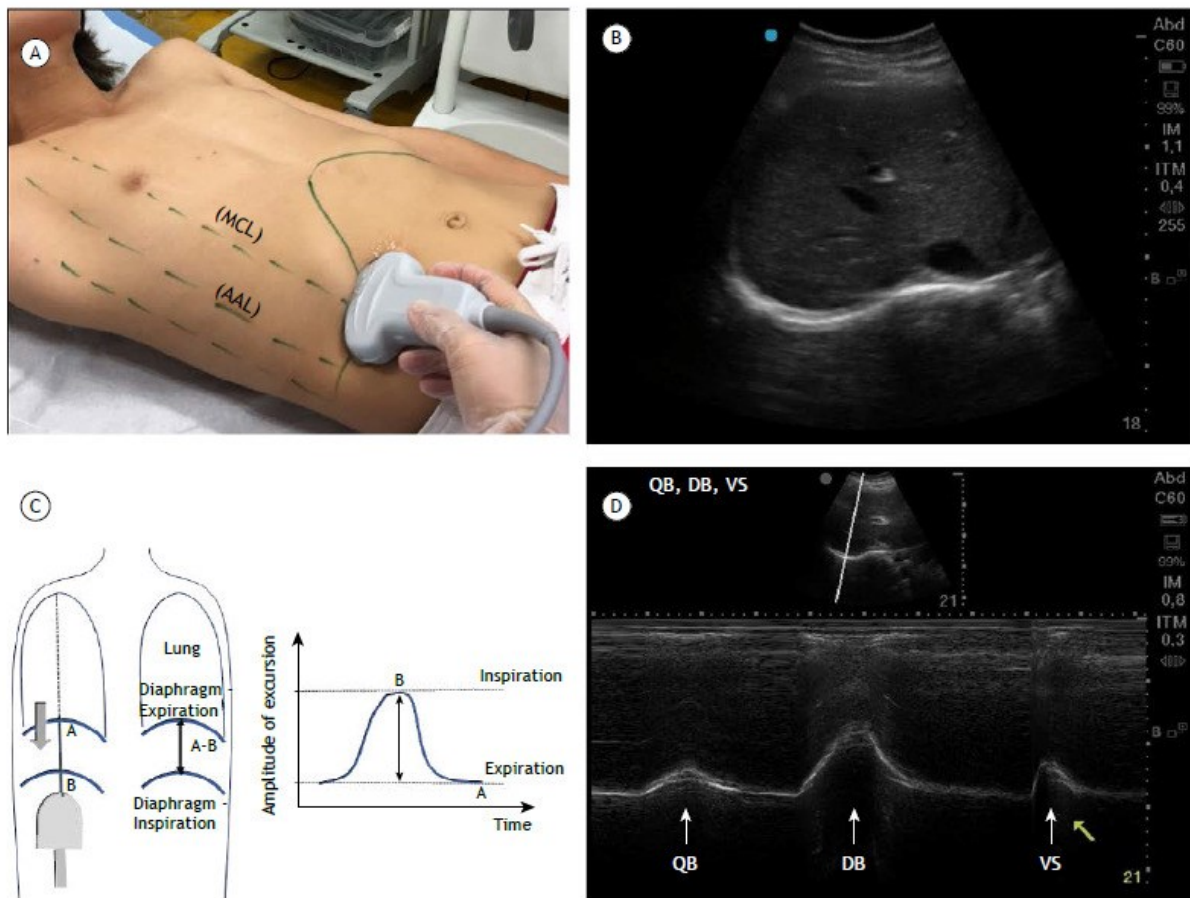


**Figure 20** - A: the range of motion of the right hemidiaphragm is measured using a convex probe located in the subcostal region between the midclavicular line (MCL) and the anterior axillary line (AAL). B: Ultrasound image of the right hemidiaphragm in the same subcostal region as A between the MCL and the AAL. C: Diagram showing the measurement of the range of motion of the diaphragm from expiration to inspiration. D: Measurement of the diaphragmatic amplitude in M mode. The upper part of the figure shows the normal right hemidiaphragm in B-mode, and the lower part shows the diaphragmatic range of motion in M mode during quiet breathing (QB), deep breathing (DB), and spontaneous sniffing (VS). Image from (Santana et al., 2020).

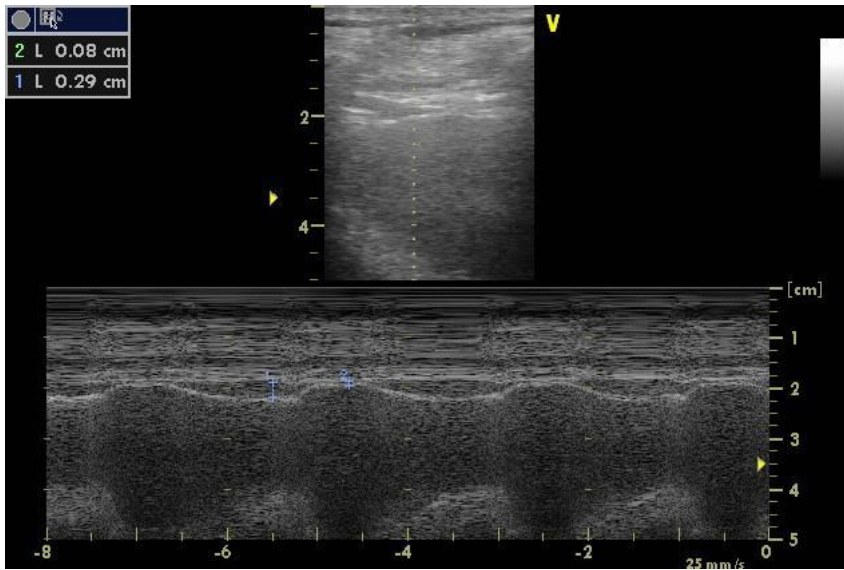


**Figure 21** - Measurement of diaphragmatic thickening on LUS.

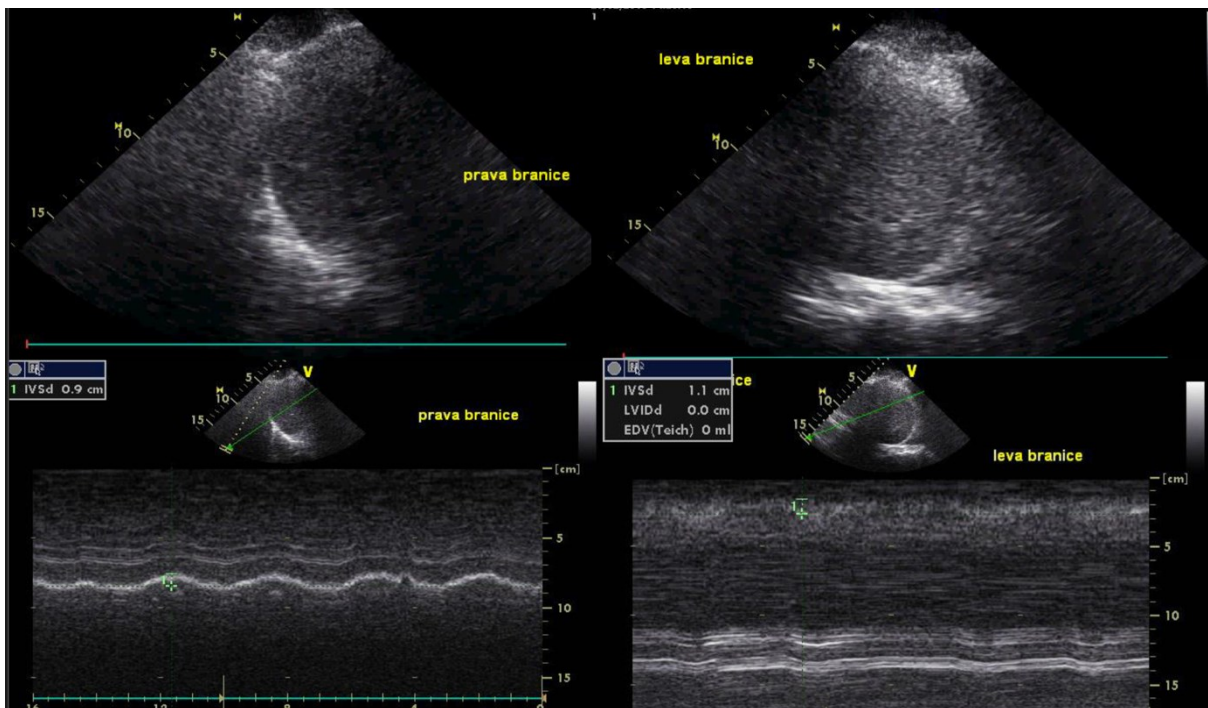


**Figure 22** - Paresis of the right diaphragm on LUS where there is a reduction in the excursion of the diaphragm.

With dysfunction of the diaphragm, there is a concomitant adaptation of the extradiaphragmatic apparatus whence the extradiaphragmatic muscles are recruited and this

manifests, for example, as the thickening of the parasternal intercostal muscles, which can be reliably measured on ultrasound and evaluated as a fraction of their thickening, which therefore provides a means for effective ventilation and pulmonary gas exchange (**Figure 23**). According to the change in thickness, the percentage of thickening of the parasternal intercostal muscles is determined as follows: Parasternal intercostal muscle thickening is equal to the maximum inspiratory thickness minus the end-expiratory thickness divided by the end-expiratory thickness, the resultant value is then multiplied by a 100 (Dres et al., 2020).

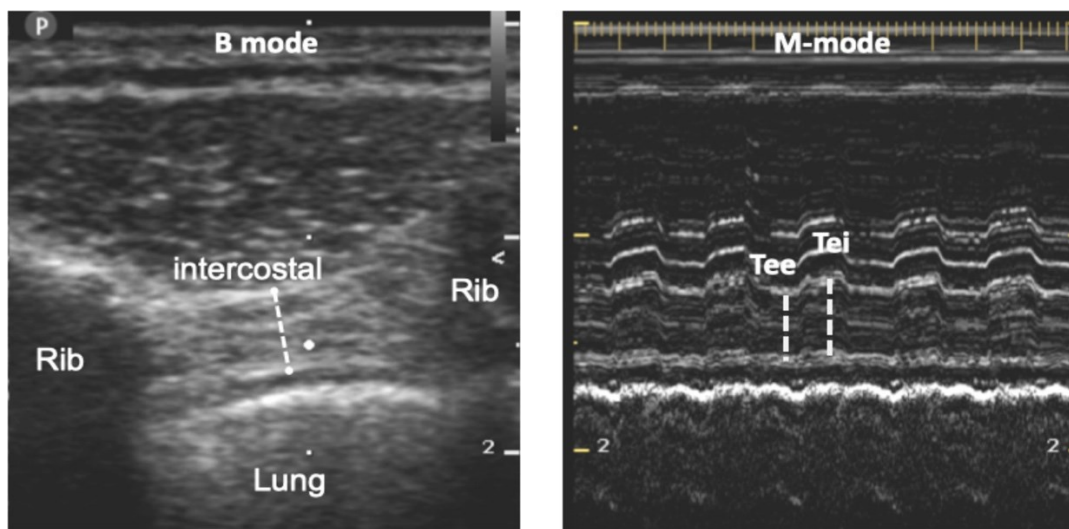


**Figure 23** - Ultrasound examination of the right parasternal intercostal muscles. Left: The parasternal intercostal muscles are seen as a tri-layered biconcave structure composed of two linear hyperechoic membranes extending from the anterior and posterior surfaces of adjacent ribs, respectively, and the medial muscular portion. Measurements in B-mode were performed at the central thinnest part of the muscle (dotted line). Right: In M mode, parasternal intercostal muscle thickness was measured at end-expiration (Tea) and end-inspiration (Tei). Image from (Dres et al., 2020).

## **2 Aims and hypotheses**

### **2.1 Aims**

- To show and demonstrate that some novel CXR indicators can be utilized to assess the positioning of CDs.
- To evaluate how CD positioning, assessed via LUS and CXR, may be associated with a residual or occult pneumothorax.
- To explore the correlation between the absence of CD detection and signs of a residual pneumothorax on LUS
- To determine if there is a prediction error when using the established gold standard method for ascertaining pleural fluid volume on LUS.
- To ascertain whether there is a causal relationship between the number of bedside serial antero-posterior supine CXRs and CT scans performed and the ICU outcomes in patients with severe COVID-19 ARDS treated with ECMO

### **2.2 Hypotheses**

Due to the above-mentioned aims, our hypotheses were as follows:

- A CD that has changed its position on a CXR should prompt further evaluation on LUS to exclude a residual pneumothorax that is occult on CXR.
- The absence of CD detection between the ventral pleural layers on the bedside LUS may be associated with signs of a residual pneumothorax.
- The established gold standard to quantify pleural effusion volume on LUS underestimates pleural fluid volume in patients with consolidated lungs, therefore,

multiple pleural separation measurements may be more useful to provide an accurate quantification of pleural fluid in these patients.

- The frequency of CXRs and CTs might not relate to ICU outcome in patients with severe COVID-19 ARDS treated with ECMO

## 3 Investigations

Our work presented in this dissertation thesis is constituted of two retrospective studies (Study 1 and Study 3) and two prospective studies (Study 2 and Study 4).

This dissertation thesis will therefore be divided into three parts: Part one will be evaluating CD positioning on CXR and LUS and residual/occult PNOs, part two will be challenging the established method of quantifying pleural fluid volume on LUS, and the last part, part three will be delving into the impact of serial imaging with the growing popularity of LUS on the ICU outcome of patients with COVID-19 ARDS treated with ECMO.

### 3.1 Part 1: Studies evaluating CD positioning on CXR and LUS

#### 3.1.1 Study 1 - X-ray indices of chest drain malposition after insertion for drainage of pneumothorax in mechanically ventilated critically ill patients

**Hypothesis:** A CD that has changed its position on a CXR should prompt further evaluation on LUS to exclude a residual pneumothorax that is occult on CXR.

#### Methods

We carried out this study between May 2015 and June 2017 in a 20-bed intensive care unit in a tertiary non-trauma centre. It was approved by the Institutional Review Board and informed consent was waived due to the retrospective design of the study.

The inclusion criteria were: (I) the presence of a CD in the pleural space inserted for PNO drainage from the safe triangle; (II) mechanical ventilation; (III) CXR and CT scan with the drainage performed less than 24 hours apart. The exclusion criteria were: (I) all anatomical CD malpositions (extrathoracic, intraparenchymal, interlobar); (II) mid-clavicular access.

The study included a total of 28 patients. These patients were divided according to the position of the CD on CT into two groups: group A with the tip of the CD anterior to the mid-axillary line (correct placement, n=24) and group B with the tip of the CD at the level of or posterior to the mid-axillary line (incorrect placement, n=4).



The parameters measured on CT and CXR are listed in **Table 3.1.1 - 1**. The foreshortening of the CD was calculated as the distance of the CD from chest entry to its tip in the coronal plane (ignoring the anteroposterior dimension) divided by its true length obtained by 3D measurement. The angle of inclination of the CD above the horizontal line at chest entry was measured on CXR (**Figure 3.1.1 - 1**). CD tortuosity was determined as the ratio of a straight distance of the CD from chest entry to its tip and the length of the CD in the patient measured on CXR (**Figure 3.1.1 - 1 and Figure 3.1.1 - 2**). CT and CXR measurements were performed by a board-certified radiologist with >10 years of experience in thoracic imaging.

**Table 3.1.1 - 1 - Parameters measured and calculated on CT and CXR.**

Measured and calculated parameters on CT and chest radiographs (CXR)

Parameter	Group A: correct placement (n=24)	Group B: incorrect placement (n=4)	P	Test
CT scan (CT)				
CD entry: intercostal space	3 [2–5]	3 [3–7]	0.82	MW
CD length in the thoracic cavity (mm)	99±24	158±53	0.001	T
CD entry to tip distance (mm)	93±21	135±46	0.005	T
CD entry to tip distance in the coronal plane (ignoring the anteroposterior dimension) (mm)	88±19	118±49	0.033	T
CD foreshortening in the coronal plane (CD entry to tip distance ignoring the anteroposterior dimension/CD entry to tip length) (%)	90±10	75±13	0.015	T
Chest radiograph (CXR)				
Entry angle (angle of inclination above the horizontal) (°)	29 (IQR 29)	53 (IQR 22)	0.042	MW
Tortuosity (entry to tip distance/entry to tip length of the CD measured on a CXR) (%)	0.99 (IQR 0.03)	0.84 (IQR 0.5)	0.16	MW

CD, chest drain; T, t-test, MW, Mann-Whitney test; IQR, interquartile range.

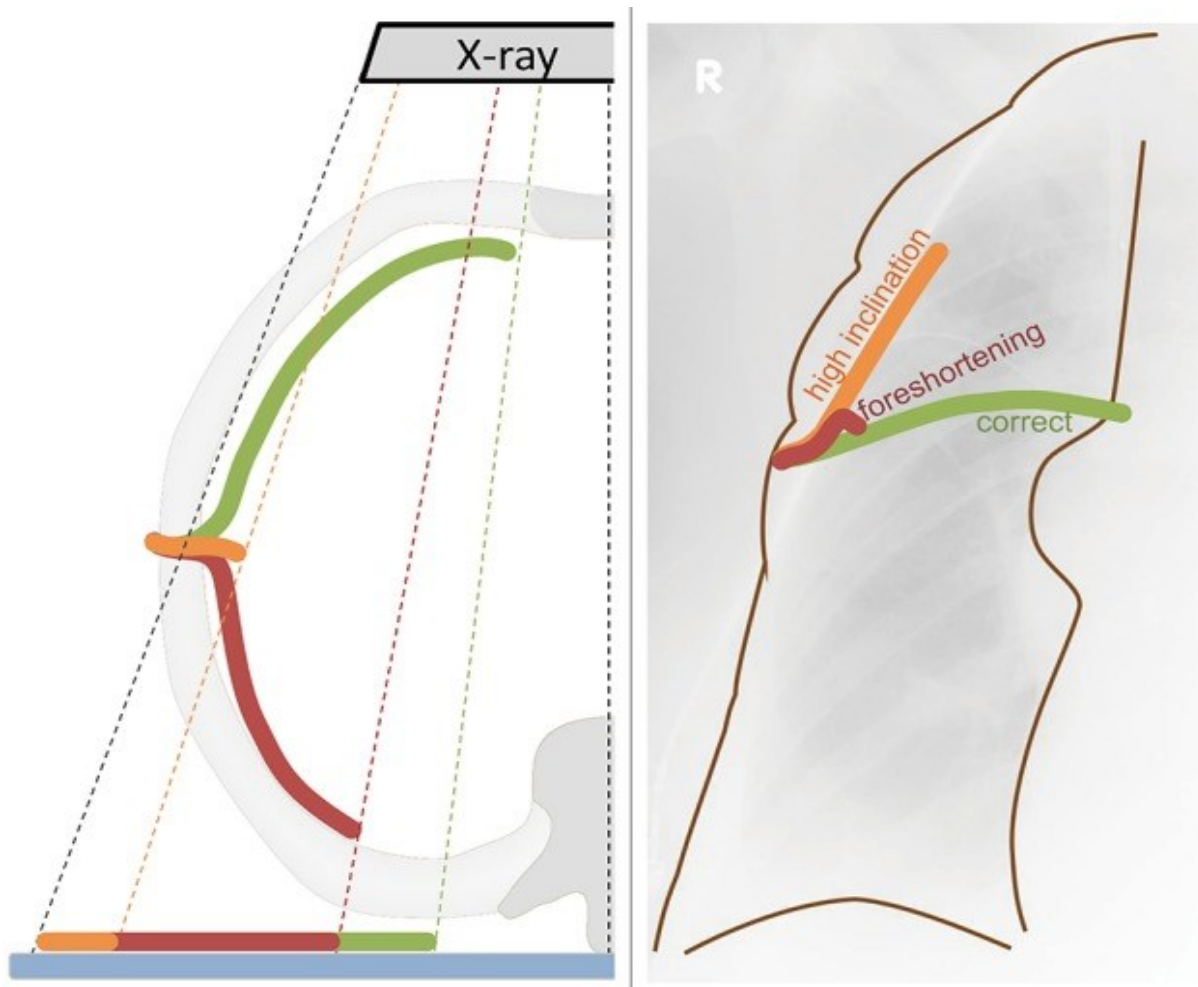


**Figure 3.1.1 - 1** - Schematic drawing of the principle of foreshortening and cranial angulation (inclination) of a CD on a CXR due to its position and divergence of X-rays (dashed lines). The green CD shows the correct position; the orange CD shows lateral migration, and the red CD shows dorsal migration.

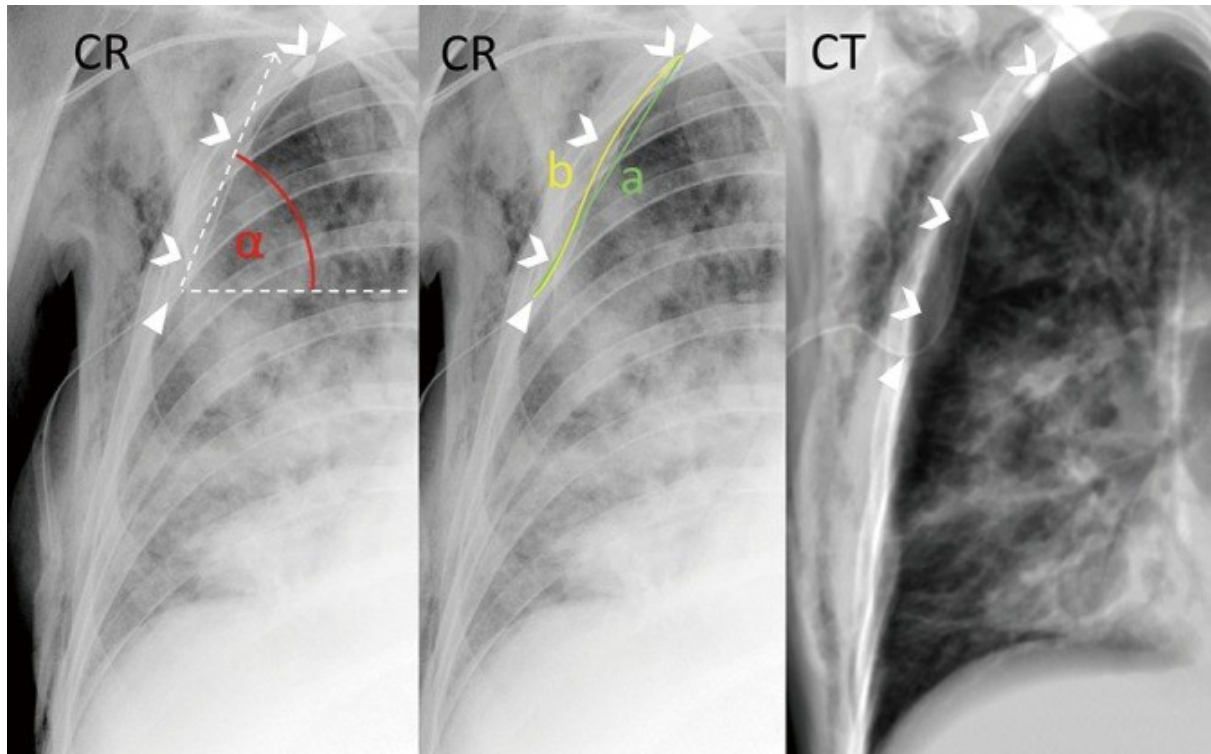


**Figure 3.1.1 - 2** - A CD (chevrons) inserted through the safe triangle for PNO drainage that had slipped laterally is shown on CXR (left and middle) and a thick slab coronal CT reformat (right). Arrowheads show chest entry and the tip of the CD.  $\alpha$  shows inclination of the CD from the horizontal line ( $61^\circ$  on CXR, left). The measurement of the straight distance (a, green) and length of the CD inside the pleural cavity (b, yellow) used for calculation ( $a/b$ ) of the tortuosity (0.97) are shown in the middle. CD foreshortening is the ratio between the straight distance (a, green, right) and the length of the CD inside the pleural cavity read on the printed rule (0.77)- for the purpose of this study measured on CT.

We analysed the data using GraphPad Prism (GraphPad Software, La Jolla, USA). We then tested the normality of the data by using the D'Agostino & Pearson omnibus test, whilst the statistical significance between the groups was tested by the  $t$ -test or the Mann-Whitney test as appropriate with a subsequent ROC analysis. A P value below 0.05 was considered significant.

## Results

The patients were  $59.5 \pm 15$  years old and 78% were males. All patients were mechanically ventilated with APACHE II  $23 \pm 6$ , SOFA  $8.9 \pm 2.5$ . The causes of the PNO were postsurgical (n=10), ventilator related in pneumonia (n=7), ventilator related in ARDS requiring ECMO (n=6), postprocedural (n=3), and spontaneous on intermittent positive pressure ventilation (IPPV, n=2).

The parameters measured on CT and CXR are presented in **Table 3.1.1 - 1**. *Greater CD foreshortening was the best clue of a misplaced CD with an AUC of 0.93 (95% CI: 0.83–1.0, P=0.0071), 100% sensitivity and 88% specificity for a cut-off value of 82% (Table 3.1.1 - 1, Figure 3.1.1 - 3)*. The angle of inclination of the CD was greater in patients with a misplaced CD with AUC of 0.83 (95% CI: 0.63–1.0, P=0.039), 75% sensitivity, and 92% specificity for a cut-off value of 50 degrees (**Figure 3.1.1 - 3**). There was no significant difference in CD tortuosity on CXR between the groups with an AUC of 0.69 (95% CI: 0.34–1.0, P=0.22).

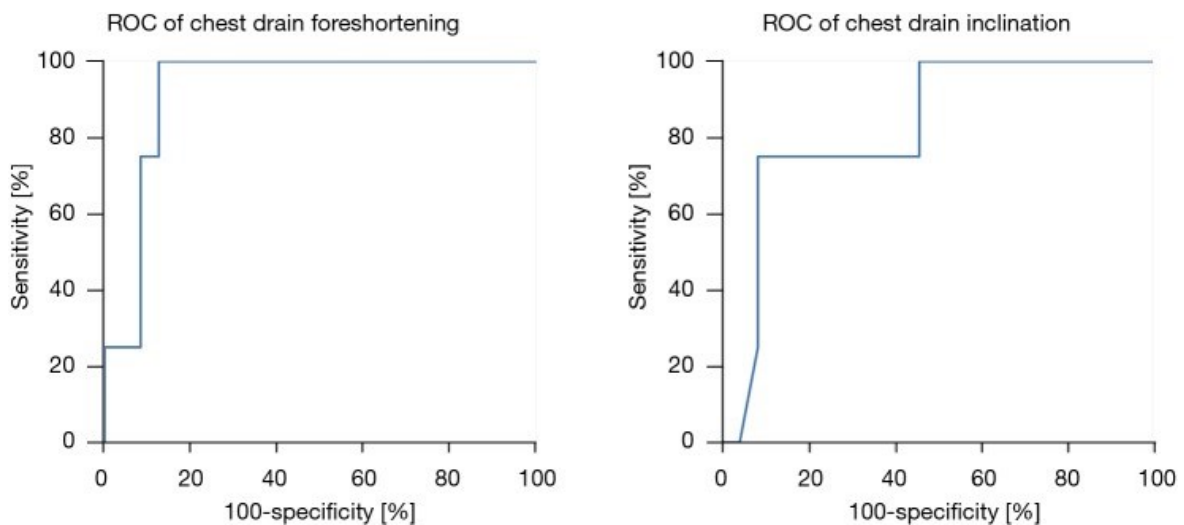


**Figure 3.1.1 - 3** - ROC of CD foreshortening and inclination as a clue of a misplaced CD with an AUC of 0.93 and 0.83, respectively. ROC, receiver operating characteristic; AUC, area under the curve.

Three of the four patients with migrated CDs had a residual ventral PNO on the CT scan. The median time between the CXR and CT examinations was 5.4 hours (IQR 3.1).

The aforementioned hypothesis (a CD that has changed its position on a CXR should prompt further evaluation on LUS to exclude a residual PNO that is occult on CXR) was thus confirmed.

### **3.1.2 Study 2 - Interpleural location of chest drain on ultrasound excludes pneumothorax and associates with a low degree of chest drain foreshortening on the antero-posterior chest x-ray**

**Hypothesis:** The absence of CD detection between the ventral pleural layers on the bedside LUS may be associated with signs of a residual pneumothorax.

#### **Methods**

We prospectively evaluated all patients between March 2020 and February 2022 with COVID-19 ARDS and with a concomitant PNO for the presence of a residual PNO on LUS, the detection of a CD between the pleural layers on LUS, and finally, for the CD foreshortening and angle of inclination of the CD both taken from the bedside CXR. All patients with a large subcutaneous emphysema or with anatomical drain malpositions were excluded.

The drainages were performed by intensivists using 16-20F CDs (Portex, UK) and utilising the blunt forceps technique in the safe triangle (Havelock et al., 2010). All CDs were connected to a closed suction system with a negative pressure of  $-20$  cmH<sub>2</sub>O. A PNO was diagnosed on LUS according to the current standards (Volpicelli et al., 2012) using a linear transducer (6–10 MHz, Vivid S6, VividS60 or Vivid I, General Electric).

Foreshortening was estimated as a decrease in the chest drain index (CDI), which should ideally be close to 1 (**Figure 3.1.2 - 2**). The CDI is equal to the length of the CD in the chest measured on an antero-posterior CXR divided by the depth of insertion read directly on a CD scale plus 5 cm (Figure 3.1.2 - 1 and 3.1.2 - 2), which is the distance from the first drainage orifice to the tip of the CD. The angle of inclination of the CD was measured as the angle between the horizontal line and the CD at pleural space entry on the CXR (**Figure 3.1.2 - 1**). The angle of inclination of the CD was judged to be higher or lower than  $50^{\circ}$  (Mokotedi et al., 2018).

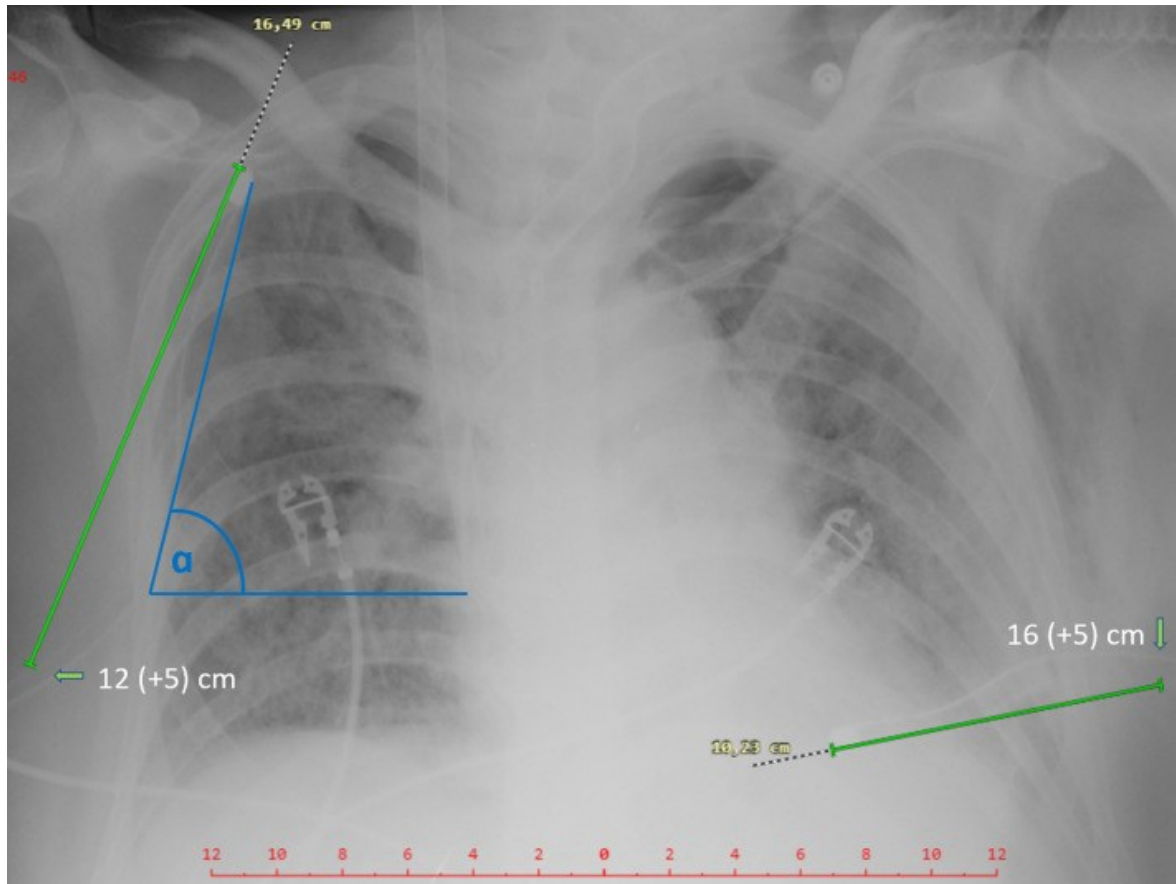


**Figure 3.1.2 - 1** - Patient on VV-ECMO with bilateral PNOs has a steep ascending right CD ( $\alpha > 50^\circ$ ) with a CDI of 0.97 ( $16.49/12 + 5$ ), and no signs of a PNO on LUS of the right hemithorax. The left CD has a CDI of 0.49 ( $10.23/16 + 5$  cm) and foreshortening due to dorsal malposition and a left ventral PNO on LUS.

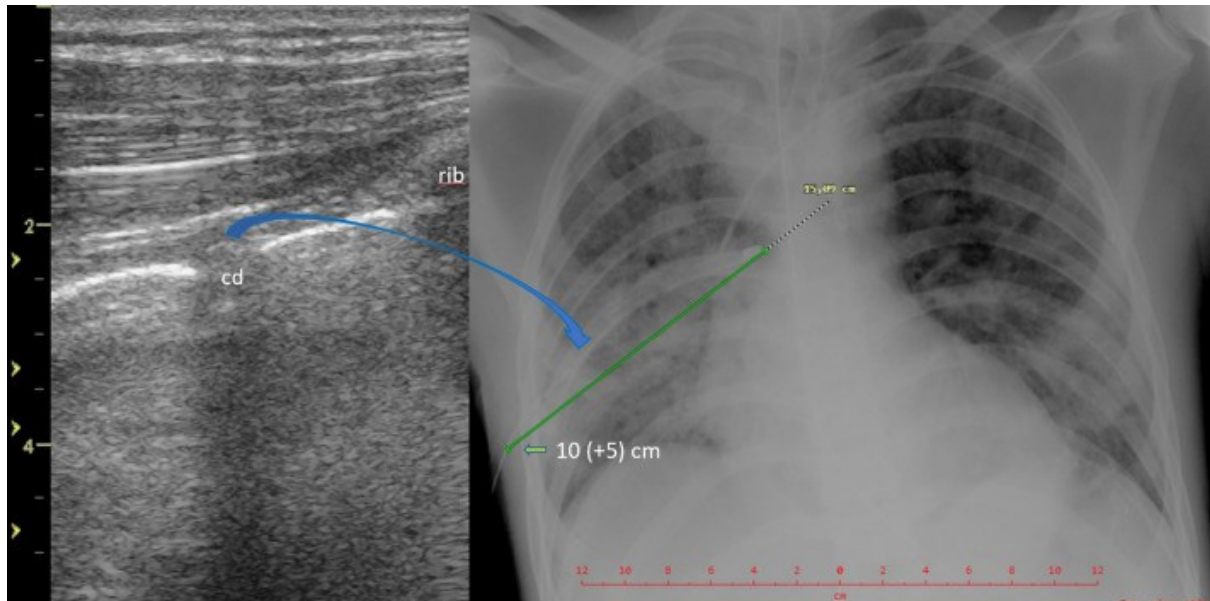


**Figure 3.1.2 - 2** - Patient with COVID-19 ARDS after CD insertion for a right ventral PNO. The linear transducer shows the transverse plane of the CD between the enhancing pleural layers under the anterior chest wall next to the rib (left LUS, blue arrow towards the drain position on the right CR). In the same patient, the CDI (here 1.00) is equal to the length of the CD in the chest measured on CR (15.09 cm) divided by the depth of insertion of the CD read directly on a CD scale plus 5 cm (10 + 5 cm).

We analysed the data using Statistica v.12 software. Normality of the data was tested using the Kolmogorov–Smirnov test and the statistical significance between the groups was tested using the Mann–Whitney U test for the numerical variables and with the Chi-square test for categorical data. The numerical data is reported as medians and interquartile ranges. The risk ratio for a PNO on LUS was calculated in relation to the CXR findings. A p-value below 0.05 was considered significant.

## Results

116 PNO drainages (75 on the right, 41 on the left) were performed and monitored in 88 patients (31 females, age  $56.2 \pm 19$ , APACHE II  $22 \pm 4$ , SOFA  $9 \pm 2.2$ ). 10 patients were excluded due to significant subcutaneous emphysema.

The aetiologies of the PNO were spontaneous on mechanical ventilation in 79 (74%), post-cannulation or due to thoracocentesis in 25 (24%) and after transbronchial biopsy in 2 (2%).

The results in groups with and without residual post-drainage PNO are given in **Table 3.1.2 - 1**. Among the 80 cases with full lung expansion on LUS (no PNO in the six zones of each hemithorax), the CD was located by LUS after drainage in 69 (86%). The median CDI was 0.99 (0.88–1.06), and the steep angle of inclination of the CD on CXR ( $> 50^\circ$ ) was found in 10 patients (12.5%).

**Table 3.1.2 - 1** - Comparison of the novel observed categorical parameters (CD location in %, its steep course in %, presence of an air leak in %) and continuous parameters (depth of CD insertion in cm, length of CD in chest in cm, CDI, all \* medians and interquartile ranges) between groups with full lung expansion on LUS (PNO excluded in all lung fields) and groups with a residual PNO on LUS.

Pneumothorax <i>n</i> = 106	Full lung expansion on post-drainage CUS ( <i>n</i> = 80, 75%)	Residual pneumothorax on post-drainage CUS ( <i>n</i> = 26, 25%)
Drain located on CUS	69 (86%)	8 (31%), ( <i>p</i> <sup>∧</sup> 0.0001)
Depth of drain insertion on CD scale (cm)*	12 (10–14)	12 (12–16), (n.s.)
Length of CD in chest on antero-posterior CR (cm)*	16.1 (14.2–17.9)	13.3 (11.4–16.5), (n.s.)
CDI*	0.99 (0.88–1.06)	0.76 (0.6–0.93), ( <i>p</i> <sup>∧</sup> 0.01)
Steep ascending drain in chest on CR	10 (12.5%)	6 (23%), (n.s.)
Continued air leak from the drain	19/80 (24%)	14/26 (55%), ( <i>p</i> <sup>∧</sup> 0.003)

26 cases had a residual PNO after drainage (24.5%), the CD was located by LUS in 8 of those (31%), the median CDI was 0.76 (0.6–0.93), *p* < 0.01, the steep angle of inclination of the inserted CD on CXR was observed in 6 patients (23%).

Of the 106 patients included, the CD was located in between the pleural layers in 77 patients, and 8 of those had a residual PNO. In contrast, the CD was not located in 29 patients, of which 18 still had a post-drainage PNO. The risk ratio for a PNO in a patient with a CD that is not visible in the interpleural space on LUS (*n* = 29) and an associated low CDI on CXR was 5.97, 95% CI [2.92–12.21], *p* < 0.0001, NNT 1.94.

For the 16 patients with a steep angle of inclination of the CD on CXR greater than  $50^\circ$ , the risk ratio for a PNO was not significant (RR 1.68, 95% CI [0.80–3.54], *p* < 0.17, NNT 6.55).



For the 33 patients with a continued air leak from the CD post drainage, the risk of a residual PNO is significant (RR 2.27, 95% CI [1.33–3.85],  $p = 0.003$ , NNT 3.32).

The aforementioned hypothesis (the absence of CD detection between the ventral pleural layers on the bedside LUS may be associated with signs of a residual pneumothorax) was thus confirmed.

## **3.2 Part 2 - Challenging the established method of quantifying pleural fluid volume on LUS in patients with consolidated lungs**

### **3.2.1 Study 3 - Pulmonary consolidation alters the ultrasound estimate of pleural fluid volume when considering chest drainage in patients on ECMO**

**Hypothesis:** The established gold standard method to quantify pleural effusion volume on LUS underestimates PEv in patients with consolidated lungs, therefore multiple pleural separation measurements may be more useful to provide an accurate quantification of PE in these patients.

#### **Methods**

In this study we prospectively collected pleural drainage data in patients with severe cardiorespiratory failure treated with ECMO for a period of 3 years (2019–2021). In addition to the presence of a PE, severe lung consolidations with a lung score of 3 in the basal lung regions and no better than a lung score of 2 in the anterior regions were diagnosed by applying a complex LUS protocol in six regions on both right and left hemithorax (Via et al., 2012). Patients were supine with the trunk elevated at a 15° angle to the horizontal, corresponding to the method described by Balik et al. (Balik et al., 2006). The key measurements were taken in expiration with transducer scanning in the transverse plane above the base of the lung in the posterior axillary line at the planned drainage spot (**Figure 3.2.1 - 1**).

All drainages were performed by intensivists using the blunt forceps technique and the CDs were pulled from the trocar into the pleural cavity. Patients with pleural separations of less than 10 mm on the initial scan and/or with an absence of extensive lung consolidations (lung score 2 to 3) were excluded, as well as patients with incomplete PE aspiration on post-drainage ultrasound.

After we excluded three effusions (5.7%) for incomplete drainage, a total of 50 PEs were evaluated and drained in 42 patients (27 males and 15 females), (age  $44 \pm 17$  years, APACHE II  $25.8 \pm 6.8$ , SOFA  $11 \pm 2.5$ , height  $174 \pm 7$  cm, body weight  $87 \pm 20$  kg). Twenty-eight patients were on veno-venous ECMO, four on veno-arterio-venous ECMO and ten on veno-arterial ECMO. The calibres of the CDs were 12F ( $n = 33$ ), 16F ( $n = 3$ ), 20F ( $n = 7$ ), 24F ( $n = 1$ ), 28F ( $n = 2$ ), 32F ( $n = 2$ ). The main character of the PE was exudate ( $n = 25$ ), clear transudate ( $n = 12$ ), sanguinolent ( $n = 8$ ) and haemothorax ( $n = 5$ ). The overall incidence of drainage-related bleeding or iatrogenic PNO was zero. All ECMO patients were on a pulmoprotective ventilation (BIPAP,  $n = 30$ , 60%; PSV,  $n = 20$ ; 40%) with plateau pressures up to 24–26 cmH<sub>2</sub>O and PEEP 8–12 cmH<sub>2</sub>O.

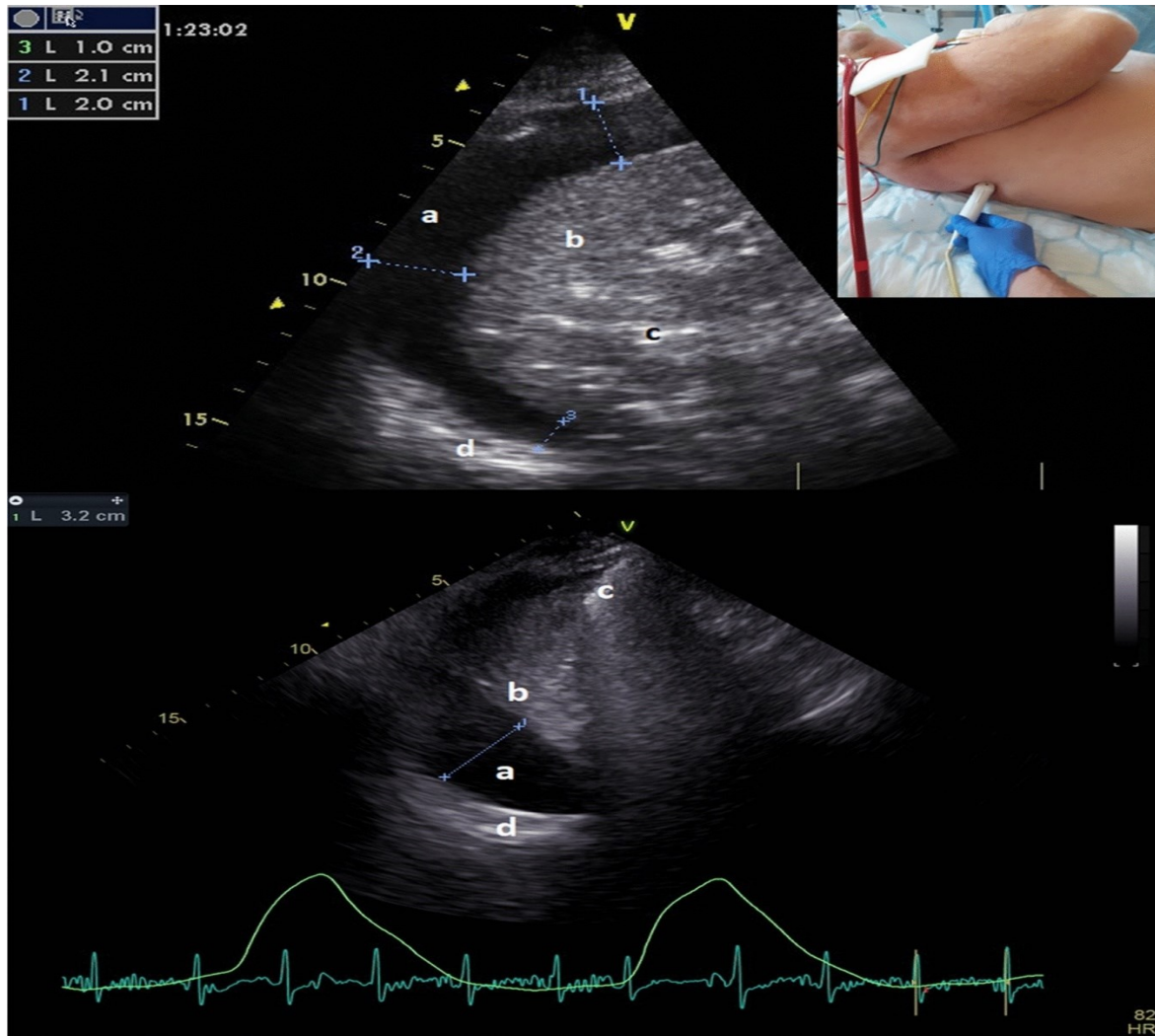


**Figure 3.2.1 - 1** - Phased array transducer scanning in the transverse plane above the base of the right lung in the posterior axillary line. The transducer is positioned at the expected chest drainage spot allowing measurements of the separation of the pleural layers in the intercostal space which contributes to the safety of the procedure (upper). Consolidated right lower lobe in a patient on ECMO with a circumferential effusion that separates the pleural layers paravertebrally (3 = Psep) 10 mm, dorsally (2 = Dsep) 21 mm and laterally (1 = Lsep) 20 mm (a pleural fluid, b consolidated lung parenchyma, c bronchogram, d rib). The drained volume of pleural fluid was 980 ml (middle). For comparison, the original method of pleural fluid estimation (Balik et al., 2006) was used in another non-ECMO cardiac patient (bottom). The maximum separation of 32 mm at the base of the lung is multiplied by 20 giving a pleural volume estimate of 640 ml. Note that there is no pleural separation and aerated lung under the posterolateral chest wall (a pleural fluid, b compressed lung parenchyma, c aerated lung, d rib).

## Results

The PEv and pleural separations showed normal distributions according to the Kolmogorov–Smirnov test. The maximum pleural separation (Msep) was  $24 \pm 7$  mm, correlating (all Pearson's correlation) with separation at the dorsal chest wall (Dsep,  $21 \pm 9$  mm,  $r = 0.88$ ,  $p = 0.0001$ ). The paravertebral (Psep) and lateral (Lsep) separations were  $17 \pm 8$  mm and  $17 \pm 7$  mm, respectively (**Figure 3.2.1 - 1**).

The classic method of PE estimation (Balik et al., 2006) produced a mean underestimation error of  $359 \pm 187$  ml, while the mean drained volume was  $837 \pm 206$  ml. The Msep value correlated significantly with the drained volume ( $r = 0.47$ ,  $p = 0.001$ ); however, the best correlation was found for the Lsep ( $r = 0.61$ ,  $r^2 = 0.37$ ,  $p = 0.0001$ , **Figure 3.2.1 - 1**).

The volume of PE can be estimated with equation  $V[ml] = 540 + 17 * Lsep[mm]$ , resulting in a mean prediction error of  $129 \pm 98$  ml. Similarly, the sum (Ssep) of the basal, lateral, and ventral pleural separations (mean  $55 \pm 18$  mm) correlated with the drained volume ( $r = 0.54$ ,  $p = 0.0001$ ), showing a mean prediction error of  $144 \pm 95$  ml. Only for the classic method, the prediction bias for the volume estimate was significantly different from zero (Bland–Altman,  $p = 0.0001$ ).

Comparison of the right and left pleural effusions did not show a significantly better correlation of Lsep of the right hemithorax ( $n = 30$ ,  $r = 0.66$ ,  $p = 0.0001$ ) compared to the left hemithorax ( $n = 20$ ,  $r = 0.52$ ,  $p = 0.02$ ;  $p = 0.49$  for comparison, Fischer's z-transformation).

The aforementioned hypothesis (the established gold standard method to quantify pleural effusion volume on LUS underestimates pleural fluid volume in patients with consolidated lungs, therefore multiple pleural separation measurements may be more useful to provide an accurate quantification of pleural fluid in these patients) was confirmed.

### **3.3 Part 3 - The impact of serial imaging with the growing popularity of LUS on the ICU outcome of patients with COVID-19 ARDS treated with ECMO.**

#### **3.3.1 Study 4 Prognostic Impact of Serial Imaging in Severe Acute Respiratory Distress Syndrome on the Extracorporeal Membrane Oxygenation**

**Hypothesis:** The frequency of CXRs and CTs might not relate to ICU outcome in patients with severe COVID-19 ARDS treated with ECMO.

#### **Methods**

Here, we retrospectively analysed patients with severe ARDS due to COVID-19 according to the Berlin 2011 criteria (Ferguson et al., 2012) admitted to a single high-volume ECMO centre between March 2020 and March 2022. We sought to determine the impact of the number of antero-posterior CXRs and CT scans on the resultant ICU outcome.

The requirements for imaging were stratified according to the body mass index (BMI), i.e., obese (BMI > 30) and non-obese (BMI ≤ 30) patients, and patients managed with and without ECMO. We excluded all patients with mild ARDS and/or the absence of a weighted bed for BMI measurement. We retrieved the data from the hospital information system and included demographic characteristics, patients' histories, clinical data—body mass index (BMI), initial status at ICU admission, and severity scores [Acute Physiology and Chronic Health Evaluation (APACHE IV), Sequential Organ Function (SOFA)]. Imaging examinations were retrieved from an existing and already published dataset (Balik et al., 2022).

#### *Statistical Analysis*

After verifying the distribution of data, continuous data is expressed as the median and interquartile range (IQR), and the differences between the groups were tested with the Mann-Whitney U test. The categorical data is expressed as the number of probands, and percentage

of a given group and evaluated using the Fischer's exact test. The Rank correlation with Spearman's coefficient is utilized for correlation analysis of the number of radiographic (RTG) records with the length of stay and outcome in the ICU. The design of the regression analysis followed the original method published previously (Balik et al., 2022), now with added data on imaging. The linear regression analysis and the Mantel-Haenszel test was performed in order to determine the odds ratio of a particular complication and its relationship to the frequency of RTG imaging. Cox proportional hazards regression analysis was used to test the various risk factors and their relationships to the outcomes. A  $p$ -value below 0.05 was considered significant.

## Results

### *Chest X-ray*

A total of 292 patients with severe ARDS were included in this analysis. Their median age was 57 years (IQR 48–69), with men comprising a total of 194 (66.4%). Out of the 292 patients, 173 were treated conservatively, and 119 (40.8%) were treated with ECMO. The characteristics of the patients relevant to chest imaging, including outcome data, are summarised in **Table 3.3.1 - 1**. The patients were divided into the obese group ( $n = 171$ , 58.6%) and the non-obese group ( $n = 121$ , 41.4%).

**Table 3.3.1 - 1 - Patient characteristics.**

	<b>BMI &gt; 30 (n = 171)</b>	<b>BMI ≤ 30 (n = 121)</b>	<b>p-Value</b>
Age (years)	56 (48–65)	61 (51–68)	<b>0.013</b>
Weight (kg)	110 (100–120)	82 (75–90)	<b>&lt;0.001</b>
Height (m)	1.74 (1.68–1.8)	1.77 (1.7–1.8)	<b>0.024</b>
BMI	35.1 (32.1–40.1)	26.3 (24.8–27.8)	<b>&lt;0.001</b>
Gender (males)	63.7% (109)	70.2% (85)	0.246
APACHE IV	87 (77–100)	90 (77–100)	0.371
SOFA	10 (8–12)	11 (8–12)	0.480
PaO <sub>2</sub> /FiO <sub>2</sub> (at admission)	75 (62–101)	75.5 (60–105)	0.883
Orotracheal intubation on admission	95.9% (164)	94.2% (114)	0.505
NIV/HFNO (days)	2 (1–4)	2 (0–5)	0.702
Tracheostomy	75.4% (129)	69.4% (84)	0.254
<b>MV parameters (at admission)</b>			
PEEP	12 (10–14)	11 (8–14)	<b>0.048</b>
driving pressure	18 (15–20)	16 (12–18)	<b>&lt;0.001</b>
plateau pressure	30 (26–34)	28 (24–30)	<b>0.002</b>
Prone position	62% (106)	59.5% (72)	0.623
VV ECMO	45% (77)	34.7% (42)	0.087
Pneumothorax	18.1% (31)	19.8% (24)	0.749
Pneumothorax in ECMO patients	26% (20)	33.3% (14)	0.404
Pneumomediastinum	8.8% (15)	9.9% (12)	0.763
Pneumomediastinum in ECMO patients	18.2% (14)	19% (8)	1.00
ICU LOS (days)	13 (7–22)	13 (6–20)	0.432
Hospital LOS (days)	27 (14–51)	27 (13–66)	0.639
ICU mortality	36.8% (63)	33.9% (41)	0.578
Hospital mortality	49.7% (85)	48.8% (59)	0.873
90-day mortality	48.5% (83)	45.5% (55)	0.603

Serial CXRs were indicated for the evaluation of respiratory apparatus (45%) and periprocedural related complications, for example, due to central line or CD placement (55%). The median number of CXRs per patient was eight (IQR 4–14) in all BMI classes. The univariate Mann–Whitney test did not find a significant relationship between the number of CXRs and ICU outcome, which was relevant for both obese (BMI > 30) and non-obese (BMI ≤ 30) patients (**Table 3.3.1 - 2**).

**Table 3.3.1 - 2** - Comparison between the number of CXRs (median, IQR) of surviving and deceased patients in the ICU.

Parameter	Surviving (Median, IQR)	Dead (Median, IQR)	p-Value
ICU outcome	7 (4; 14), <i>n</i> = 187	8 (5; 15.5), <i>n</i> = 104	0.23
ICU outcome BMI > 30	8 (5; 14.8), <i>n</i> = 107	8 (5; 13), <i>n</i> = 62	0.69
ICU outcome BMI ≤ 30	7 (3.5; 12), <i>n</i> = 80	8.5 (5; 17), <i>n</i> = 42	0.21

The number of CXRs strongly correlated with the length of stay of both the survivors and the deceased in the ICU ( $r = 0.87, p < 0.0001$ ,  $r = 0.83, p < 0.0001$ , respectively, **Figure 3.3.1 - 1**).

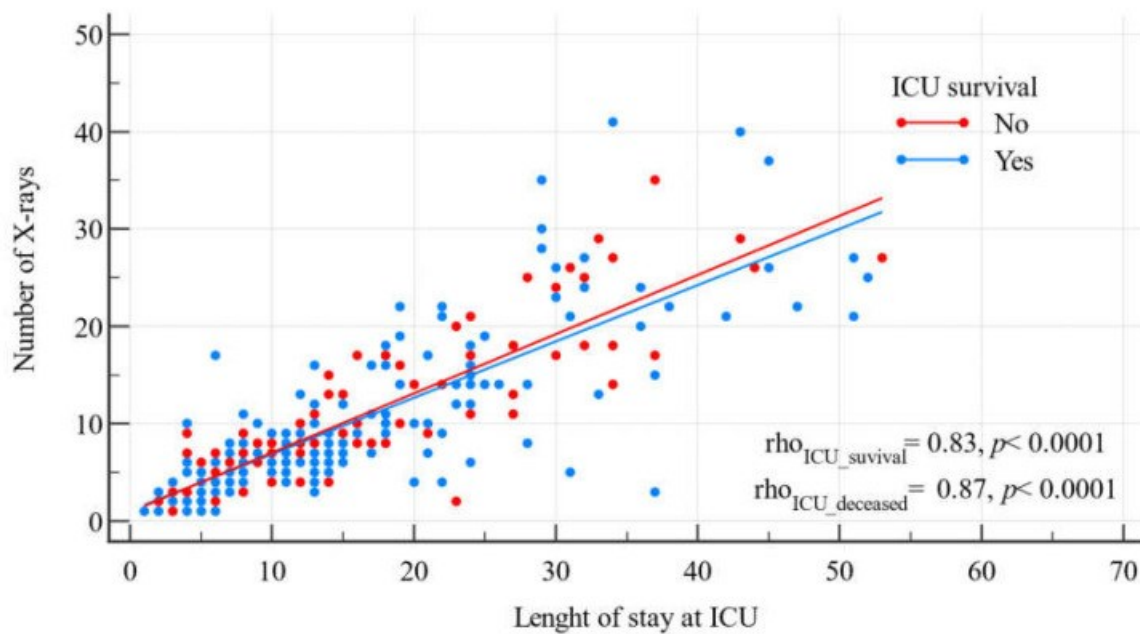


**Figure 3.3.1 - 1** - A scatter diagram showing the relationship between the number of CXRs and the length of stay in the ICU. Blue line is for ICU deceased, red line for ICU survival.

The relationship between the length of stay and ICU survival was not significant ( $p = 0.54$ ). Furthermore, to eliminate the effect of the length of stay in the ICU, the mean number of CXRs per day in the ICU unit was analysed for relationship to outcome. The mean number of CXRs per day in the ICU was  $0.7 \pm 0.32$  and did not show a significant relationship with the ICU outcome ( $p = 0.37$ ). The odds ratio (OR) for the number of CXRs per day in the



ICU for the ICU outcome was 1.2 (0.57–2.49;  $p = 0.63$ ). In addition, we analysed the multivariable combination of selected clinical factors and the mean number of CXRs per day in the ICU by multivariable logistic regression (**Table 3.3.1 - 3**). The relationship was not significant ( $p = 0.45$ ).

**Table 3.3.1 - 3** - Multivariable logistic regression for selected complications, adverse outcome, and mean number of CXRs per day in the ICU (BMI body mass index, DM diabetes mellitus, HT hypertension, and IHD chronic intermittent haemodialysis). The significant  $p$ -values below 0.05 are in bold.

Variable	Odds Ratio	95% CI	$p$ Value
Age > 50	2.59	1.22–5.09	<b>0.006</b>
Gender male	1.25	0.7–2.22	0.44
BMI > 30	1.16	0.64–2.08	0.63
ECMO yes	2.11	1.13–3.94	<b>0.02</b>
DM yes	1.39	0.73–2.62	0.32
HT yes	0.96	0.54–1.69	0.88
IHD yes	1.18	0.53–2.64	0.68
Chronic immunosuppressive therapy yes	1.71	0.69–4.21	0.25
Immunosuppression > 8 mg Dexamethasone or 40 mg Methylprednisolone yes	1.31	0.67–2.56	0.43
Pneumothorax	1.26	0.63–2.51	0.51
Barotrauma yes	0.42	0.16–1.12	0.08
Major bleeding event yes	2.1	1.01–4.37	<b>0.046</b>
Number of X-rays per day in the ICU	1.35	0.61–2.98	0.45

### *Computed Tomography*

The median number of CT scans per patient was zero (IQR 0–1) because only 26.5% of patients with a BMI of 18–40 had at least one CT scan per ICU stay. A total of 145 CT scans were ordered for 77 patients with severe ARDS from the entire cohort of 291 patients. The rates of CT scanning were 26–33% across the classes of BMI, except for the morbidly obese patients (BMI > 40) who required a CT scan in 14% of the cases. The highest BMI of a patient with a CT scan was 44.2. The median number of CT scans in those who had at least one CT scan was one (IQR 1–2).

The indications for CT scans were mainly CT of the brain for a suspected intracranial pathology (74 scans), CT angiography indicated typically for a suspected pulmonary embolism (50 scans), and CT of the trunk obtained mostly to search for the source of sepsis or abdominal pathology (21 scans).

The relationship between the number of CT scans and the ICU outcome was evaluated with respect to the BMI (18–44.2) and ECMO therapy. The study did not find any differences in outcomes related to the presence of a CT scan performed, ECMO therapy, or the length of stay in the ICU (**Table 3.3.1 - 4**).

**Table 3.3.1 - 4** - Comparison of CT scan rates (percentage, numbers) between survivors and deceased in the ICU.

Parameter	% CT among Surviving (No. of Probands)	% CT among Dead (No. of Probands)	<i>p</i> -Value
ICU outcome	29% (49)	25.8% (25)	0.67
ICU outcome ECMO	42.9% (24)	30.6% (15)	0.23
ICU outcome without ECMO	22.3% (25)	20.8% (10)	1.0
ICU LOS (days)	12 (6–19)	12 (8–20)	0.45

The ICU outcome of all patients treated with ECMO who required a CT scan (only patients with BMI < 45) was not different (49% rates of ECMO in the surviving vs. 60% in the deceased,  $p = 0.46$ ). The absence of a CT scan in patients on ECMO, however, predicted the prognosis of patients (29.1% in survivors vs. 47.4% in deceased in the ICU,  $p = 0.01$ ). The odds ratio (OR) for survival associated with ordering a CT scan (Cox analysis) for ECMO patients was 0.48,  $p = 0.01$ .

To evaluate the impact of selected diagnostic and therapeutic factors in relation to the purchased CXRs, CT scans, and ICU outcome, we performed the Mantel-Haenszel analysis, which calculated the OR for the presence of a particular complication. For the analysis, we used the mean CXR number per day in the ICU as a cut-off value (**Figure 3.3.1 - 1**). CT scanning was shown to be not statistically significant in relation to the length of stay in the ICU and an adverse outcome. The Mantel-Haenszel analysis showed a total effect of the

various selected clinical factors on the impact of less or more frequent radiographic imaging close to one (0.9,  $p = 0.15$ ), which was not significant.

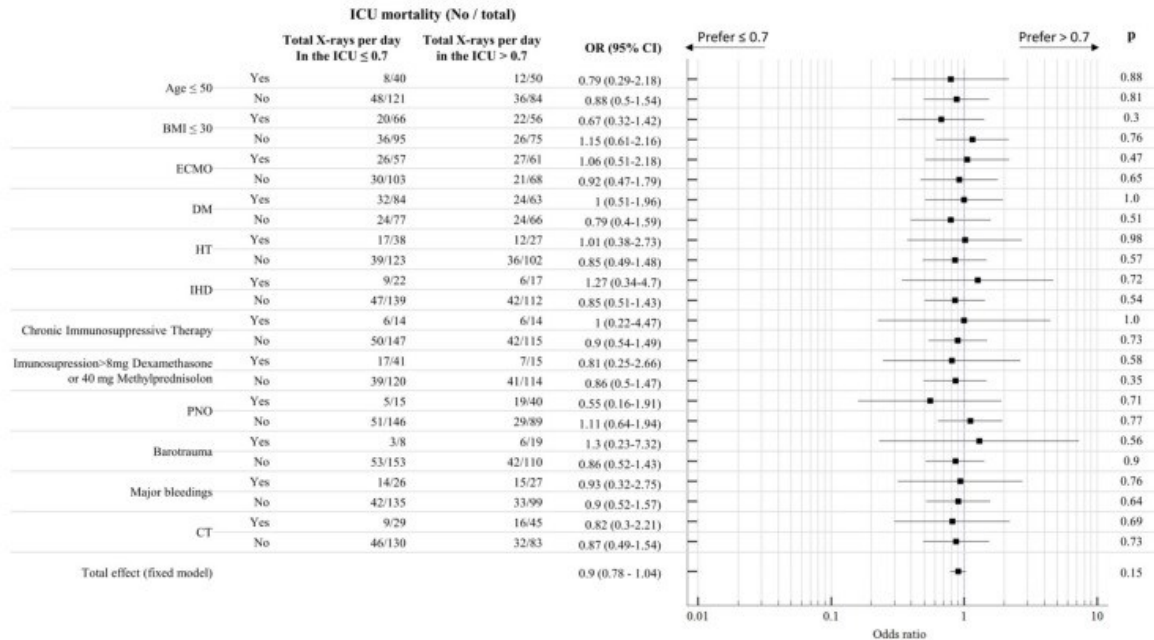


**Figure 3.3.1 - 1** - Mantel–Haenszel analysis of factors tested for their relationship to the adverse outcome (death in the ICU) - the mean CXR number per day in the ICU and ICU outcome. The total effect of 0.9 represents the impact of selected variables on the impact of imaging on the patient's outcome.

Financial analysis of our data calculated an average cost of EUR 459 for a whole-body CT scan and EUR 304 for a head or chest CT. With CT scan rates in our cohort being 27%, the estimated savings on 292 patients with severe ARDS was EUR 98.685 if a CT had been ordered in all 100% cases over two years, compared to only 27% of the patients in whom the CT scans were indicated.

The aforementioned hypothesis (the frequency of CXRs and CTs might not relate to ICU outcome in patients with severe COVID-19 ARDS treated with ECMO) was confirmed.

## 4 Discussion

LUS has cemented itself in the area of critical care as the workhorse of critical care imaging. Our work which has been presented herein investigated 3 aspects: CD positioning on CXR and LUS, challenging the established method of quantifying PE<sub>v</sub> on LUS in patients with heavily consolidated lungs and the impact of serial imaging with the growing popularity of LUS on the ICU outcome of patients with COVID-19 ARDS treated with ECMO.

The detection of malposition of CD inserted for PNO in supine CXR is difficult because it is not readily obvious and there are no specific signs to identify it. Our **first study** thus evaluated simple parameters measured or derived from bedside CXR (gold standard follow-up method after CD insertion) that could raise suspicion of CD malposition after insertion for PNO drainage through the safe triangle in non-trauma mechanically ventilated critically ill patients. Greater foreshortening of the CD and a steep angle of inclination of the CD above the horizontal at chest entry should raise suspicion of CD migration and mandate further investigation by LUS to rule out a residual PNO occult on CXR. In this study, we assumed that a migrating CD inserted from the safe triangle would turn upward and laterally and later dorsally and that this trajectory would result in the CD pointing steeply upward after entering the pleural cavity and later foreshortening on CXR (**Figure 4.1**).

It is important to consider the implications of detecting CD malposition, especially in the context of non-trauma patients with respiratory failure on aggressive IPPV. While some suggested that hemodynamically stable mechanically ventilated patients should be only observed (C. G. Ball et al., 2010; Kirkpatrick et al., 2013), other studies were inconclusive (Ouellet et al., 2009). In contrast to occult PNOs in trauma that do not always require chest drainage (C. G. Ball et al., 2010; Kirkpatrick et al., 2013; Ouellet et al., 2009) the rates of PNO progression may be higher in non-trauma patients and those with respiratory failure on aggressive IPPV as they may therefore potentially enlarge due to positive respiratory pressure (Brook et al., 2009).

The potential consequences of a secondary occult or small residual ventral PNO in patients on IPPV may limit lung recruitment, and as thus cause increased requirements for mechanical ventilation, and hindered weaning, and may potentially enlarge and progress into a life-

threatening tension PNO (Baldt et al., 1995; Ball et al., 2003; Enderson et al., 1993; Karnik & Khan, 2001; Lim et al., 2005). This highlights the importance of accurately identifying CD malposition in these patients.

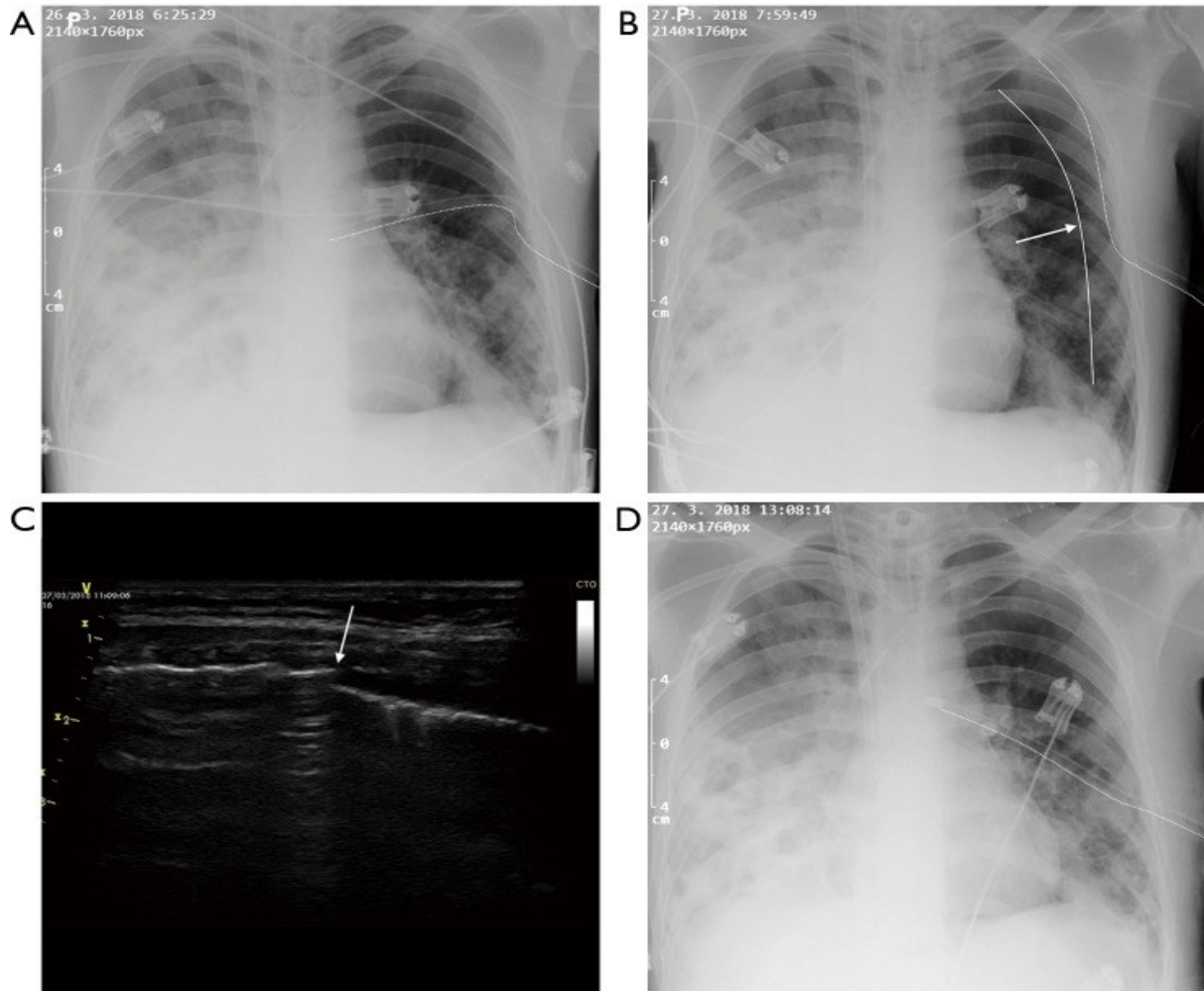


**Figure 4.1** - An example of a supine CXR after CD (white dotted line) insertion for left-sided spontaneous PNO in a patient on veno-arterio-venous ECMO (A). The next supine CXR (B, after 24 h) taken whilst the patient was on pressure support ventilation showed apparent axillar dislocation of the CD that had not moved at the insertion site. The patient's status was complicated by a recurrent PNO diagnosed with LUS by the typical appearance of the lung-point (C, here in the 5<sup>th</sup> intercostal space). The PNO was medial from the solid white line (see B) drawn through the lung point depicted by LUS (C). The control CXR (D, after re-drainage) showed a correct position of the CD (white dotted line) inserted for PNO from the safe triangle.

To our best knowledge, this is the first study to systematically evaluate the malposition of a CD for PNO drainage from parameters assessed on CXR.

In the **second study**, we went further to utilize LUS to locate the CD post-drainage, since LUS provides a non-invasive and bedside method that can potentially rule out the presence of a residual PNO post-drainage and potentially eliminating the need for a thoracic CT scan and reducing the risk associated with patient transport.

This study shows that a CD may be located on LUS under the anterior chest wall in 86% of patients post-drainage and represents an important sign of successful pleural drainage with full lung expansion, an aspect that has not been described so far (**Figure 4.2**) to the best of our knowledge. Failure to locate the CD carries a significant risk of a residual PNO occult on CXR, which must be excluded on LUS (Volpicelli et al., 2012). The presence of a CD in between the pleural layers on LUS represents an additional important sign excluding a residual PNO, particularly in the apical lung regions with limited lung sliding and lung pulse (Lichtenstein & Menu, 1995). With its limitations caused by interfering ribs, the findings may help to exclude a PNO particularly in lung hyperinflation like in COPD, bullous emphysema, post thoracic surgery, and in patients with consolidated lungs on ECMO and a lung-protective mechanical ventilation. Furthermore, a parallel course of the CD to a rib was found in 10% of patients without any other LUS signs of a PNO.

This finding coupled with the findings of the 1st study may further optimise patient care, seeing as the degree of CD foreshortening on CXR estimated with the help of a CDI implies a high risk of an occult ventral pneumothorax (**Figure 3.1.2 - 2**). Another clinical finding that warrants the exclusion of an occult/residual PNO by LUS is a continuous air leak from the inserted CD. In contrast to the conclusions of the 1st study, the risk of a residual/occult pneumothorax is likely not significant with a steep angle of inclination of the CD found on CXR.

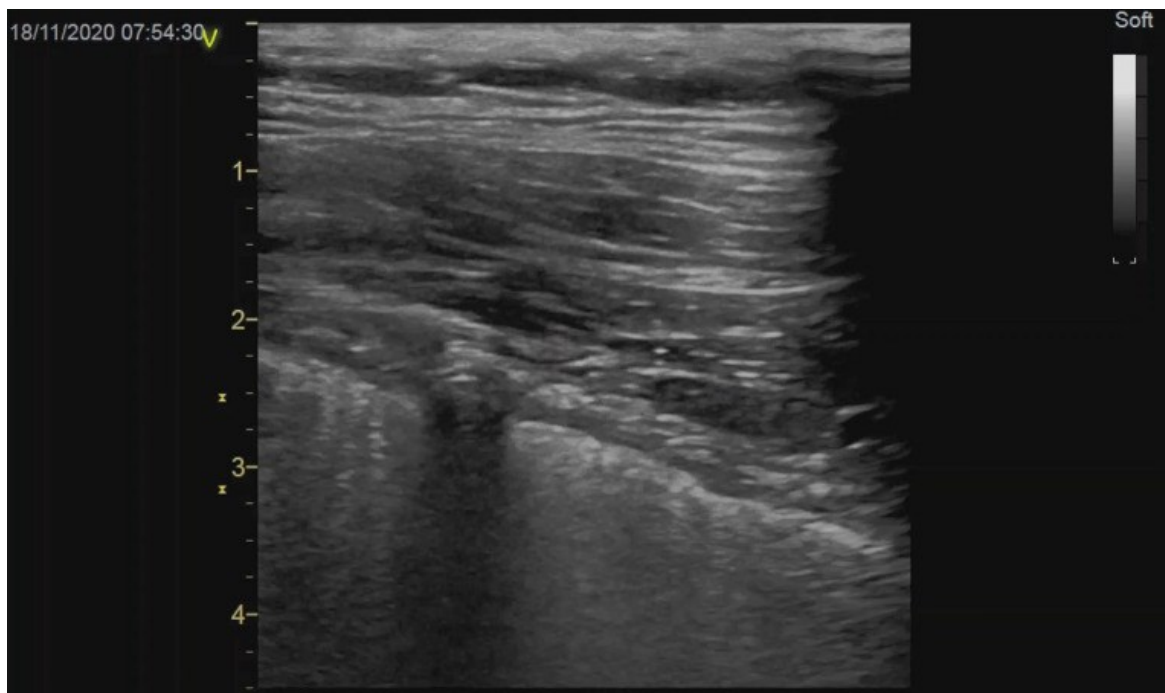


**Figure 4.2** - Chest ultrasound of the anterior chest wall in a patient with COVID-19 ARDS after drainage of a PNO due to barotrauma. The linear transducer depicts a CD in the transverse plane in between the enhancing visceral and parietal pleura.

In part two (**Study 3**), LUS has proven to be a valuable tool in the assessment of PE and PEv in patients with severe ARDS treated with ECMO. As our research highlights, there are certain factors that can impact the accuracy of the assessment of PEv in these patients. The method of multiplying the maximum transverse pleural separation at the base of the lung in millimetres by 20 has been formulated and independently verified in mechanically ventilated patients (Balik et al., 2006; Peris et al., 2010). This method assumes an aerated lung floating in pleural fluid but may not be accurate in extensively consolidated and less buoyant lungs which greatly displace the PE, particularly in severe ARDS treated with ECMO. This inaccuracy opens the door to large prediction errors and an underestimation of the PEv in patients with extensive lung consolidations which may therefore be detrimental to patient care.

In the concluding part of our work (**Study 4**), we sought to shed light on the impact of radiographic imaging methods on the ICU outcomes of critically ill patients with severe ARDS. The findings revealed intriguing insights into the potential benefits of routine bedside

CXR imaging in aggressively ventilated patients with severe cardiorespiratory failure, particularly those undergoing ECMO treatment. In this arena, our study showed potential benefit of routine bedside CXRs in aggressively ventilated patients with severe cardiorespiratory failure. Considering the ventilator settings (**Table 3.3.1 - 1**) and the barotrauma rates of up to 33%, this approach seems to be fully justified. Importantly, 2/3 of the patients were obese, and 1/5 were morbidly obese (Balik et al., 2022), increasing the side effects and risks of mechanical ventilation. Obesity causes functional changes in the respiratory system, leading to decreased end-expiratory lung volume, increased incidence of airway closure, and atelectasis formation, as well as modifications in lung and chest wall mechanics. These changes account for the high incidence of gas exchange impairment, alterations in respiratory mechanics, and hemodynamic compromise (Ball & Pelosi, 2019; De Jong et al., 2020). From a pathophysiological perspective, it is also worth noting that adiposity is linked to the production of various inflammatory mediators and hormones (e.g. leptin) (Silva et al., 2012).

Albeit retrospective, this study shows that, besides some primary indications, the need for CT scanning did not correlate with better survival outcomes in the ICU, suggesting that the frequency of radiographic imaging was not a determining factor in the ICU outcome of aggressively ventilated patients. It should be noted that patients who needed fewer CT scans tended to experience a more favourable disease course, indicating a potential link between the frequency of radiographic imaging and disease-related complications.

A combination of ultrasound, echocardiography, and CXR appeared to be sufficient for up to 3/4 of patients with severe ARDS, avoiding the need for a CT scan. The CT scanning approach can have negative implications due to the transfer of ICU patients to the radiology suite, which is not always safe in severe illnesses with the risk of instability associated with transport (Beckmann et al., 2004; Foley et al., 2002; Revel et al., 2020; Richmond et al., 2018). There is also an increased transport-associated workload for the ICU staff, which can be a sensitive issue at times of shortage. Epidemiology issues and the transmission of contagious diseases, e.g., COVID-19, are important factors with implications for an out-of-ICU environment where disinfection and cleaning are required in the CT suite, which can interrupt routine work.



Moreover, whilst delving into the financial implications of CT imaging on the reimbursement of care, coupled with the logistical challenges and safety concerns associated, we found that the rates of CT in our cohort around 27%, therefore, the estimated savings on 292 patients with severe ARDS were up to EUR 100.000 if a CT had been ordered in 100% of cases over the period of two years. This underscores the multifaceted impact of imaging methods on the healthcare system as a whole.

### **Limitations and challenges of the studies**

Lung ultrasound is a valuable diagnostic tool for various respiratory conditions, but it does have some limitations. One of the main limitations is that it can be less sensitive in detecting small or distant lesions compared to other imaging techniques such as CT scans. Additionally, the interpretation of lung ultrasound images can be subjective and may vary between clinicians interpreting the images. Furthermore, the quality of the images may be affected by patient factors such as obesity, chest dressings, chest deformations, and subcutaneous emphysema, as well. Finally, lung ultrasound may not be suitable for all patients, particularly those with severe respiratory distress.

In **part one**, due to the retrospective nature of the study one, the study was limited by the small number of patients with malpositioned CDs, which therefore raises important considerations for further research. Future studies may benefit from a prospective design with a larger patient population to investigate and validate the utility of CD foreshortening and the angle of inclination of the CD. Furthermore, exploring the potential impact of different radiographic techniques on the measured parameters could provide valuable information on the reliability and reproducibility of these findings in clinical practice. The limitations posed by interobserver variability in the study warrant further exploration in the form of a multivariate analysis combining significant findings such as CD position on LUS, CDI, and air leak, which could lead to a more precise interpretation.

In **part two** (study 3), potential sources of error included variability of mean airway pressures regardless of a PEEP close to 10cmH<sub>2</sub>O in all patients on ECMO, and interobserver variability, which sheds light on the potential challenges in accurately assessing pleural fluid volume and lung consolidations using LUS.

In **part three** (study 4), the retrospective nature of the analysis and the lack of data on potential further imaging methods undertaken post-discharge from the ICU may have impacted the assessment of hospital outcomes. Furthermore, seeing as the CT table has a weight limitation, availability of this method for some extremely obese patients may have been limited.

### **Benefit of our work**

Addressing the aforementioned shortcomings and research gaps, the whole purpose of this dissertation work was to comprehensively explore the relationship between radiographic imaging methods (CT/CXR) in critically ill patients in the era of growing use of LUS which provides valuable insight into the potential benefits and considerations associated with different imaging modalities. The findings underscore the need for a nuanced approach to imaging in the intensive care setting, considering not only patient safety, but also clinical efficacy, financial, logistical, and patient-centred factors to provide tailored, high-quality patient care.

LUS can be used in resource limited settings, especially in third world countries where there is a lack of trained radiologists and infrastructure limitations pertaining to CT scan availability. This means that clinicians who are well trained can offer and provide accurate care and make clinical decisions that will better benefit the patient.

In the context of Czech Republic, where LUS is largely being done by pulmonologists and critical care clinicians, there should be a push for radiologists to integrate into the training of LUS in the form of courses and lectures, so they can be better versed with the aspects of LUS and participate in the image gently movement (paediatric imaging) and the ALARA principle.

### **Future trends**

One future trend in LUS is the increasing use of artificial intelligence (AI), deep learning (DL), and machine learning algorithms (MLA) which can be used to analyse LUS images

automatically and to aid the non-expert clinician in interpreting the images. This can help to improve the accuracy and speed of diagnosis, as well as to identify early signs of lung disease (Khan et al., 2023; Kuroda et al., 2023; Nhat et al., 2023; Russell et al., 2021; Wang et al., 2022). Furthermore, in the advent of infectious diseases, such as the recent COVID-19, where there is use of AI-robotics and tele-examination to remotely examine patients in order to curb cross contamination in these instances (Akbari et al., 2021; Al-Zogbi et al., 2021; Wang et al., 2021, 2022).

Another interesting emerging avenue pertaining to LUS is the use of contrast enhanced lung ultrasound (CEUS). So far, studies have looked at peripheral consolidations where they sought to differentiate neoplastic from non-neoplastic peripheral consolidations (Sartori et al., 2013). Trenker et al. (Trenker et al., 2017) sought to objectivise findings of peripheral pleural consolidations in patients with no signs on PE on CT but are clinically suspected of a PE and concluded that these consolidations likely represented embolic consolidations. Other studies (Tee et al., 2020; Yusuf et al., 2022) in this field have recently looked at subpleural consolidations seen in COVID-19 patients and have characterized them as microinfarcts as they were found to be avascular.

## 5 Conclusion

LUS has cemented itself in the area of critical care as the workhorse of critical care imaging where different lung pathologies can be examined.

Our work investigated CD positioning on CXR and LUS and we showed that it can be related to residual pneumothoraces which are potentially harmful in mechanically ventilated patients. We also challenged the established method of quantifying PEv on LUS in patients with heavily consolidated lungs on ECMO and we found out that there is an underestimation of PEv in this subset of patients. Lastly, a combination of LUS, echocardiography, and CXR appeared to be sufficient in up to 3/4 of patients with severe ARDS, avoiding the need for serial CT scanning as it did not correlate with better survival outcomes in the ICU.

As more clinicians receive training in lung ultrasound, and ultrasound technology continues to advance (CEUS, AI), widespread integration of LUS into clinical practice is expected, especially in third world countries where resources are limited. Overall, lung ultrasound holds great promise as a cost-effective and efficient diagnostic modality for respiratory diseases not only in the critically ill, but also in patients with various pulmonary pathologies. Furthermore, we also advocate for LUS to be incorporated into the training of radiologists so that they participate in the image gently movement (paediatric imaging) and the ALARA principle.

## 6 References

- Agricola, E., Bove, T., Oppizzi, M., Marino, G., Zangrillo, A., Margonato, A., & Picano, E. (2005). "Ultrasound comet-tail images": A marker of pulmonary edema - A comparative study with wedge pressure and extravascular lung water. *Chest*, 127(5), 1690–1695. <https://doi.org/10.1378/chest.127.5.1690>
- Akbari, M., Carriere, J., Meyer, T., Sloboda, R., Husain, S., Usmani, N., & Tavakoli, M. (2021). Robotic Ultrasound Scanning With Real-Time Image-Based Force Adjustment: Quick Response for Enabling Physical Distancing During the COVID-19 Pandemic. *Frontiers in Robotics and AI*, 8, 645424. <https://doi.org/10.3389/FROBT.2021.645424/BIBTEX>
- Al-Zogbi, L., Singh, V., Teixeira, B., Ahuja, A., Bagherzadeh, P. S., Kapoor, A., Saeidi, H., Fleiter, T., & Krieger, A. (2021). Autonomous Robotic Point-of-Care Ultrasound Imaging for Monitoring of COVID-19–Induced Pulmonary Diseases. *Frontiers in Robotics and AI*, 8, 645756. <https://doi.org/10.3389/FROBT.2021.645756/BIBTEX>
- Andy Adam, Adrian K. Dixon, Jonathan H Gillard, & Cornelia Schaefer-Prokop (Eds.). (2021). *Grainger & Allison's Diagnostic Radiology* (7th ed., Vol. 1). Elsevier.
- Baldt, M. M., Bankier, A. A., Germann, P. S., Pöschl, G. P., Skrbensky, G. T., & Herold, C. J. (1995). Complications after emergency tube thoracostomy: assessment with CT. *Radiology*, 195(2), 539–543. <https://doi.org/10.1148/RADIOLOGY.195.2.7724780>
- Balik, M., Maly, M., Huptych, M., Mokotedi, M. C., & Lambert, L. (2023). Prognostic Impact of Serial Imaging in Severe Acute Respiratory Distress Syndrome on the Extracorporeal Membrane Oxygenation. *Journal of Clinical Medicine* 2023, Vol. 12, Page 6367, 12(19), 6367. <https://doi.org/10.3390/JCM12196367>
- Balik, M., Mokotedi, M. C., Maly, M., Otahal, M., Stach, Z., Svobodova, E., Flaksa, M., Rulisek, J., Brozek, T., & Porizka, M. (2022). Pulmonary consolidation alters the ultrasound estimate of pleural fluid volume when considering chest drainage in patients on ECMO. *Critical Care*, 26(1), 1–4. <https://doi.org/10.1186/S13054-022-04018-9/FIGURES/1>
- Balik, M., Plasil, P., Waldauf, P., Pazout, J., Fric, M., Otahal, M., & Pachtl, J. (2006). Ultrasound estimation of volume of pleural fluid in mechanically ventilated patients. *Intensive Care Medicine*, 32(2), 318–321. <https://doi.org/10.1007/s00134-005-0024-2>

- Balik, M., Svobodova, E., Porizka, M., Maly, M., Brestovansky, P., Volny, L., Brozek, T., Bartosova, T., Jurisinova, I., Mevaldova, Z., Misovic, O., Novotny, A., Horejsek, J., Otahal, M., Flaksa, M., Stach, Z., Rulisek, J., Trachta, P., Kolman, J., ... Blaha, J. (2022). The impact of obesity on the outcome of severe SARS-CoV-2 ARDS in a high volume ECMO centre: ECMO and corticosteroids support the obesity paradox. *Journal of Critical Care*, 72, 154162. <https://doi.org/10.1016/J.JCRC.2022.154162>
- Ball, C. G., Dente, C. J., Kirkpatrick, A. W., Shah, A. D., Rajani, R. R., Wyrzykowski, A. D., Vercurysse, G. A., Rozycki, G. S., Nicholas, J. M., Salomone, J. P., & Feliciano, D. V. (2010). Occult pneumothoraces in patients with penetrating trauma: Does mechanism matter? *Canadian Journal of Surgery*, 53(4), 251. <https://doi.org/10.1016/j.yccm.2010.11.046>
- Ball, C. G., Hameed, S. M., Evans, D., Kortbeek, J. B., & Kirkpatrick, A. W. (2003). Occult pneumothorax in the mechanically ventilated trauma patient. In *Canadian Journal of Surgery* (Vol. 46, Issue 5, pp. 373–379). Canadian Medical Association. </pmc/articles/PMC3211710/?report=abstract>
- Ball, L., & Pelosi, P. (2019). How i ventilate an obese patient. *Critical Care*, 23(1), 1–3. <https://doi.org/10.1186/S13054-019-2466-X/FIGURES/1>
- Beckmann, U., Gillies, D. M., Berenholtz, S. M., Wu, A. W., & Pronovost, P. (2004). Incidents relating to the intra-hospital transfer of critically ill patients. An analysis of the reports submitted to the Australian Incident Monitoring Study in Intensive Care. *Intensive Care Medicine*, 30(8), 1579–1585. <https://doi.org/10.1007/S00134-004-2177-9>
- Boles, J.-M., Bion, J., Connors, A., Herridge, M., Marsh, B., Melot, C., Pearl, R., Silverman, H., Stanchina, M., Vieillard-Baron, A., & Welte, T. (2007). Weaning from mechanical ventilation. *European Respiratory Journal*, 29(5), 1033–1056. <https://doi.org/10.1183/09031936.00010206>
- Bompard, F., Monnier, H., Saab, I., Tordjman, M., Abdoul, H., Fournier, L., Sanchez, O., Lorut, C., Chassagnon, G., & Revel, M. P. (2020). Pulmonary embolism in patients with COVID-19 pneumonia. In *European Respiratory Journal* (Vol. 56, Issue 1). European Respiratory Society. <https://doi.org/10.1183/13993003.01365-2020>
- Bouhemad, B., Dransart-Rayé, O., Mojoli, F., & Mongodi, S. (2018). Lung ultrasound for diagnosis and monitoring of ventilator-associated pneumonia. *Annals of Translational Medicine*, 6(21), 5–5. <https://doi.org/10.21037/ATM.2018.10.46>

- Bouhemad, B., Mongodi, S., Via, G., & Rouquette, I. (2015). Ultrasound for “lung monitoring” of ventilated patients. In *Anesthesiology* (Vol. 122, Issue 2, pp. 437–447). Lippincott Williams and Wilkins. <https://doi.org/10.1097/ALN.0000000000000558>
- Bouhemad, B., Zhang, M., Lu, Q., & Rouby, J. J. (2007). Clinical review: Bedside lung ultrasound in critical care practice. In *Critical Care* (Vol. 11, Issue 1, p. 205). <https://doi.org/10.1186/cc5668>
- Brook, O. R., Beck-Razi, N., Abadi, S., Filatov, J., Ilivitzki, A., Litmanovich, D., & Gaitini, D. (2009). Sonographic detection of pneumothorax by radiology residents as part of extended focused assessment with sonography for trauma. *Journal of Ultrasound in Medicine : Official Journal of the American Institute of Ultrasound in Medicine*, 28(6), 749–755. <https://doi.org/10.7863/JUM.2009.28.6.749>
- Caltabeloti, F. P., Monsel, A., Arbelot, C., Brisson, H., Lu, Q., Gu, W. J., Zhou, G. J., Auler, J. O. C., & Rouby, J. J. (2014). Early fluid loading in acute respiratory distress syndrome with septic shock deteriorates lung aeration without impairing arterial oxygenation: A lung ultrasound observational study. *Critical Care*, 18(3), R91. <https://doi.org/10.1186/cc13859>
- Corradi, F., Brusasco, C., & Pelosi, P. (2014). Chest ultrasound in acute respiratory distress syndrome. *Current Opinion in Critical Care*, 20(1), 98–103. <https://doi.org/10.1097/MCC.0000000000000042>
- De Jong, A., Wrigge, H., Hedenstierna, G., Gattinoni, L., Chiumello, D., Frat, J. P., Ball, L., Schetz, M., Pickkers, P., & Jaber, S. (2020). How to ventilate obese patients in the ICU. *Intensive Care Medicine*, 46(12), 2423. <https://doi.org/10.1007/S00134-020-06286-X>
- Dres, M., Dubé, B. P., Goligher, E., Vorona, S., Demiri, S., Morawiec, E., Mayaux, J., Brochard, L., Similowski, T., & Demoule, A. (2020). Usefulness of Parasternal Intercostal Muscle Ultrasound during Weaning from Mechanical Ventilation. *Anesthesiology*, 132(5), 1114–1125. <https://doi.org/10.1097/ALN.00000000000003191>
- Enderson, B. L., Abdalla, R., Frame, S. B., Casey, M. T., Gould, H., & Maull, K. (1993). Tube thoracostomy for occult pneumothorax: a prospective randomized study of its use. *The Journal of Trauma*, 35(5), 726–729; discussion 729. <https://doi.org/10.1097/00005373-199311000-00013>
- Engdahl, O., Toft, T., & Boe, J. (1993). Chest Radiograph—A Poor Method for Determining the Size of a Pneumothorax. *Chest*, 103(1), 26–29. <https://doi.org/10.1378/CHEST.103.1.26>

- Esmadi, M., Lone, N., Ahmad, D. S., Onofrio, J., & Brush, R. G. (2013). Multiloculated pleural effusion detected by ultrasound only in a critically-ill patient. *American Journal of Case Reports*, *14*, 63–66. <https://doi.org/10.12659/AJCR.883816>
- Ferguson, N. D., Fan, E., Camporota, L., Antonelli, M., Anzueto, A., Beale, R., Brochard, L., Brower, R., Esteban, A., Gattinoni, L., Rhodes, A., Slutsky, A. S., Vincent, J. L., Rubinfeld, G. D., Taylor Thompson, B., & Marco Ranieri, V. (2012). The Berlin definition of ARDS: An expanded rationale, justification, and supplementary material. *Intensive Care Medicine*, *38*(10), 1573–1582. <https://doi.org/10.1007/S00134-012-2682-1/TABLES/4>
- Foley, D. S., Pranikoff, T., Younger, J. G., Swaniker, F., Hemmila, M. R., Remenapp, R. A., Copenhaver, W., Landis, D., Hirschl, R. B., & Bartlett, R. H. (2002). A review of 100 patients transported on extracorporeal life support. *ASAIO Journal (American Society for Artificial Internal Organs : 1992)*, *48*(6), 612–619. <https://doi.org/10.1097/00002480-200211000-00007>
- Goligher, E. C., Leis, J. A., Fowler, R. A., Pinto, R., Adhikari, N. K. J., & Ferguson, N. D. (2011). Utility and safety of draining pleural effusions in mechanically ventilated patients: A systematic review and meta-analysis. *Critical Care*, *15*(1). <https://doi.org/10.1186/cc10009>
- Guérin, C., Albert, R. K., Beitler, J., Gattinoni, L., Jaber, S., Marini, J. J., Munshi, L., Papazian, L., Pesenti, A., Vieillard-Baron, A., & Mancebo, J. (2020). Prone position in ARDS patients: why, when, how and for whom. *Intensive Care Med*, *46*, 2385–2396. <https://doi.org/10.1007/s00134-020-06306-w>
- Havelock, T., Teoh, R., Laws, D., & Gleeson, F. (2010). Pleural procedures and thoracic ultrasound: British Thoracic Society pleural disease guideline 2010. *Thorax*, *65*(SUPPL. 2). <https://doi.org/10.1136/thx.2010.137026>
- Huang, C., Wang, Y., Li, X., Ren, L., Zhao, J., Hu, Y., Zhang, L., Fan, G., Xu, J., Gu, X., Cheng, Z., Yu, T., Xia, J., Wei, Y., Wu, W., Xie, X., Yin, W., Li, H., Liu, M., ... Cao, B. (2020). Clinical features of patients infected with 2019 novel coronavirus in Wuhan, China. *The Lancet*, *395*(10223), 497–506. [https://doi.org/10.1016/S0140-6736\(20\)30183-5](https://doi.org/10.1016/S0140-6736(20)30183-5)
- Ibarra-Estrada, M., Gamero-Rodríguez, M. J., García-De-Acilu, M., Roca, O., Sandoval-Plascencia, L., Aguirre-Avalos, G., García-Salcido, R., Aguirre-Díaz, S. A., Vines, D. L., Mirza, S., Kaur, R., Weiss, T., Guerin, C., & Li, J. (2020). *Lung ultrasound response*



*to awake prone positioning predicts the need for intubation in patients with COVID-19 induced acute hypoxemic respiratory failure: an observational study.*  
<https://doi.org/10.1186/s13054-022-04064-3>

- Ibitoye, B. O., Idowu, B. M., Ogunrombi, A. B., & Afolabi, B. I. (2018). Ultrasonographic quantification of pleural effusion: Comparison of four formulae. *Ultrasonography*, 37(3), 254–260. <https://doi.org/10.14366/usg.17050>
- Karnik AM, & Khan FA. (2001). *Pneumothorax and barotrauma* (Parillo JE & Dellinger RP., Eds.; 2nd ed). Mosby.
- Khan, U., Afrakhteh, S., Mento, F., Fatima, N., De Rosa, L., Custode, L. L., Azam, Z., Torri, E., Soldati, G., Tursi, F., Macioce, V. N., Smargiassi, A., Inchingolo, R., Perrone, T., Iacca, G., & Demi, L. (2023). Benchmark methodological approach for the application of artificial intelligence to lung ultrasound data from COVID-19 patients: From frame to prognostic-level. *Ultrasonics*, 132, 106994. <https://doi.org/10.1016/J.ULTRAS.2023.106994>
- Kirkpatrick, A. W., Rizoli, S., Ouellet, J. F., Roberts, D. J., Sirois, M., Ball, C. G., Xiao, Z. J., Tiruta, C., Meade, M., Trottier, V., Zhu, G., Chagnon, F., & Tien, H. (2013). Occult pneumothoraces in critical care: A prospective multicenter randomized controlled trial of pleural drainage for mechanically ventilated trauma patients with occult pneumothoraces. *Journal of Trauma and Acute Care Surgery*, 74(3), 747–755. <https://doi.org/10.1097/TA.0B013E3182827158>
- Klein, J. S., Brant, W. E., Helms, C. A., & Vinson, E. N. (Eds.). (2019). *Brant and Helms' Fundamentals of Diagnostic Radiology* (5th ed.). Lippincott Williams & Wilkins (LWW).
- Ko, J. P., Liu, G., Klein, J. S., Mossa-Basha, M., & Azadi, J. R. (2020). Pulmonary COVID-19: Multimodality Imaging Examples. *RadioGraphics*, 40(7), 1893–1894. <https://doi.org/10.1148/rg.2020200158>
- Kuroda, Y., Kaneko, T., Yoshikawa, H., Uchiyama, S., Nagata, Y., Matsushita, Y., Hiki, M., Minamino, T., Takahashi, K., Daida, H., & Kagiya, N. (2023). Artificial intelligence-based point-of-care lung ultrasound for screening COVID-19 pneumoniae: Comparison with CT scans. *PLOS ONE*, 18(3), e0281127. <https://doi.org/10.1371/JOURNAL.PONE.0281127>

- Lê, M. P., Jozwiak, M., & Laghnam, D. (2022). Current Advances in Lung Ultrasound in COVID-19 Critically Ill Patients: A Narrative Review. *Journal of Clinical Medicine* 2022, Vol. 11, Page 5001, 11(17), 5001. <https://doi.org/10.3390/JCM11175001>
- Lichtenstein, D. (2017). Novel approaches to ultrasonography of the lung and pleural space: Where are we now? In *Breathe* (Vol. 13, Issue 2, pp. 100–111). European Respiratory Society. <https://doi.org/10.1183/20734735.004717>
- Lichtenstein, D. A. (2014). *Lung ultrasound in the critically ill*. <http://www.annalsofintensivecare.com/content/4/1/1>
- Lichtenstein, D. A. (2015). BLUE-Protocol and FALLS-Protocol: Two applications of lung ultrasound in the critically ill. *Chest*, 147(6), 1659–1670. <https://doi.org/10.1378/chest.14-1313>
- Lichtenstein, D. A., & Menu, Y. (1995). A Bedside Ultrasound Sign Ruling Out Pneumothorax in the Critically III: Lung Sliding. *Chest*, 108(5), 1345–1348. <https://doi.org/10.1378/CHEST.108.5.1345>
- Lichtenstein, D. A., & Mezière, G. A. (2008a). Relevance of Lung Ultrasound in the Diagnosis of Acute Respiratory Failure. *Chest*, 134(1), 117. <https://doi.org/10.1378/CHEST.07-2800>
- Lichtenstein, D. A., & Mezière, G. A. (2008b). Relevance of lung ultrasound in the diagnosis of acute respiratory failure the BLUE protocol. *Chest*, 134(1), 117–125. <https://doi.org/10.1378/chest.07-2800>
- Lichtenstein, D., Mezière, G., & Seitz, J. (2009). The dynamic air bronchogram: A lung ultrasound sign of alveolar consolidation ruling out atelectasis. *Chest*, 135(6), 1421–1425. <https://doi.org/10.1378/chest.08-2281>
- Lim, K. E., Tai, S. C., Chan, C. Y., Hsu, Y. Y., Hsu, W. C., Lin, B. C., & Lee, K. T. (2005). Diagnosis of malpositioned chest tubes after emergency tube thoracostomy: Is computed tomography more accurate than chest radiograph? *Clinical Imaging*, 29(6), 401–405. <https://doi.org/10.1016/J.CLINIMAG.2005.06.032>
- Maly, M., Mokotedi, M. C., Svobodova, E., Flaksa, M., Otahal, M., Stach, Z., Rulisek, J., Brozek, T., Porizka, M., & Balik, M. (2022). Interpleural location of chest drain on ultrasound excludes pneumothorax and associates with a low degree of chest drain foreshortening on the antero-posterior chest X-ray. *Ultrasound Journal*, 14(1), 1–7. <https://doi.org/10.1186/S13089-022-00296-0/FIGURES/5>

- Maw, A. M., Hassanin, A., Ho, P. M., McInnes, M. D. F., Moss, A., Juarez-Colunga, E., Soni, N. J., Miglioranza, M. H., Platz, E., DeSanto, K., Sertich, A. P., Salame, G., & Daugherty, S. L. (2019). Diagnostic Accuracy of Point-of-Care Lung Ultrasonography and Chest Radiography in Adults With Symptoms Suggestive of Acute Decompensated Heart Failure: A Systematic Review and Meta-analysis. *JAMA Network Open*, 2(3), e190703. <https://doi.org/10.1001/JAMANETWORKOPEN.2019.0703>
- Mokotedi, C. M., & Balik, M. (2017). Is the mechanism of re-expansion pulmonary oedema in a heart-lung interaction? *BMJ Case Reports*, 2017. <https://doi.org/10.1136/bcr-2017-219340>
- Mokotedi, M. C., Lambert, L., Simakova, L., Lips, M., Zakharchenko, M., Rulisek, J., & Balik, M. (2018). X-ray indices of chest drain malposition after insertion for drainage of pneumothorax in mechanically ventilated critically ill patients. *Journal of Thoracic Disease*, 10(10), 5695–5701. <https://doi.org/10.21037/jtd.2018.09.64>
- Mokotedi, M. C., Malý, M., & Balík, M. (2023). Imaging of COVID-19 in critical care with a focus on chest ultrasound. *Anesteziologie a Intenzivní Medicina*, 34(2), 61–68. <https://doi.org/10.36290/AIM.2023.022>
- Nazerian, P., Vanni, S., Volpicelli, G., Gigli, C., Zanobetti, M., Bartolucci, M., Ciavattone, A., Lamorte, A., Veltri, A., Fabbri, A., & Grifoni, S. (2014). Accuracy of point-of-care multiorgan ultrasonography for the diagnosis of pulmonary embolism. *Chest*, 145(5), 950–957. <https://doi.org/10.1378/chest.13-1087>
- Nazerian, P., Volpicelli, G., Gigli, C., Becattini, C., Papa, G. F. S., Grifoni, S., & Vanni, S. (2017). Diagnostic Performance of Wells Score Combined With Point-of-care Lung and Venous Ultrasound in Suspected Pulmonary Embolism. *Academic Emergency Medicine*, 24(3), 270–280. <https://doi.org/10.1111/ACEM.13130>
- Nhat, P. T. H., Van Hao, N., Tho, P. V., Kerdegari, H., Pisani, L., Thu, L. N. M., Phuong, L. T., Duong, H. T. H., Thuy, D. B., McBride, A., Xochicale, M., Schultz, M. J., Razavi, R., King, A. P., Thwaites, L., Van Vinh Chau, N., Yacoub, S., Thao, D. P., Kien, D. T., ... Gomez, A. (2023). Clinical benefit of AI-assisted lung ultrasound in a resource-limited intensive care unit. *Critical Care*, 27(1), 1–8. <https://doi.org/10.1186/S13054-023-04548-W/FIGURES/4>
- Ouellet, J. F., Trottier, V., Kmet, L., Rizoli, S., Laupland, K., Ball, C. G., Sirois, M., & Kirkpatrick, A. W. (2009). The OPTICC trial: a multi-institutional study of occult

- pneumothoraces in critical care. *The American Journal of Surgery*, 197(5), 581–586. <https://doi.org/10.1016/J.AMJSURG.2008.12.007>
- Peris, A., Tutino, L., Zagli, G., Batacchi, S., Cianchi, G., Spina, R., Bonizzoli, M., Migliaccio, L., Perretta, L., Bartolini, M., Ban, K., & Balik, M. (2010). The Use of Point-of-Care Bedside Lung Ultrasound Significantly Reduces the Number of Radiographs and Computed Tomography Scans in Critically Ill Patients. *Anesthesia & Analgesia*, 111(3), 687–692. <https://doi.org/10.1213/ANE.0b013e3181e7cc42>
- Price, L. C., McCabe, C., Garfield, B., & Wort, S. J. (2020). Thrombosis and COVID-19 pneumonia: The clot thickens! In *European Respiratory Journal* (Vol. 56, Issue 1). European Respiratory Society. <https://doi.org/10.1183/13993003.01608-2020>
- Razazi, K., Thille, A. W., Carteaux, G., Beji, O., Brun-Buisson, C., Brochard, L., & Dessap, A. M. (2014). Effects of pleural effusion drainage on oxygenation, respiratory mechanics, and hemodynamics in mechanically ventilated patients. *Annals of the American Thoracic Society*, 11(7), 1018–1024. <https://doi.org/10.1513/AnnalsATS.201404-152OC>
- Remérand, F., Dellamonica, J., Mao, Z., Ferrari, F., Bouhemad, B., Jianxin, Y., Arbelot, C., Lu, Q., Ichai, C., & Rouby, J. J. (2010). Multiplane ultrasound approach to quantify pleural effusion at the bedside. *Intensive Care Medicine*, 36(4), 656–664. <https://doi.org/10.1007/s00134-010-1769-9>
- Revel, M. P., Parkar, A. P., Prosch, H., Silva, M., Sverzellati, N., Gleeson, F., & Brady, A. (2020). COVID-19 patients and the radiology department – advice from the European Society of Radiology (ESR) and the European Society of Thoracic Imaging (ESTI). *European Radiology*, 30(9), 4903–4909. <https://doi.org/10.1007/S00330-020-06865-Y/FIGURES/5>
- Richmond, K. M., Warburton, K. G., Finney, S. J., Shah, S., & Reddi, B. A. J. (2018). Routine CT scanning of patients retrieved to a tertiary centre on veno-venous extracorporeal membrane oxygenation: a retrospective risk benefit analysis. *Perfusion*, 33(6), 438–444. <https://doi.org/10.1177/0267659118763266>
- Rocca, E., Zanza, C., Longhitano, Y., Piccolella, F., Romenskaya, T., Racca, F., Savioli, G., Saviano, A., Piccioni, A., & Mongodi, S. (2023). Lung Ultrasound in Critical Care and Emergency Medicine: Clinical Review. *Advances in Respiratory Medicine 2023, Vol. 91, Pages 203-223*, 91(3), 203–223. <https://doi.org/10.3390/ARM91030017>

- Roch, A., Bojan, M., Michelet, P., Romain, F., Bregeon, F., Papazian, L., & Auffray, J.-P. (n.d.). *Usefulness of Ultrasonography in Predicting Pleural Effusions > 500 mL in Patients Receiving Mechanical Ventilation\**. [www.chestjournal.org](http://www.chestjournal.org)
- Roncon, L., Zuin, M., Barco, S., Valerio, L., Zuliani, G., Zonzin, P., & Konstantinides, S. V. (2020). Incidence of acute pulmonary embolism in COVID-19 patients: Systematic review and meta-analysis. *European Journal of Internal Medicine*, *82*, 29–37. <https://doi.org/10.1016/J.EJIM.2020.09.006>
- Routsi, C., Stanopoulos, I., Kokkoris, S., Sideris, A., & Zakyntinos, S. (n.d.). Weaning failure of cardiovascular origin: how to suspect, detect and treat-a review of the literature. *Annals of Intensive Care*. <https://doi.org/10.1186/s13613-019-0481-3>
- Russell, F. M., Ehrman, R. R., Barton, A., Sarmiento, E., Ottenhoff, J. E., & Nti, B. K. (2021). B-line quantification: comparing learners novice to lung ultrasound assisted by machine artificial intelligence technology to expert review. *Ultrasound Journal*, *13*(1), 1–7. <https://doi.org/10.1186/S13089-021-00234-6/TABLES/5>
- Santana, P. V., Cardenas, L. Z., de Albuquerque, A. L. P., de Carvalho, C. R. R., & Caruso, P. (2020). Diaphragmatic ultrasound: A review of its methodological aspects and clinical uses. *Jornal Brasileiro de Pneumologia*, *46*(6), 1–17. <https://doi.org/10.36416/1806-3756/e20200064>
- Sartori, S., Postorivo, S., Vece, F. Di, Ermili, F., Tassinari, D., & Tombesi, P. (2013). Contrast-enhanced ultrasonography in peripheral lung consolidations: What's its actual role? *World Journal of Radiology*, *5*(10), 372. <https://doi.org/10.4329/WJR.V5.I10.372>
- Schaefer-Prokop, C. (2011). *Critical Care Radiology*. Georg Thieme Verlag.
- Silva, P. L., Pelosi, P., & Rocco, P. R. M. (2012). *Mechanical ventilation in obese patients*.
- Silva, S., Ait Aissa, D., Cocquet, P., Hoarau, L., Ruiz, J., Ferre, F., Rousset, D., Mora, M., Mari, A., Fourcade, O., Riu, B., Jaber, S., & Bataille, B. (2017). Combined Thoracic Ultrasound Assessment during a Successful Weaning Trial Predicts Postextubation Distress. *Anesthesiology*, *127*(4), 666–674. <https://doi.org/10.1097/ALN.0000000000001773>
- Silveri, N. G., Soldati, G., Testa, A., Sher, S., Pignataro, G., La, M., Monica, ;, & Sala, L. (2008). *Occult Traumatic Pneumothorax\* Diagnostic Accuracy of Lung Ultrasonography in the Emergency Department*. *133*, 204–211. <https://doi.org/10.1378/chest.07-1595>

- Silvia Mongodi, A., Bouhemad, B., Orlando, A., Stella, A., Tavazzi, G., Via, G., Antonio Iotti, G., Braschi, A., & Mojoli, F. (2017). Modified Lung Ultrasound Score for Assessing and Monitoring Pulmonary Aeration Modifizierter Lungen-US-Score zur Bewertung und Überwachung der Belüftung der Lunge. *Modified Lung Ultrasound Ultraschall in Med*, 37, 530–537. <https://doi.org/10.1055/s-0042-120260>
- Smith, M. J., Hayward, S. A., Innes, S. M., & Miller, A. S. C. (2020). Point-of-care lung ultrasound in patients with <scp>COVID</scp> -19 – a narrative review. *Anaesthesia*, 75(8), 1096–1104. <https://doi.org/10.1111/anae.15082>
- Soldati, G., Smargiassi, A., Inchingolo, R., Buonsenso, D., Perrone, T., Briganti, D. F., Perlini, S., Torri, E., Mariani, A., Mossolani, E. E., Tursi, F., Mento, F., & Demi, L. (2020). Is There a Role for Lung Ultrasound During the COVID-19 Pandemic? In *Journal of Ultrasound in Medicine* (Vol. 39, Issue 7, pp. 1459–1462). John Wiley and Sons Ltd. <https://doi.org/10.1002/jum.15284>
- Soummer, A., Perbet, S., Brisson, H., Arbelot, C., Constantin, J. M., Lu, Q., & Rouby, J. J. (2012). Ultrasound assessment of lung aeration loss during a successful weaning trial predicts postextubation distress. *Critical Care Medicine*, 40(7), 2064–2072. <https://doi.org/10.1097/CCM.0b013e31824e68ae>
- Suh, Y. J., Hong, H., Ohana, M., Bompard, F., Revel, M.-P., Valle, C., Gervaise, A., Poissy, J., Susen, S., Hékimian, G., Artifoni, M., Periard, D., Contou, D., Delaloye, J., Sanchez, B., Fang, C., Garzillo, G., Robbie, H., & Yoon, S. H. (2021). Pulmonary Embolism and Deep Vein Thrombosis in COVID-19: A Systematic Review and Meta-Analysis. *Radiology*, 298(2), E70–E80. <https://doi.org/10.1148/radiol.2020203557>
- Tee, A., Wong, A., Yusuf, G. T., Rao, D., & Sidhu, P. S. (2020). Contrast-enhanced ultrasound (CEUS) of the lung reveals multiple areas of microthrombi in a COVID-19 patient. *Intensive Care Medicine*, 46(8), 1660–1662. <https://doi.org/10.1007/S00134-020-06085-4/FIGURES/1>
- Trenker, C., Apitzsch, J. C., Pastor, S., Bartelt, S., Neesse, A., & Goerg, C. (2017). Detection of peripheral embolic consolidations using contrast-enhanced ultrasonography in patients with no evidence of pulmonary embolism on computed tomography: A pilot study. *Journal of Clinical Ultrasound*, 45(9), 575–579. <https://doi.org/10.1002/JCU.22511>
- Trezzi, M., Torzillo, D., Ceriani, E., Costantino, G., Caruso, S., Damavandi, P. T., Genderini, A., Cicardi, M., Montano, N., & Cogliati, C. (2013). Lung ultrasonography for the

- assessment of rapid extravascular water variation: Evidence from hemodialysis patients. *Internal and Emergency Medicine*, 8(5), 409–415. <https://doi.org/10.1007/s11739-011-0625-4>
- Via, G., Storti, E., Gulati, G., Neri, L., Mojoli, F., & Braschi, A. (2012). *Lung ultrasound in the ICU: from diagnostic instrument to respiratory monitoring tool*.
- Volpicelli, G. (2011). Sonographic diagnosis of pneumothorax. In *Intensive Care Medicine* (Vol. 37, Issue 2, pp. 224–232). Springer. <https://doi.org/10.1007/s00134-010-2079-y>
- Volpicelli, G., Elbarbary, M., Blaivas, M., Lichtenstein, D. A., Mathis, G., Kirkpatrick, A. W., Melniker, L., Gargani, L., Noble, V. E., Via, G., Dean, A., Tsung, J. W., Soldati, G., Copetti, R., Bouhemad, B., Reissig, A., Agricola, E., Rouby, J. J., Arbelot, C., ... Petrovic, T. (2012). International evidence-based recommendations for point-of-care lung ultrasound. *Intensive Care Medicine*, 38(4), 577–591. <https://doi.org/10.1007/s00134-012-2513-4>
- Volpicelli, G., Skurzak, S., Boero, E., Carpinteri, G., Tengattini, M., Stefanone, V., Luberto, L., Anile, A., Cerutti, E., Radeschi, G., & Frascisco, M. F. (2014). Lung Ultrasound Predicts Well Extravascular Lung Water but Is of Limited Usefulness in the Prediction of Wedge Pressure. *Anesthesiology*, 121(2), 320–327. <https://doi.org/10.1097/ALN.0000000000000300>
- Wang, J., Peng, C., Zhao, Y., Ye, R., Hong, J., Huang, H., & Chen, L. (2021). Application of a Robotic Tele-Echography System for COVID-19 Pneumonia. *Journal of Ultrasound in Medicine*, 40(2), 385–390. <https://doi.org/10.1002/JUM.15406>
- Wang, J. ;, Yang, X. ;, Zhou, B. ;, Sohn, J. J. ;, Zhou, J. ;, Jacob, J. T. ;, Higgins, K. A. ;, Bradley, J. D. ;, Liu, T., Wang, J., Yang, X., Zhou, B., Sohn, J. J., Zhou, J., Jacob, J. T., Higgins, K. A., Bradley, J. D., & Liu, T. (2022). Review of Machine Learning in Lung Ultrasound in COVID-19 Pandemic. *Journal of Imaging 2022, Vol. 8, Page 65*, 8(3), 65. <https://doi.org/10.3390/JIMAGING8030065>
- Yusuf, G. T., Wong, A., Rao, D., Tee, A., Fang, C., & Sidhu, P. S. (2022). The use of contrast-enhanced ultrasound in COVID-19 lung imaging. *Journal of Ultrasound*, 25(2), 319–323. <https://doi.org/10.1007/S40477-020-00517-Z/FIGURES/3>
- Zhang, Y., Xue, H., Wang, M., He, N., Lv, Z., & Cui, L. (2021). Lung ultrasound findings in patients with coronavirus disease (COVID-19). *American Journal of Roentgenology*, 216(1), 80–84. <https://doi.org/10.2214/AJR.20.23513>





## A Appendix

### A.1 Publications included in this thesis

Mokotedi, M. C., Lambert, L., Simakova, L., Lips, M., Zakharchenko, M., Rulisek, J., & Balik, M. (2018). X-ray indices of chest drain malposition after insertion for drainage of pneumothorax in mechanically ventilated critically ill patients. *Journal of Thoracic Disease*, *10*(10), 5695–5701. <https://doi.org/10.21037/jtd.2018.09.64> **IF 2.5**

Maly, M., Mokotedi, M. C., Svobodova, E., Flaksa, M., Otahal, M., Stach, Z., Rulisek, J., Brozek, T., Porizka, M., & Balik, M. (2022). Interpleural location of chest drain on ultrasound excludes pneumothorax and associates with a low degree of chest drain foreshortening on the antero-posterior chest X-ray. *The ultrasound journal*, *14*(1), 45. <https://doi.org/10.1186/s13089-022-00296-0> **IF 3.4**

Balik, M., Maly, M., Huptych, M., Mokotedi, M. C., & Lambert, L. (2023). Prognostic Impact of Serial Imaging in Severe Acute Respiratory Distress Syndrome on the Extracorporeal Membrane Oxygenation. *Journal of clinical medicine*, *12*(19), 6367. <https://doi.org/10.3390/jcm12196367> **IF 3.9**

Balik, M., Mokotedi, M. C., Maly, M., Otahal, M., Stach, Z., Svobodova, E., Flaksa, M., Rulisek, J., Brozek, T., & Porizka, M. (2022). Pulmonary consolidation alters the ultrasound estimate of pleural fluid volume when considering chest drainage in patients on ECMO. *Critical care (London, England)*, *26*(1), 144. <https://doi.org/10.1186/s13054-022-04018-9> **IF 15.1**

### A.2 Publications on the topic not included in this thesis

Mokotedi, C. M., & Balik, M. (2017). Is the mechanism of re-expansion pulmonary oedema in a heart-lung interaction? *BMJ Case Reports*, *2017*. <https://doi.org/10.1136/bcr-2017-219340> **IF 0.9**

Mokotedi, M.C., Malý, M., & Balík, M. (2023). Zobrazovací metody u těžkých forem covid-19 se zaměřením na hrudní ultrasonografii. *Anesteziologie a intenzivní medicína*, 34(2), 61-68 **IF 0.1**